Structural Layout Optimization Framework of Tall Buildings Subjected to Wind Load

A thesis

submitted to the Faculty of Graduate Studies

in partial fulfilment of the requirements for the

Degree of Doctor of Philosophy

in

Civil Engineering

Lakehead University

By

Magdy Alanani

Supervisor:

Dr. Ahmed Elshaer

Associate Professor – Department of Civil Engineering

ABSTRACT

Conventional design methodology for tall buildings is a time-consuming and repetitive trial-and-error procedure with a limited probability of yielding an optimal solution that satisfies architectural, structural and serviceability requirements. Tall buildings are typically slender structures and mainly depend on a Main Wind Force Resisting System (MWFRS) (e.g., shear walls, cores, and bracing systems) to withstand the lateral load of wind events, where a minor change in their layout, size, or shape will affect the cost tremendously. Consequently, a structural layout optimization procedure will result in a more economical and sustainable design. Most previous studies focused on developing optimization frameworks and algorithms that rely on using static wind loads. Even with the adoption of dynamic wind load, the focus was on the vertical layout of the lateral load-resisting systems in a simplified form and as a single objective optimization due to the demanding computational costs. Therefore, the first and main objective of this research is to develop a novel structural-wind optimization framework (SWOF) to find the optimal horizontal (e.g., shear wall) layout of tall buildings subjected to wind loads. SWOF is considered a genetic algorithm-based framework that uses a data-driven surrogate model to evaluate its constraints and objective functions. These surrogate models rely on a training dataset prepared using the Finite Element Method (FEM), which has been created using an open application program interface (OAPI) MATLAB code. The second objective is to adopt a multi-objective optimization algorithm to increase the exploration capabilities of the search domain and to find a Pareto Front of multiple optimal layouts. The multi-objective optimization handles contradicting objective functions from which the decision-maker can choose the perfect compromise. The third objective is to extend the use of the developed SWOF framework to include performance-based wind design (PBWD) concepts by relying on dynamic wind load time history

analysis to enable the inclusion of dynamically very sensitive tall buildings. This is primarily achieved by developing an experimentally validated computational fluid dynamics (CFD) model to generate wind load time history and combining the developed framework with the PBWD requirements. The fourth and last objective of this thesis is to examine different data-driven surrogate models to ensure their efficiency in capturing the relationship between the crude topology of tall buildings and the structural response required for optimization. In addition, reducing the computational time required for objective functions and constraints evaluations and makes the framework computationally affordable. An optimization problem is presented to show SWOF's efficiency. SWOF showed significant capabilities in recognizing load direction, critical load cases and inertia concepts without explicitly defining them through the developed code.

KEYWORDS

Structural optimization; Topology optimization; Tall buildings; Wind load; Genetic algorithm; Neural networks; Surrogate model; Machine learning; Deep Learning; Computational Fluid Dynamics (CFD); Finite Element Method (FEM); Large Eddy Simulation (LES); Shear walls; Performance-based Wind Design (PBWD).

CO-AUTHORSHIP STATEMENT

This thesis has been prepared in accordance with the regulations for an Integrated-Article format stipulated by the Faculty of Graduate Studies at Lakehead University. Information presented from outside sources, which has been used for analysis or discussion, has been cited where appropriate. This thesis has been co-authored as:

Chapter 2: ANN-based optimization framework for the design of wind load resisting system of tall buildings

Alanani, M., & Elshaer, A. (2023). ANN-based optimization framework for the design of wind load resisting system of tall buildings. *Engineering Structures*, *285*, 116032.

Chapter 3: Multi-objective structural layout optimization of tall buildings subjected to dynamic wind loads

Alanani, M., Brown, T., & Elshaer, A. (2024). Mulit-objective structural layout optimization of tall buildings subjected to dynamic wind loads. *Journal of Structural Engineering, ASCE*, 1–30. https://doi.org/10.1061/JSENDH/STENG-12366

Chapter 4: Performance-based layout optimization framework of tall buildings subjected to dynamic wind load

Alanani, M., & Elshaer, A. (2024). Performance-based layout optimization framework of tall buildings subjected to dynamic wind load (under review). *Journal of Wind Engineering and Industrial Aerodynamics.*

Chapter 5: Data-driven surrogate models for estimating tall building wind response

Alanani, M., Allam, M., & Elshaer, A. (2024). Data-driven surrogate models for estimating tall building wind response (under review). *Journal of Building Engineering*

DEDICATION

To those who lost their lives, families, homes and dreams

ACKNOWLEDGEMENTS

In the name of Allah, the Most Gracious, the Most Merciful. I am deeply grateful to Allah Almighty for granting me the opportunity to embark on this Ph.D. journey, guiding me through unexpected paths, and blessing me with the strength and perseverance to see it through to completion. I am thankful to Allah for the hardship before ease.

I would like to express my deepest gratitude to my supervisor, Dr. Ahmed Elshaer, for his unwavering support, guidance and advice. This endeavour would not have been possible without his mentorship, which has been vital in shaping my research and academic growth. From providing insightful feedback on my work to offering invaluable advice on navigating the challenges of academia and beyond, his dedication and commitment to my success have been truly remarkable.

I am also indebted to the members of my thesis committee, Prof. “Yanglin Gong,” Prof. “Wilson Wang”, and Prof. “Wael El-Dakhakhni,” for their scholarly insights, constructive feedback, and invaluable contributions to shaping this research. Their expertise and guidance have been instrumental in refining the scope of the dissertation. I would also like to extend my thanks to my previous supervisors. Without their advice, I would not have made it to the Ph.D., Prof. Maguid Hasan”, Prof. “Hamed Salem,” Prof. “Marwan Shedid” and “Dr. Mariem Ehab.”

To my beloved parents, who have been the cornerstone throughout my whole life, I owe an immeasurable debt of gratitude. I am acutely aware that I am their most significant project. Their endless love and sacrifices have been the driving force behind every step. I am also grateful to my sisters for all that they do, from providing emotional support during challenging times to celebrating every milestone with unwavering enthusiasm. My warmest thanks to my grandparents for all the unconditional love they gave. Special thanks to my uncle “Dr. Sherif” for his guidance, mentorship and motivation.

Thanks should also go to the members of my research group, “SWERL” for their encouragement and support. I want to use this space to thank them, in no specific order: “Mutaz,” “Raghdah,” “Mostafa,” “Tristen,” “Stephen,” “Amir,” and “Kendra.” Your collaboration and company have enriched my academic experience and made this journey more fulfilling. Whether it was research feedback or offering words of encouragement, I am grateful for the friendships and professional relationships built during this time. Also, thanks are extended to my office mates, “Mehran,”

“Ahmed,” “Aysen,” “Zahra,” “Maral,” and “Ali.” I would also like to thank “Marwa Allam” for the technical advice, revision and guidance that helped me get into new technical fields.

To my dear roommates, “Elian,” “Ishak,” “Ali,” “Mouaad,” “Deeb,” “Elshafey,” “Mondeir,” and “Anas” who have become like family to me, thank you for your companionship, support, and understanding. Your presence has made the challenges more bearable and the successes more meaningful, from late-night talks, celebrations of achievements, outings, travelling, activities and gatherings. I cherish the memories we have created together and am thankful for your friendship.

I am immensely thankful to those who generously extended their kindness and assistance, particularly my childhood friend “Ahmed Hesham” and his family, for their support and hospitality. I am grateful for all the warm gatherings that I had the privilege to attend, which made me feel at home and like a family. Also, I am thankful to my old friends who joined me here in Canada “Omar Elmeligy,” and “Amgad Mahrous.” In addition to the support of my friends back home, your prayers reached me, and having you here would have meant a lot.

I am deeply grateful for the unexpected blessings I encountered in Thunder Bay. What began as a new chapter in an unfamiliar city quickly transformed into a journey filled with genuine connections and unwavering support from its remarkable community. I am profoundly thankful for their generosity and helpfulness. Listing all will be hard if not impossible; therefore, I take this opportunity to extend my heartfelt gratitude to a few, without any particular order: “Dr. Yasser,” “Dr. Mohannad,” “Dr. Hassan,” “Haj Munawar,” “Dr. Najam,” “Dr. Samer,” “Dr. Malek,” “Dr. Ibrahim,” “Dr. Hamza,” “Dr. Ahwiadi,” “Khaled,” “ Faisal,” “Joy,” “ Fouad,” and “Mourad.”

I would be remiss in not mentioning the Lakehead University community through the Ph.D. journey. I was welcomed with open arms and fostered an atmosphere of inclusivity. Special thanks to the international office team, Faculty of Engineering, FGS, LUSU, LUGSA and LUMSA. To all helping hand and offered words of encouragement throughout my journey, your generosity and support have not gone unnoticed.

Last but not least, I acknowledge the countless times I troubleshot a code, messed up nonsense errors, rewrote a paper, and patiently waited for validations to be correct. It’s true we learn from failure much more than from success. As Thomas Edison famously said, *“Just because something doesn't do what you planned it to do doesn't mean it's useless.”*

LIST OF JOURNAL PUBLICATIONS

Alanani, M., & Elshaer, A. (2023). ANN-based optimization framework for the design of wind load resisting system of tall buildings. Engineering Structures, 285, 116032. https://doi.org/10.1016/j.engstruct.2023.116032

Alanani, M., Brown, T., & Elshaer, A. (2024). Mulit-objective structural layout optimization of tall buildings subjected to dynamic wind loads. Journal of Structural Engineering, ASCE, 1–30. https://doi.org/10.1061/JSENDH/STENG-12366

Alanani, M., Allam, M., & Elshaer, A. (2024). Data-driven surrogate models for estimating tall building wind response (under review). Journal of Building Engineering

Alanani, M., & Elshaer, A. (2024). Performance-based layout optimization framework of tall buildings subjected to dynamic wind load (under review). Journal of Wind Engineering and Industrial Aerodynamics.

Brown, T., Alanani, M., Elshaer, A., & Issa, A. (2024). Formulation of Separation Distance to Mitigate Wind-Induced Pounding of Tall Buildings. Buildings, 14(2), 479. https://doi.org/10.3390/buildings14020479

LIST OF CONFERENCE PUBLICATIONS

Alanani, M., & Elshaer, A. (2021). Improving wind performance of structural systems of tall buildings using topology modifications. The Canadian Society of Civil Engineering Annual Conference 2021, 244(May), 1–9. https://doi.org/10.1007/978-981-19-0656-5_41

Alanani, M., & Elshaer, A. (2022). Structural Layout Optimization of Tall Buildings Against Wind Load. Proceedings of the Canadian Society of Civil Engineering Annual Conference 2022.

Alanani, M., Brown, T., & Elshaer, A. (2023). Automated shear wall layout optimization framework of tall buildings subjected to dynamic wind loads. Proceedings of the Canadian Society of Civil Engineering Annual Conference, 1–13.

Alanani, M., & Elshaer, A. (2023). AI-driven topology optimization framework for tall buildings subjected to dynamic wind excitation. 16th International Conference on Wind Engineering, 1–4.

Table of Contents

Abstract I
Keywords III
Co-Authorship Statement IV
Dedication VI
Acknowledgements VII
List of Journal Publications IX
List of Conference Publications IX
List of Tables XII
List of Figures XIII
Chapter 1 1
1. Introduction 1
1.1. Background 1
1.2. Research Gap 7
1.3. Scope of Thesis 8
1.4. Organization of thesis 9
1.5. References 12
Chapter 2 16
2. ANN-based optimization framework for the design of wind load resisting system of tall buildings 16
2.1. Introduction 16
2.2. Structural Wind optimization Framework (SWOF) 19
2.3. Optimization problem definition 22
2.4. Optimization problems description and results 34
2.5. Conclusion 49
2.6. References 52
Chapter 3 55
3. Multi-objective structural layout optimization of tall buildings subjected to dynamic wind loads 55
3.1. Introduction 55
3.2. Structural-Wind optimization Framework (SWOF) 60
3.3. Optimization problem definition 69
3.4. Optimization problem description and results 82
3.5. Conclusion 90

3.6. References 92
Chapter 4 97
4. Performance-based layout optimization framework of tall buildings subjected to dynamic wind load 97
4.1. Introduction 97
4.2. Adopting Performance-Based Wind Design for tall building optimization 104
4.3. Structural-Wind Optimization Framework (SWOF) 108
4.4. Surrogate model development 112
4.5. Optimization Problem definition 114
4.6. Results and discussion 116
4.7. Conclusion 125
4.8. References 127
Chapter 5 132
5. Data-driven surrogate models for estimating tall building wind response 132
5.1. Introduction 132
5.2. Usage of surrogate model in PBWD optimization framework 136
5.3. Regression Models 140
5.4. Development of surrogate models 147
5.5. Results and Discussion 151
5.6. Conclusion 160
5.7. References 162
Chapter 6 167
6. Conclusions and recommendations 167
6.1. Summary 167
6.2. Main Contributions 168
6.3. Future work and recommendations 171

LIST OF TABLES

Table 2-1 Optimization problems matrix for objective function and constraints 35

Table 2-2 GA parameters of the optimization Problem-1 36

Table 2-3 Validation results of optimization Problem-1 37

Table 2-4 GA parameters of optimization Problem-2 41

Table 2-5 Validation results of optimization Problem-2 42

Table 2-6 GA parameters of optimization Problem-3 43

Table 2-7 Validation results of optimization Problem-3 44

Table 2-8 GA parameters of optimization Problem-4 47

Table 2-9 Validation results of optimization Problem-4 49

Table 3-1. Objective functions definition 62

Table 3-2 ANN regression performance metrics 69

Table 3-3. Building and computational domain dimensions 73

Table 3-4: Steel sections for the examined structures at a mean wind velocity of 40 m/s (Brown et al., 2024) 79

Table 3-5: Design wind loads for Building 1 subjected to a design mean wind velocity of 40 m/s (Brown et al., 2024) 80

Table 3-6. NSGA-II parameters of the optimization problem 83

Table 4-1 NSGA-II parameters 116

Table 5-1 Hyperparameters configuration for each ML model 150

Table 5-2 Statistical performance metrics 151

LIST OF FIGURES

Fig. 1-1 Number of completed tall buildings each year starting from 1980 (CTBUH, 2021)..... 1

Fig. 1-2 Interrelations of tall building design considerations (Park et al., 2005) 3

Fig. 1-3 Information flow model for the structural design process (Anwar et al., 2005) 3

Fig. 1-4 Design stages level of influence (Kanyilmaz et al., 2023)..... 4

Fig. 1-5 Structural wind optimization categories: (a) Outer shape aerodynamic optimization, structural system optimization: (b) Elevation layout, and (c) Plan layout. (Alanani & Elshaer, 2023)..... 7

Fig. 2-1 Structure wind optimization framework (SWOF) flowchart 21

Fig. 2-2 (a) Slab plan layout, (b) shear wall segment and (c) column cross-section 24

Fig. 2-3 (a) Architectural plan view and (b) possible shear wall locations 25

Fig. 2-4 Surrogate model building flowchart..... 27

Fig. 2-5 Schematic diagram for general ANN architecture 29

Fig. 2-6 Change of regression coefficient with the training sample (training of the σM)..... 29

Fig. 2-7 Sensitivity analysis for the interstorey drift ANN hidden layer size..... 31

Fig. 2-8 Regression coefficient for intersorey drift ANN in (a) Y-direction and (b) X-direction 31

Fig. 2-9 Error Histogram for interstorey drift ANN in (a) Y-direction and (b) X-direction 31

Fig. 2-10 Optimal shear wall layout of optimization Problem-1-1..... 37

Fig. 2-11 (a) Interstorey drift of optimization Problem-1-1 (b) Interstorey drift of optimization Problem-1-1 37

Fig. 2-12 Optimal shear wall layout of optimization Problem-1-2..... 38

Fig. 2-13 (a) Fitness curve for the total number of shear wall segments of optimization Problem-1-2, (b) Interstorey drift of optimization Problem-1-2 39

Fig. 2-14 (a) Various population size fitness curves of optimization Problem-1-3, (b) Interstorey drift of optimization Problem-1-3 40

Fig. 2-15 Optimal shear wall layout optimization Problem-1-3 40

Fig. 2-16 (a) Fitness curve for the total number of shear wall segments of optimization Problem-2, (b) Optimal shear wall layout of optimization Problem-2 41

Fig. 2-17 (a) Interstorey drift, and (b) distance between the center of mass and center of rigidity of the best fitness candidate in each generation of optimization Problem-2 42

Fig. 2-18 (a) Fitness curve for the total number of shear wall segments of optimization Problem-3, and (b) optimal shear wall layout of optimization Problem-3 44

Fig. 2-19 (a) Interstorey drift, and (b) standard deviation of base moments of optimization Problem-3 44

Fig. 2-20 (a) Histogram for base maximum bending moment of optimization Problem-3, and (b) probability distribution function for three different generated layouts 45

Fig. 2-21 Maximum bending moment around the local perpendicular axis of piers 45

Fig. 2-22 Fitness curve for (a) the total number of piers and (b) the number of shear wall segments of optimization Problem-4 47

Fig. 2-23 Optimal shear wall layout of optimization Problem-4 48

Fig. 2-24 (a) Three-dimensional FEM model for the optimal layout of optimization Problem-4, and (b) Demand/capacity ratio histogram and probability distribution function for all piers of the optimization Problem-4 48

Fig. 2-25 (a) Interstorey drift, (b) distance between the center of mass and center of rigidity, and (c) standard deviation of the base moment. 49

Fig. 2-26 (a) FEM and ANN outputs for interstorey drift, (b) Regression coefficient for Intersotrey drift of optimization Problem-4 49

Fig. 3-1. Structure wind optimization framework (SWOF) flowchart 63

Fig. 3-2 Non-dominant Sorting Genetic Algorithm (NSGA-II) flowchart 65

Fig. 3-3 Sensitivity analysis for the training sample size of $eCMCR$ 66

Fig. 3-4. Regression coefficient of (a) interstorey drift in the Y-direction δy, (b) eccentricity $eCMCR$, and (c) standard deviation of the base moment (σM). 68

Fig. 3-5 Error Histogram of (a) interstorey drift in the Y-direction δy, (b) eccentricity $eCMCR$, and (c) standard deviation of the base moment (σM). 68

Fig. 3-6. CAARC standard full-scale dimensions 70

Fig. 3-7. Computational domain details and boundary conditions 72

Fig. 3-8. (a) mean wind velocity and (b) turbulence intensity profiles used for the inflow boundary condition (Elshaer et al., 2016)..... 72

Fig. 3-9 Computational grid (a) near target buildings, (b) inlet, (c) ground and (c) 3d view for the computational domain. 73

Fig. 3-10 Mean velocity magnitude with flow streamlines 74

Fig. 3-11. (a) $mean\ CP$ (b) $RMS\ CP$ distribution over the horizontal section of the building at 2/3 H against BLWT test results..... 75

Fig. 3-12. (a) Longitudinal and across wind forces time history at 10th floor, (b) Highlighted derived surface for the 10^{th} floor 76

Fig. 3-13 (a) Slab plan layout, (b) shear wall segment and (c) column cross-section 77

Fig. 3-14. (a) Architectural plan view and (b) possible shear wall locations 78

Fig. 3-15 (a) FEM CAARC model dimensions, (b) maximum deflection of storeys, and (c) maximum inter-storey drift in the along-wind direction (Brown et al., 2024)..... 80

Fig. 3-16 (a) 3D Finite Element model and (b) 10th story displacement 81

Fig. 3-17. Selection of optimal solutions on the Pareto Front 85

Fig. 3-18 Pareto Front optimal layouts and corresponding objective function values. 85

Fig. 3-19 Values of objective functions for a sample of optimal solutions on the Pareto Front .. 87

Fig. 3-20. Drift constraint values for a sample of optimal solutions on the Pareto Front 88

Fig. 3-21. Demand/capacity ratio histogram and probability distribution function for all piers for a sample of optimal solutions on the Pareto Front. 89

Fig. 3-22. Probability distribution function for 5 optimal solutions on the Pareto Front 89

Fig. 4-1 ASCE PBWD pre-standards procedure (Abdelwahab et al., 2023)..... 104

Fig. 4-2 Outline of PBWD MWFRS analysis and acceptance methods for each performance objective (ASCE, 2019)..... 105

Fig. 4-3 Method 1 procedure for Continuous Occupancy performance objective of MWFRS.. 107

Fig. 4-4 Structure wind optimization framework (SWOF) flowchart (Alanani et al., 2024) 108

Fig. 4-5 The case study building plan layout with structural details and domain. 110

Fig. 4-6. (a) Longitudinal and across wind forces and torsional wind moment time history at the 10th floor, AOA=$0o$ (b) Highlighted derived surface for the 10^{th} floor 111

Fig. 4-7 Proposed Deep Neural Network (DNN) architecture. 113

Fig. 4-8 Mean Square Error for $D/Cwall$ DNN 114

Fig. 4-9 (a) Error Histogram, and (b) Regression plot for $D/Cwall$ results..... 114

Fig. 4-10 Fitness function of the eccentricity objective function through different population sizes 117

Fig. 4-11 NSGA-II procedure (based on (Deb et al., 2002b)) 118

Fig. 4-12 3D Pareto Front with five samples of possible MWFRS layouts 119

Fig. 4-13 Selected optimal layout-A 119

Fig. 4-14 Structural response via along wind load: (a) peak drift, (b) storey drift, (c) base shear, and (d) overturning moment of layout-A 121

Fig. 4-15 Structural response via across wind load: (a) peak drift, (b) storey drift, (c) base shear, and (d) overturning moment of layout-A 121

Fig. 4-16 Peak drift in the (a) x-direction, (b) y-direction and (c) the rotation time history at the top story by LC2 123

Fig. 4-17 (a) Performance D/C results for shear walls, and (b) strength capacity results for columns..... 124

Fig. 4-18 Edge fiber stress-strain results for (a) concrete and (b) steel reinforcement at Pier-2 124

Fig. 4-19 $P1-M2-M3$ Interaction diagram for Pier-2 with internal loads due to $0o\ and\ 225o$ Angles of Attack (AOA) 125

Fig. 5-1 Surrogate model attached to an optimization algorithm. 139

Fig. 5-2 The process of preparing a training database for the proposed ML-based surrogate model. 139

Fig. 5-3 Structural response data distribution for 1000 generated samples using LHS..... 148

Fig. 5-4 ML-based surrogate model's developing pipeline..... 149

Fig. 5-5 Coefficient of determination box plot for 5-fold through the cross-validation training of different ML models: (a) peak deflection, (b) peak interstory drift, (c) maximum D/C in shear walls and (d) maximum D/C in columns..... 153

Fig. 5-6 Actual and predicted values representation for: (a) peak deflection, (b) peak interstory drift, (c) maximum D/C in walls and (d) maximum D/C in columns 155

Fig. 5-7 Error distribution percentage of different ML models for: (a) peak deflection, (b) peak interstory drift, (c) maximum D/C in shear walls and (d) maximum D/C in columns..... 156

Fig. 5-8 Performance metrics of different ML-based surrogate models (a) peak deflection, (b) peak interstory drift, (c) maximum D/C in shear walls and (d) maximum D/C in columns..... 157

Fig. 5-9 A comparison of different ML models for a 1 AOA scenario using: (a) error %, (b) actual and predicted values representation, (c) 5-fold coefficient of determination distribution, and (d) performance metrics. 159

Fig. 5-10 A comparison between best performing ML models for 1 and 8 AOA scenarios: (a) error %, (b) coefficient of determination, (c) 5-fold coefficient of determination distribution, and (d) performance metrics. 159

CHAPTER 1

1. INTRODUCTION

1.1. Background

With the rapid increase in population accompanied by vast technological development, the world is shifting towards more dense urban cities (Roser et al., 2019). In 2020, 56.2% of the world's population lived in urban cities. A key element in shaping those cities is tall buildings with their relatively small footprint that crop up more spaces. Tall buildings are growing taller, and the need for more tall buildings is increasing. In 2018, as shown in Fig. 1-1, a new record was accomplished as more than 160 tall buildings of 200 meters or more were constructed, including 20 supertall buildings exceeding 300 meters (CTBUH, 2021)

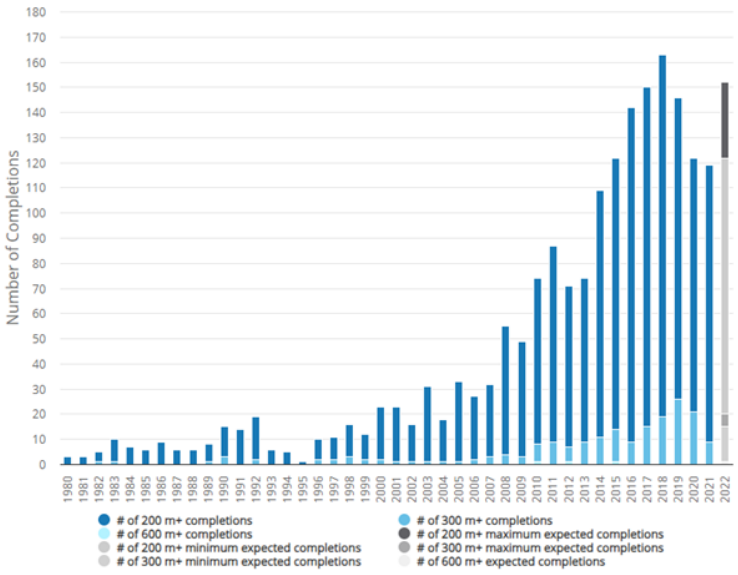

Fig. 1-1 Number of completed tall buildings each year starting from 1980 (CTBUH, 2021)

It is not only about the aesthetics of tall buildings but also about the adequate solutions provided for the housing problem. Yet more innovative solutions should be provided to overcome the associated challenges with tall buildings. One of these challenges is their slenderness and sensitivity to wind loads. It was noted that the number of natural climate disasters, especially

extreme wind events, increased in the last three decades (Reidmiller et al., 2018). Consequently, the wind resiliency of tall structures should increase. Yet, the construction cost will increase, using conventional design and construction methodology, which will increase the cost of housing. Another challenge that faces tall buildings is the amount of carbon emissions resulting from the process of building such structures, starting from materials acquisition to putting the building to function. With these current design practices, the construction industry becomes responsible for almost 40% of global energy-related carbon emissions (WGBC, 2019).

The conventional design procedure of tall buildings goes through an interconnected, interdisciplinary, continuous process, as illustrated in Fig. 1-2. The collaboration between structural engineers and architects reaches its peak through the initial design steps to identify the buildings' overall form. Structural design procedure can be divided into stages as follows: conception, modelling, analysis, design, detailing, drafting, and costing, as shown in Fig. 1-3. Each design stage varies in the amount of influence on the total cost and the amount of carbon emission, where it can be noticed that the conceptual design has the highest effect, as presented in Fig. 1-4. Besides the effect of the design stages, each structural element has its contribution to the budget and the environment. (Cho et al., 2004) found that the unit direct construction cost of MWFRS (i.e., shear walls) can reach 52% in some tall building projects. This percentage is inevitable, and the tuning of the structural layout at the conceptual design stages plays a significant role in reducing the project's total cost with less environmental impact. Consequently, it becomes a crucial objective for structural designers to provide more optimized and cost-effective structures while maintaining the balance between aesthetics, serviceability, and safety of structures (Beghini et al., 2014). One of the most efficient solutions to address structural optimization's problem is structural topology optimization. This methodology proved its efficiency in other fields like material,

industrial, biomedical, automotive and aeronautical fields (Sigmund, 2000). It can be defined as finding the best distribution of material within a design domain (Bendsøe & Sigmund, 2004).

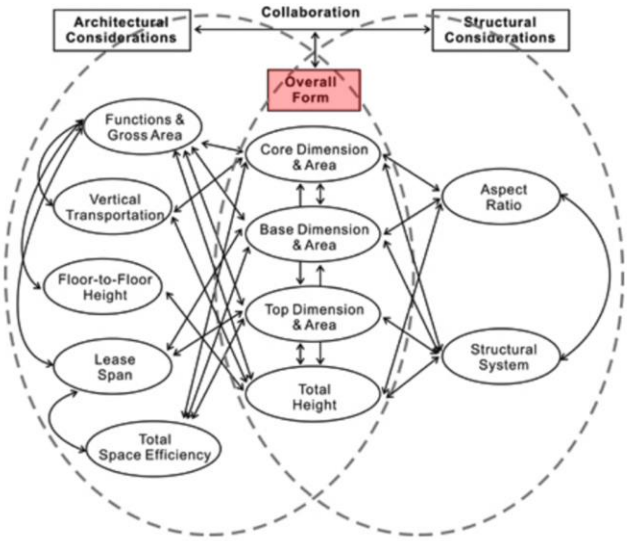

Fig. 1-2 Interrelations of tall building design considerations (Park et al., 2005)

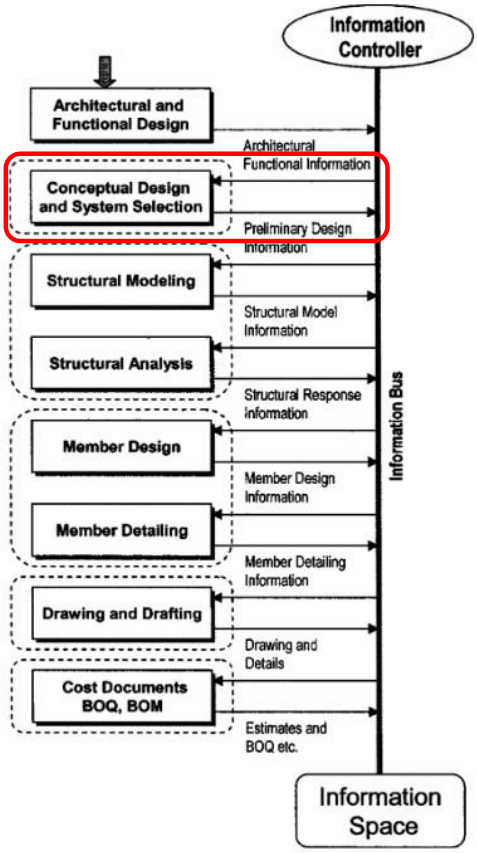

Fig. 1-3 Information flow model for the structural design process (Anwar et al., 2005)

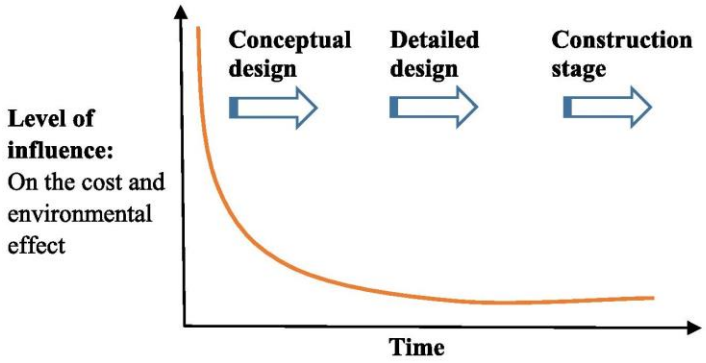

Fig. 1-4 Design stages level of influence (Kanyilmaz et al., 2023)

As for tall buildings, structural wind optimization can be categorized into two main categories, which are outer shape aerodynamic optimization and structural system optimization, as shown in Fig. 1-5. Outer shape aerodynamic optimization relies on altering the shape of the bluff body to reduce the amount of wind forces that will be generated, as shown in Fig. 1-5 (a). This alteration process can be done either locally by adding modifications to corners (e.g., corner chamfering, recession and roundness) (Bernardini, Spence, Wei, et al., 2015; Elshaer, Bitsuamlak, & El-Damatty, 2017; Kareem et al., 1999, 2013b; Tamura & Miyagi, 1999) or globally by inducing significant changes to the building's form (e.g., twisting, tapering and openings) (Elshaer & Bitsuamlak, 2018; Kelly et al., 2012; Tanaka et al., 2012). On the other hand, structural system optimization, which is the focus of this thesis, depends on finding an optimal structural system capable of resisting lateral loads (e.g., wind and seismic). Structural topology optimization aims towards finding the optimal thickness for structural elements of a prescribed structure layout (Bendsøe & Sigmund, 2004; Sigmund, 2000) within a predefined set of structural and architectural constraints. For example, (C.-M. Chan et al., 1995) developed a lateral load-resisting system steel design framework based on an optimality criterion optimization algorithm that automates the selection of structural steel members on a predefined layout subjected to drift, strength and size constraints. In comparison, shape optimization is based on changing the shape of the structural resisting system without changing the used structural member or material. This is presented

through the study by (Akbari Hamed et al., 2022), in which the opening shape within the steel plate shear wall was optimized using the optimality criterion algorithm. In contrast, topology optimization targets the structural system's layout by finding the materials' connection and distribution through the predefined domain. This can be tackled either on the elevation layout like finding the optimal bracing system shape, as shown in Fig. 1-5(b), or on the plan layout as finding the optimal shear walls layout, as shown in Fig. 1-5 (c).

Previous studies have focused on optimizing the elevation layout of lateral load resisting systems against wind loads, particularly in steel structures, due to the versatility offered by those structures (Baldock et al., 2005; C. M. Chan & Wong, 2008a; Es-haghi & Sarcheshmehpour, 2022). For plan layout optimization, few studies are found in the literature. Multiple limitations were challenging for those frameworks. For example, (Y. Zhang & Mueller, 2017) developed an optimization framework based on a modified evolutionary algorithm. However, the precalculations of shear walls' capacity with a limited dataset of selections limit the capabilities of exploring more layouts that might be more optimal. Thus, developing an optimization framework for the main wind force-resisting system (MWFRS) with affordable computational capabilities is needed. Detailed literature about horizontal layout optimization, especially for shear wall systems, will be found in Chapter 2.

The consideration of static wind load is typically adopted in optimization frameworks with single objective optimization. Yet the inclusion of static wind is a simplified approach that reduces the analysis accuracy and optimization output as well. As a result, dynamic wind loads should be adopted in MWFRS optimization frameworks (Bobby et al., 2014; Gomez et al., 2021; Suksuwan & Spence, 2019). The consideration of multi-objective optimization with dynamic wind load is still not comprehensively studied, so finding a compromise between contradicting objective

functions and design variables is required (Alanani et al., 2024a), and it will be discussed in detail in Chapter 3.

Seeking optimal design would be less efficient if uncertainties dominate the design process (Bezabeh et al., 2020; S. M. J. Spence & Arunachalam, 2022). Thus, applying the performance-based design (PBD) approach overperformed the deterministic approach while allowing for controlled inelastic deformations through nonlinear time history analysis (NLTHA) (ASCE, 2019). As a result, it is recommended to couple the PBD procedure with an optimization algorithm that can handle the cumbersome design procedure (S. M. J. Spence & Kareem, 2014). Chapter 4 shows the literature about performance-based design and how it can be deployed within an optimization procedure.

Finally, adopting PBD in an optimization framework might require a high computational cost that can be affordable using surrogate models (Esteghamati et al., 2021). Machine learning models have shown efficiency in capturing structural response at the element-based level (Haggag et al., 2024; G. Ma et al., 2023; Solorzano & Plevris, 2023a) and system-based level (Hareendran & Alipour, 2022; Micheli, Alipour, et al., 2020a; Tseranidis et al., 2016). Yet, an efficient surrogate model that can capture the relationship between the crude topology of the shear wall system and the tall building's structural response is still missing. More detailed literature on machine learning applications in tall building design and how it can be used for developing an ML-based surrogate model is shown in Chapter 5.

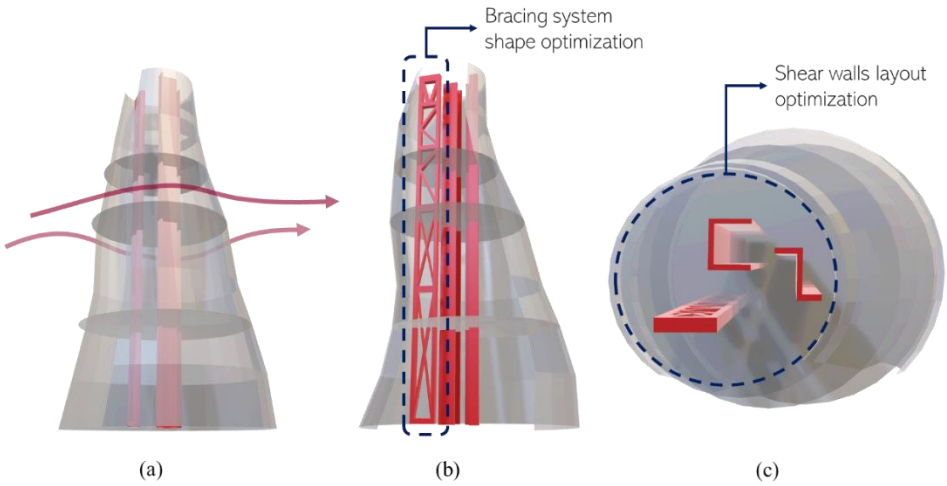

Fig. 1-5 Structural wind optimization categories: (a) Outer shape aerodynamic optimization, structural system optimization: (b) Elevation layout, and (c) Plan layout. (Alanani & Elshaer, 2023)

1.2. Research Gap

Despite the advancement in the field of structural optimization, most of the earlier studies tackled the optimization problem of the elevation (i.e., vertical) layout of the Main Wind Force Resisting System (MWFRS). The focus was on deploying topology optimization in a theoretical approach that provides a holistic indication of the structural system layout. Steel has been intensely investigated, especially the bracing system layout, thanks to the versatile nature of steel formwork. On the other hand, limited studies tackled the plan (i.e., horizontal) layout problem of the MWFRS, particularly shear walls, which are considered one of the most used resisting systems for lateral loads. Moreover, most of the aforementioned research simplified the lateral load behaviour into equivalent deterministic static loads. However, lateral loads have stochastic dynamic behaviours that affect the structural vibrational modes; therefore, these simplifications might fall short of yielding an optimal or near-optimal solution. Tall buildings' structural layout optimization is characterized by a complex search space of multiple objectives and constraints (e.g., serviceability limits). Thus, the practicality of any proposed framework relies on balancing the contradicting

objective functions to better explore the design domain. Consequently, providing a multi-objective optimization framework will enable a reasonable compromise for various objective functions required in a practical application. In addition to the rising demand for Performance-based Wind design (PBWD), different approaches should be taken into account to avoid conservative design at the conceptual stage and allow performance-based design that pushes the design to its limit through detailed analysis and better quantification of uncertainties. Finally, the main challenge in providing an efficient optimization framework is the nature of the structural layout problem as a non-convex optimization problem. The heuristic optimization algorithm provides a decent resolution of this problem, yet the computational time for such algorithms is a concern. While surrogate models can provide an affordable solution for those cumbersome computations, they are still immature for the structural layouts of tall buildings.

1.3. Scope of Thesis

Based on the aforementioned research gaps, the main objective of the thesis is to develop a computationally efficient structural wind optimization framework (SWOF) to systematically find the MWFRS layout at the conceptual design stage. In fulfillment of the mentioned goal, the following specific objectives were considered:

1. Develop a genetic algorithm-based optimization framework to find the optimal shear wall layout subjected to wind loads based on the National Building Code of Canada (NBCC, 2020). Through this stage, structural response and parameters required for optimization are investigated to see the effect of each parameter on the final layout using an Artificial Neural Network-based surrogate model.
2. Adopt a multi-objective optimization algorithm to find a Pareto Front of possible optimal layout using dynamic wind load.

3. Extend the developed framework to be compatible with the performance-based wind design (PBWD) approach by exploring the framework outputs using multi-objective optimization.
4. Explore the potential of using machine learning models as a surrogate model for predicting the structural parameters required by PBWD to reduce the computational cost for the framework.

1.4. Organization of thesis

This thesis has been prepared in an "Integrated-Article" format, and it consists of 6 chapters:

1.4.1. Chapter 1 Introduction

This chapter (the current chapter) introduces the motivation, Research gap and objectives of the thesis, along with providing brief background relevant to the research project.

1.4.2. Chapter 2 ANN-based optimization framework for the design of wind load resisting system of tall buildings

This chapter discusses the development of a novel structural-wind optimization framework (SWOF) to find the optimal shear wall layout of tall buildings subjected to wind loads. SWOF is considered a genetic algorithm-based framework that uses an Artificial Neural Network (ANN) surrogate model to evaluate its constraints and objective function. These surrogate models rely on a training dataset prepared using a validated Finite Element Method (FEM), which has been created using an open application program interface (OAPI) via MATLAB code. A case study building is presented to show SWOF's efficiency and the effect of each structural parameter on the optimization outputs.

1.4.3. Chapter 3 Multi-objective structural layout optimization of tall buildings subjected to dynamic wind loads

In this chapter, the developed SWOF will be extended to deploy a multi-objective optimization algorithm to handle the practical contradicting objective functions (i.e., structural parameters). A CFD model is adopted to generate the wind load time history required to be applied to the study building. Adopting a time history analysis is considered challenging through the optimization process due to the cumbersome analysis that involves simplification of the structural system as presented in the literature. The developed framework in this chapter relies on an ANN surrogate model for constraints and objective function evaluation. This integration of dynamic response analysis and surrogate modelling was previously lacking in the literature. A multi-objective optimization is conducted to identify the optimal shear wall layout against dynamic wind load and gravity loads provided.

1.4.4. Chapter 4 Performance-based layout optimization framework of tall buildings

In this chapter, SWOF is developed to adhere to the performance constraints based on the ASCE PBWD prestandards by using a non-dominated sorting genetic algorithm-II to overcome the challenges of the domain complexity. The developed framework focuses on Continuous Occupancy (CO) performance with Linear Time History Analysis (LTHA) using wind load time histories of multiple wind angles of attack. Furthermore, a comparison is made between the framework's optimal layout behaviour, the ASCE 7-22 directional procedure generated wind loads, and nonlinear time history analysis (i.e., FNA method) to quantify the effectiveness of the developed framework.

1.4.5. Chapter 5 Data-driven surrogate models for estimating tall building wind response

This chapter comprehensively assesses different data-driven models to develop a surrogate model of tall buildings subjected to dynamic wind loads based on their structural system layout. A training

and testing dataset has been prepared using Finite Element Method (FEM) for a case study building subjected to wind load time history generated by an experimentally validated Computational Fluid Dynamics (CFD) model. For a fair comparison, each developed surrogate model is trained using a grid search algorithm through a k-fold cross-validation process to achieve optimal parameters and hyperparameters of each model. The investigation involves a detailed analysis of statistical performance metrics applied to training and testing datasets.

1.4.6. Chapter 6 Conclusions and recommendations

This chapter summarizes the key findings, insights, and contributions made through the research. It has significant results and implications within the context of the structural design of tall buildings. Moreover, it addresses the limitations encountered during the research process and suggests avenues for future research to build upon the current findings.

1.5. References

Akbari Hamed, A., Samadi, A., & Charkhtab Basim, M. (2022). Topology and shape optimization of steel plate shear walls for enhancing the seismic energy dissipation capacity. *Journal of Building Engineering*, *57*(May), 104828. https://doi.org/10.1016/j.jobe.2022.104828

Alanani, M., Brown, T., & Elshaer, A. (2024). Mulit-objective structural layout optimization of tall buildings subjected to dynamic wind loads. *Journal of Structural Engineering, ASCE*, 1–30. https://doi.org/10.1061/JSENDH/STENG-12366

Alanani, M., & Elshaer, A. (2023). ANN-based optimization framework for the design of wind load resisting system of tall buildings. *Engineering Structures*, *285*, 116032. https://doi.org/10.1016/j.engstruct.2023.116032

Anwar, N., Kanok-Nukulchai, W., & Batanov, D. N. (2005). Component-Based, Information Oriented Structural Engineering Applications. *Journal of Computing in Civil Engineering*, *19*(1), 45–57. https://doi.org/10.1061/(ASCE)0887-3801(2005)19:1(45)

ASCE. (2019). Prestandard for Performance-Based Wind Design V1.1. In *Prestandard for Performance-Based Wind Design V1.1*. American Society of Civil Engineers. https://doi.org/10.1061/9780784484739

Baldock, R., Shea, K., & Eley, D. (2005). Evolving optimized braced steel frameworks for tall buildings using modified pattern search. *Proceedings of the 2005 ASCE International Conference on Computing in Civil Engineering*, 631–642. https://doi.org/10.1061/40794(179)60

Beghini, L. L., Beghini, A., Katz, N., Baker, W. F., & Paulino, G. H. (2014). Connecting architecture and engineering through structural topology optimization. *Engineering Structures*, *59*, 716–726. https://doi.org/10.1016/j.engstruct.2013.10.032

Bendsøe, M. P., & Sigmund, O. (2004). Topology Optimization. In Topology Optimization. Springer Berlin Heidelberg. https://doi.org/10.1007/978-3-662-05086-6Bernardini, E.,

Spence, S. M. J., Wei, D., & Kareem, A. (2015). Aerodynamic shape optimization of civil structures: A CFD-enabled Kriging-based approach. *Journal of Wind Engineering and Industrial Aerodynamics*, *144*, 154–164.

Bezabeh, M., Bitsuamlak, G., & Tesfamariam, S. (2020). Performance-based wind design of tall buildings: Concepts, frameworks, and opportunities. *Wind and Structures*, *31*(2), 103–142. https://doi.org/10.12989/was.2020.31.2.103

Bobby, S., Spence, S. M. J., Bernardini, E., & Kareem, A. (2014). Performance-based topology optimization for wind-excited tall buildings: A framework. *Engineering Structures*, *74*, 242–255. https://doi.org/10.1016/j.engstruct.2014.05.043

Chan, C.-M., Grierson, D. E., & Sherbourne, A. N. (1995). Automatic Optimal Design of Tall Steel Building Frameworks. *Journal of Structural Engineering*, *121*(5), 838–847. https://doi.org/10.1061/(asce)0733-9445(1995)121:5(838)

Chan, C. M., & Wong, K. M. (2008). Structural topology and element sizing design optimisation of tall steel frameworks using a hybrid OC-GA method. *Structural and Multidisciplinary Optimization*, *35*(5), 473–488. https://doi.org/10.1007/s00158-007-0151-1

Cho, H., Co, H., Roh, S., Co, H., Byun, Y., Co, H., Yom, K., Co, H. E., Buildings, T., Cho, U. H. H., Roh, S., Byun, Y., Cho, H., Roh, S., Byun, Y., & Yom, K. (2004). Structural Quantity Analysis of Tall Buildings. *CTBUH 2004 Seoul Conference*, 662–668.

CTBUH. (2021). *2021 Year in Review - The Skyscraper Center*. Council on Tall Buildings and Urban Habitat. https://www.skyscrapercenter.com/year-in-review/2021

Elshaer, A., & Bitsuamlak, G. (2018). Multiobjective Aerodynamic Optimization of Tall Building Openings for Wind-Induced Load Reduction. *Journal of Structural Engineering*, *144*(10), 4018198. https://doi.org/10.1061/(ASCE)ST.1943-541X.0002199

Elshaer, A., Bitsuamlak, G., El-Damatty, A., & El Damatty, A. (2017). Enhancing wind performance of tall buildings using corner aerodynamic optimization. *Engineering Structures*, *136*, 133–148. https://doi.org/10.1016/j.engstruct.2017.01.019

Es-haghi, M. S., & Sarcheshmehpour, M. (2022). *A Novel Strategy for Tall Building Optimization via the Combination of AGA and Machine Learning Methods*. 4. https://doi.org/10.3390/ioca2021-10882

Esteghamati, M. Z., Rodriguez-Marek, A., Flint, M. M., Leon, R. T., Charney, F. A., & Zobel, C. W. (2021). *A DATA-DRIVEN FRAMEWORK TO SUPPORT RESILIENT AND SUSTAINABLE EARLY DESIGN*.

Gomez, F., Spencer, B. F., & Carrion, J. (2021). Topology optimization of buildings subjected to stochastic wind loads. *Probabilistic Engineering Mechanics*, *64*(July 2020), 103127. https://doi.org/10.1016/j.probengmech.2021.103127

Haggag, M., Elruby, A. Y., Ismail, M. K., AbdelAleem, B. H., & El-Dakhakhni, W. (2024). Failure mode and capacity prediction for bolted T-stub connections using ensemble learning. *Journal of Constructional Steel Research*, *212*, 108288. https://doi.org/10.1016/J.JCSR.2023.108288

Hareendran, S. P., & Alipour, A. (2022). Prediction of nonlinear structural response under wind loads using deep learning techniques. *Applied Soft Computing*, *129*, 109424. https://doi.org/10.1016/j.asoc.2022.109424

Kanyilmaz, A., Hoi Dang, V., & Kondratenko, A. (2023). How does conceptual design impact the cost and carbon footprint of structures? *Structures*, *58*(October), 105102. https://doi.org/10.1016/j.istruc.2023.105102

Kareem, A., Kijewski, T., & Tamura, Y. (1999). Mitigation of motions of tall buildings with specific examples of recent applications. *Wind and Structures*, *2*(3), 201–251. https://doi.org/10.12989/was.1999.2.3.201

Kareem, A., Spence, S. S. S., Bernardini, E., Bobby, S., & Wei, D. (2013). Using Computational Fluid Dynamics to Optimize Tall Building Design. *International Journal on Tall Buildings and Urban Habitat*, *CTBUH Journal 2013 Issue III*.

Kelly, D., Poon, D., Irwin, P., & Xie, J. (2012). Wind Engineering of the Shanghai Center Tower. *Advances in Hurricane Engineering*, 426–436. https://doi.org/10.1061/9780784412626.037

Ma, G., Wang, Y., & Hwang, H. J. (2023). Genetic programming-based backbone curve model of reinforced concrete walls. *Engineering Structures*, *283*, 115824. https://doi.org/10.1016/J.ENGSTRUCT.2023.115824

Micheli, L., Alipour, A., & Laflamme, S. (2020). Multiple-Surrogate Models for Probabilistic Performance Assessment of Wind-Excited Tall Buildings under Uncertainties. *ASCE-ASME Journal of Risk and Uncertainty in Engineering Systems, Part A: Civil Engineering*, *6*(4), 1–12. https://doi.org/10.1061/ajrua6.0001091

NBCC. (2020). National Building Code of Canada. In *Government of Canada* (Vol. 1).

Park, S. M., Sharpe, D. C., & Krawczyk, R. J. (2005). Innovative tall building form development. *CTBUH 2005 - 7th World Congress Renewing the Urban Landscape, Proceedings*.

Reidmiller, D., Avery, C., Easterling, D., Kunkel, K., & Lewis, K. (2018). Fourth National Climate Assessment: Report-in-Brief. In *US Global Change Research Program: Vol. II*.

Roser, M., Ritchie, H., & Ortiz-Ospina, E. (2019). *World Population Growth - Our World in Data*. https://ourworldindata.org/world-population-growth

Sigmund, O. (2000). Topology optimization: a tool for the tailoring of structures and materials. *Philosophical Transactions of the Royal Society of London. Series A: Mathematical, Physical and Engineering Sciences*, *358*(1765), 211–227. https://doi.org/10.1098/rsta.2000.0528

Solorzano, G., & Plevris, V. (2023). An Open-Source Framework for Modeling RC Shear Walls Using Deep Neural Networks. *Advances in Civil Engineering*, *2023*. https://doi.org/10.1155/2023/7953869

Spence, S. M. J., & Arunachalam, S. (2022). *Performance-Based Wind Engineering : Background and State of the Art*. *8*(March), 1–11. https://doi.org/10.3389/fbuil.2022.830207

Suksuwan, A., & Spence, S. M. J. J. (2019). Performance-based design optimization of uncertain wind excited systems under system-level loss constraints. *Structural Safety*, *80*(June 2018), 13–31. https://doi.org/10.1016/j.strusafe.2019.03.004

Tamura, T., & Miyagi, T. (1999). The effect of turbulence on aerodynamic forces on a square cylinder with various corner shapes. *Journal of Wind Engineering and Industrial Aerodynamics*, *83*(1–3), 135–145. https://doi.org/10.1016/S0167-6105(99)00067-7

Tanaka, H., Tamura, Y., Ohtake, K., Nakai, M., Chul Kim, Y., Chul, Y., & Chul Kim, Y. (2012). Experimental investigation of aerodynamic forces and wind pressures acting on tall buildings with various unconventional configurations. *Journal of Wind Engineering and Industrial Aerodynamics*, *107–108*, 179–191. https://doi.org/10.1016/j.jweia.2012.04.014

Tseranidis, S., Brown, N. C., & Mueller, C. T. (2016). Data-driven approximation algorithms for rapid performance evaluation and optimization of civil structures. *Automation in Construction*, *72*, 279–293. https://doi.org/10.1016/j.autcon.2016.02.002

WGBC. (2019). *Embodied carbon call to action report | World Green Building Council*. https://www.worldgbc.org/embodied-carbon

Zhang, Y., & Mueller, C. (2017). Shear wall layout optimization for conceptual design of tall buildings. *Engineering Structures*, *140*, 225–240. https://doi.org/10.1016/j.engstruct.2017.02.059

CHAPTER 2

2. ANN-BASED OPTIMIZATION FRAMEWORK FOR THE DESIGN OF WIND LOAD RESISTING SYSTEM OF TALL BUILDINGS

2.1. Introduction

Most of the earlier studies tackled the optimization problem of the elevation layout of the lateral load resisting systems against wind loads, focusing on steel structures. (Baldock et al., 2005) developed a procedure for finding the optimal bracing system layout using a pattern search algorithm. (C. M. Chan & Wong, 2008b) used a hybrid optimization algorithm of optimality criterion and GA to find the optimal bracing system layout of the steel structure in addition to finding the optimal steel structure members that can satisfy both strength and serviceability conditions against wind loads. Moreover, different load cases of wind loads are considered by (H. Lu et al., 2019) to find the optimal bracing system layout for a pre-existing frame structure. Alongside the usage of static loads based on design code regulations, dynamic loads extracted from boundary layer wind tunnels can also be incorporated into the optimization process to find the optimal lateral load resisting layout. The latter approach has been discussed by (Bobby et al., 2014), who developed an approach to find the optimal bracing system layout based on a performance-based design framework on two-dimensional sections of a tall building. The aforementioned studies adopted the "truss problem" concept based on a ground structure, a fully connected truss where all neurons are joined together with bracing elements. A continuous approach using the Solid Isotropic Material with Penalization (SIMP) method can be adopted to find the density of the material within the design domain, similar to the work done by (Luo et al., 2017). They extended the two-dimensional section optimization problem to a three-dimensional problem to find the optimal lateral load resisting system against wind loads extracted from a wind tunnel.

Altering the elevation layout of the lateral load resisting system is not the only way to optimize tall structures against various lateral loads, but also changing the location of these systems within the structure domain can affect the overall structural performance. Few studies focused on plan layout optimization of the structural system, especially reinforced concrete (RC) shear walls, against wind loads. (Y. Zhang & Mueller, 2017) developed an optimization framework based on a modified evolutionary algorithm to find the optimal RC shear wall layout taking into consideration prespecified architectural constraints. The developed framework considered only two load combinations: one for serviceability and another one for ultimate limit state design for dead, live and wind loads. In addition to the architectural constraints like openings, this framework considered serviceability (i.e., drift) and strength constraints (i.e., torsion, shear strength and flexural strength). Although this framework achieved exceptional results and formulations, the non-flexibility of calculating the flexural capacity of formulated shear wall groups and the complexity of replicating the framework on different buildings as it relies only on a Python-based computational system could be enhanced. Accordingly, (Talatahari & Rabiei, 2020) developed a shear wall layout optimization framework with more flexibility in calculating the flexural capacity of the formulated shear wall groups. In 2018, (Behmanesh, 2018) focused on size optimization by using the Monte Carlo approach to find the optimal shear wall thickness, outrigger beams thicknesses and column sizes. (H. P. Lou et al., 2021) developed an optimization framework, based on the Evolutionary Structure Optimization (ESO) algorithm, to find the optimal shear wall layout against multiple load cases of wind and seismic. The objective function was chosen to be the structure's weight, where the algorithm aimed to minimize the weight of the building without violating serviceability constraints according to the Chinese building design code of JGJ 3-2010 (Ministry of Housing and Urban-Rural Development of the People’s Republic of China., 2010).

Nevertheless, this framework provides a more user-friendly algorithm to structural designers compared to previous studies. It is worth noting that this study is considered to be more computationally expensive as every single group of the proposed variable parameter is evaluated using Finite Element Analysis (FEM) directly through ETABS. Moreover, the limit state of each structural component was not considered in that framework. Another framework was provided by (H. Lou et al., 2021a) that solved the time-consuming issue in the aforementioned framework by using a surrogate model based on a Support Vector Machine (SVM). This study adopted a non-changing columns layout, which limited the domain of the shear walls' possible locations. An alternative approach was adopted by (Pizarro & Massone, 2021a), which relied on a deep neural network trained on a database of previously accepted designs to propose a shear wall layout (i.e., thickness and length) for new structure designs. This approach can produce accepted constructible designs, yet these designs are not guaranteed an optimal shear wall layout.

Based on the discussed literature, the current chapter aims to address some of the presented limitations by developing an automated optimization framework for lateral load resisting system (i.e., shear walls) layout of tall buildings against gravity and wind loads based on the (National Building Code of Canada, 2015) and the Canadian Standards Association 2019 (CSA, 2019). The developed framework will first build a surrogate model using Artificial Neural Networks (ANN), which can estimate the structural response of proposed models after being trained by the FEM-generated results using ETABS (CSI, 2018). The usage of the surrogate model will reduce the computational time needed for the optimization process. Then, this model is coupled with a genetic algorithm to identify the optimal layout of shear walls by reducing the number of shear wall segments that will be used within predefined architectural and serviceability constraints (e.g., interstory drift). In this study, a new constraint (i.e., the standard deviation of base bending

moment) is introduced to be used through the automated optimization framework, which will indirectly include the limit state of shear walls. This constraint will efficiently distribute induced base moments over the proposed shear wall segments. Finally, the selection of suitable locations of columns will be adequately chosen based on the generated locations of shear walls, which will result in a more realistic distribution of both columns and shear walls, in addition to maintaining a consistent design of slabs, which is commensurate with the consistency of the spans of the slab. The chapter is organized into five sections. Section 2.1 presents an introduction and literature review on building aerodynamic mitigations. In Section 2.2, a description of the developed SWOF is provided. Section 2.3 presents the optimization application on a case study building, focusing on minimizing the number of shear wall segments used while considering architectural and structural constraints. Section 2.4 presents results, discussions of the optimization problems, and verification for the near-optimal solutions using FEM. Finally, Section 2.5 presents the conclusions and findings of the developed SWOF.

2.2. Structural Wind optimization Framework (SWOF)

The proposed automated Structural Wind Optimization Framework (SWOF) is developed to overcome the numerous trial and error procedures accompanied by the design process of lateral load resisting system (i.e., shear walls) to find the optimal structural system layout. This study will focus on the shear wall layout; however, SWOF is developed generically to incorporate different materials and structural systems. The main purpose of the SWOF proposed in this study is to minimize the total weight of the structural system by reducing the number of used shear wall segments within the predefined layout to enhance the structure's wind performance without violating architectural and serviceability constraints. As shown in Fig. 2-1, a flowchart represents the procedure of structural wind optimization. The procedure starts with defining the optimization

problem, which includes the definition of the objective function (or fitness function) that is responsible for evaluating possible solutions generated by the optimization algorithm, which is minimizing the total weight of the shear walls, and this can be tackled in different forms that will be explained later. The second part that will be defined for the optimization problem is the design variables. For this problem, design variables are the possible location and orientation of the shear walls. Due to architectural requirements. The design variables cannot be located anywhere within the plan boundaries; they are considered constrained (or bounded) binary variables based on a predefined domain. They have been chosen to be binary (0 or 1) to indicate the availability of the shear wall segment, either available (1) or not available (0). This domain went through a preprocessing phase where it got discretized into finite elements (shear wall segments) based on the accuracy required. The architectural preferences are not the only constraints; the design code limits are also included as constraints, in addition to any supplementary parameters required by the designer. In this study, the optimization problem is tackled through a stochastic approach, which is a Genetic Algorithm (GA) due to its complexity. GA relies on numerous evaluations of the objective function by altering design variables systematically using mutation and crossover operators until an optimum value is reached.

The execution of the evaluation function through FEM is computationally costly. Consequently, a surrogate model will be used to estimate the structural response of tall buildings after being trained with a database of Layout alternatives with their corresponding performances. For example, the optimization process of all load cases and all parameters in section 2.4.4 takes 58 minutes and 15 seconds to evaluate 10^4 candidates in each generation for 1745 generations on an Intel ® Core ™ i7-4790 CPU @3.60 GHz, 3601 MHz, 4 cores(s), 8 Logical Processors and 32 GB RAM DDR3 RAM. While building and evaluating one FEM model takes 2 to 4 minutes. The surrogate model

used in the SWOF is an Artificial Neural Network (ANN). In order to build this surrogate model, a group of random training models was prepared using FEM in order to train the ANN for predefined parameters required either for the objective function or the constraint(s) (e.g., Drift in X and Y directions). A detailed explanation of the surrogate model's building process is included in section 2.3.2. After building the surrogate model, it will be used to represent these constraints and objective functions. The optimal solution that resulted from the previously described process will be evaluated and validated through the FEM using ETABS (CSI 2018).

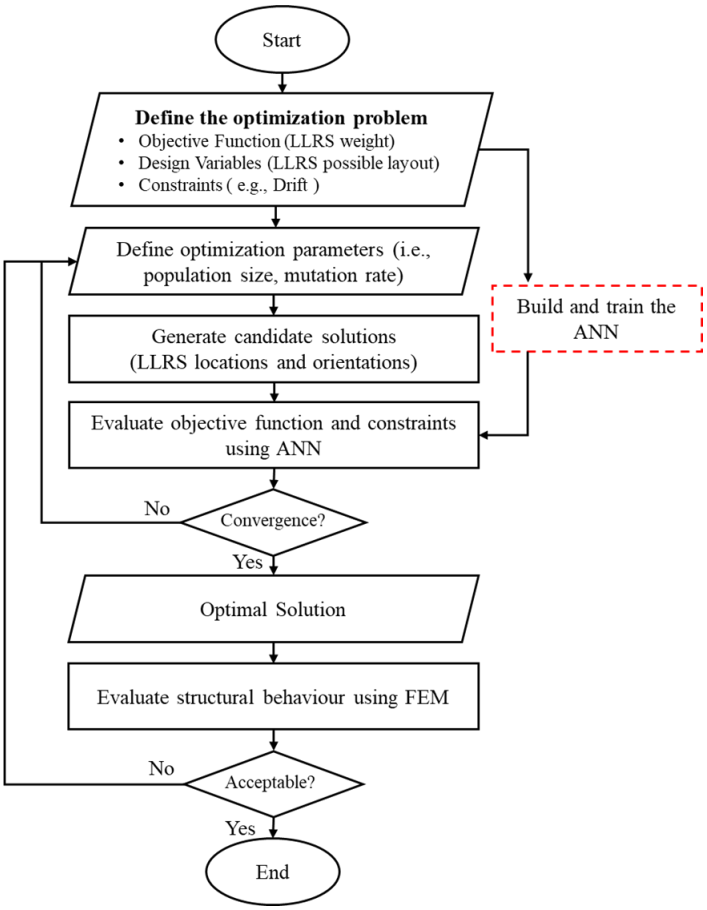

Fig. 2-1 Structure wind optimization framework (SWOF) flowchart

2.3. Optimization problem definition

2.3.1. Structural details of the Case study

In the demonstration problems, a multistory residential building of 20 floors, with a story height of $3.5\,m$, is adopted, which follows the structures described in previous studies (Alanani & Elshaer, 2021; Y. Zhang & Mueller, 2017). A single symmetric layout of rectangular-shaped flat slabs with dimensions of $24.75\,m \times\ 18.75\,m$ is used. It is expected that wind load could be the governing load for medium to high tall buildings if they fall in regions that are of elevated wind loads with a lower seismic hazard (e.g., Atlantic Canada). Moreover, a study by Aly and Abburu 2015 (Aly & Abburu, 2015) found that high-rise buildings could be more critical for similar buildings if they have lower mass and are located in low-risk seismic regions. Therefore, the building has been selected to be of $70\,m$ in height so it can be classified as a dynamically sensitive structure and follow the dynamic analysis procedure based on the NBCC 2015 (*National Building Code of Canada*, 2015). A superimposed dead load of $5\ kN/m^2$ and a live load of $1.9\ kN/m^2$are applied to all slabs. RC columns dimensions and shear wall thicknesses are set to be fixed. Since design of structural elements is dependent on the structural system's layout, which will be identified after the optimization problem, initial values can be used for the main structural elements of altering layout (i.e., column cross-section and shear wall segments). Later on, these values can be changed based on the developed layout. The layout shown in Fig. 2-2 is designed according to the Canadian Standards Association CSA 23.3-14 (CSA, 2019) using concrete of compressive strength fc'=35 MPa and steel reinforcement ASTM992 of grade 50. The ultimate limit state and serviceability limit load combinations are used for designing structural elements. In contrast to previous studies, this optimization framework took into consideration all possible wind load cases based on clause 4.1.7.9. (*National Building Code of Canada*, 2015). Different angles of attacks and load eccentricities are also considered. The selected building is designed to resist a mean-

hourly wind velocity pressure, q, of $0.74\ kPa$, importance factor, Iw, of 1.0, and topographic factor, C_t of 1.0. The terrain is considered open terrain with no topology effect. An architectural layout is proposed for two flats per story, as shown in Fig. 2-3 (a). Based on the proposed architectural layout, possible locations for shear walls are identified to fulfill architectural objectives, as illustrated in Fig. 2-3 (b). A preprocessing stage is implemented to prepare the optimization problem described in detail in the following sections. The dark grey lines in Fig. 2-3 (b) are considered the shear walls domain. To identify the length and shape of shear walls, a discretization of this domain is performed based on a rectangular mesh of a predefined base size of 1.0 meters. As a result, the domain will be divided into 170 segments of shear walls, each of 1.0 meters. For each model, different locations of columns will be identified to avoid overlapping between shear wall segments and columns. Column distribution is based on a rectangular mesh of a $6\ m$ span. This mesh minimizes the changes in the slab's straining actions as vertical supports are located at specific locations, either columns or shear walls in those spaces. Each shear wall segment is $1000\ mm$ in length and $300\ mm$ in thickness, as illustrated in Fig. 2-2 (b). Each floor is supported by a number of columns of $750 \times 750\ mm$ cross-section dimensions and 2.5% steel reinforcement, as shown in Fig. 2-2 (c).

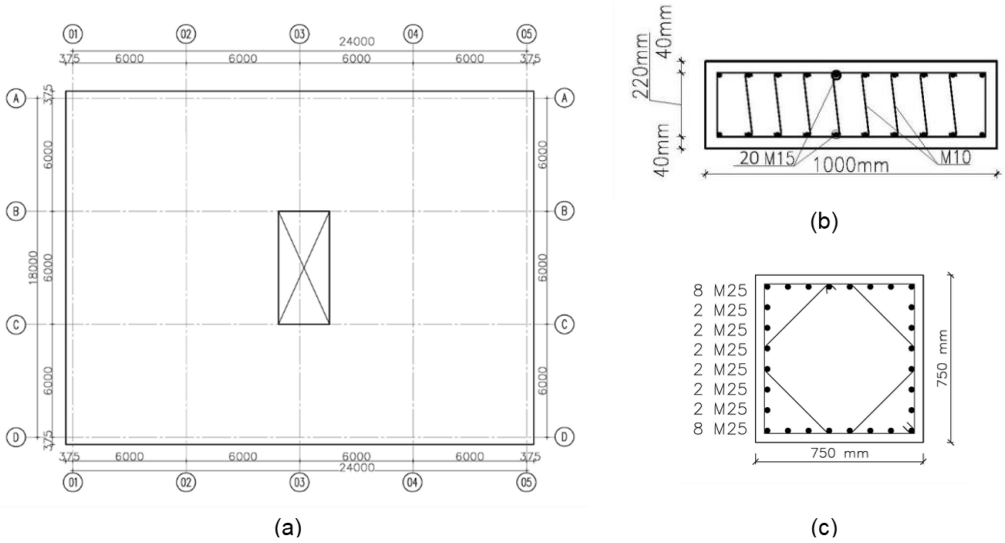

Fig. 2-2 (a) Slab plan layout, (b) shear wall segment and (c) column cross-section

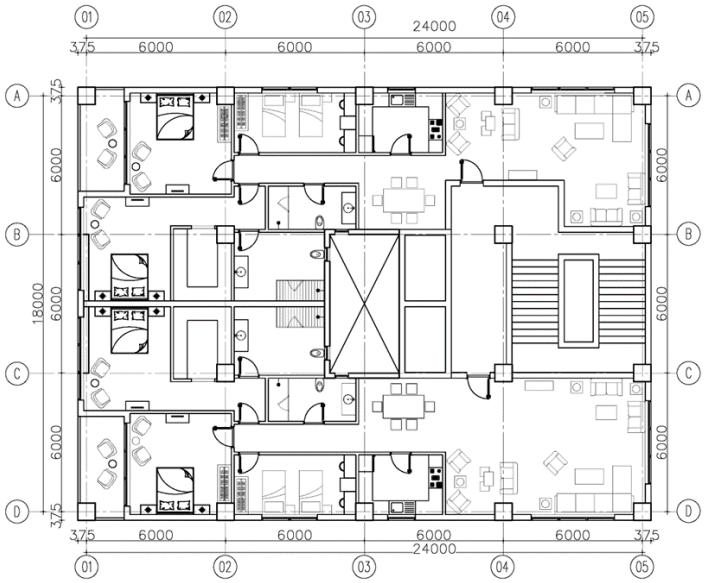

(a)

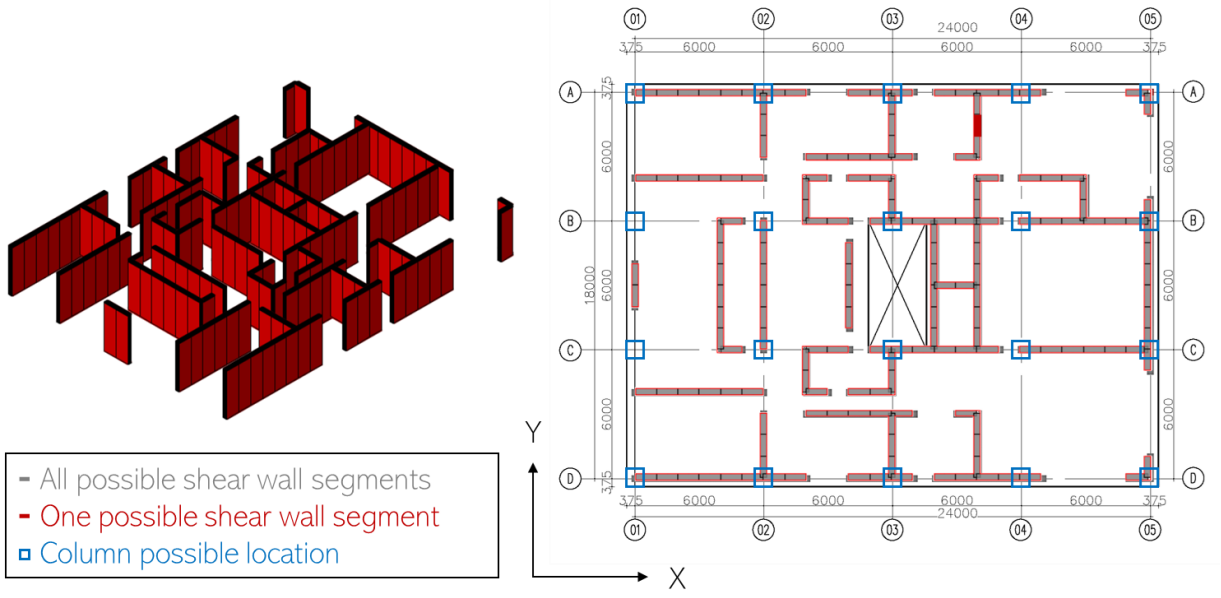

(b)

Fig. 2-3 (a) Architectural plan view and (b) possible shear wall locations

2.3.2. Training procedure of ANN (Surrogate Model)

Most engineering design problems require constructing computationally affordable functions that can be used in optimization (Forrester et al., 2008). It can be defined as an estimation model for computationally complicated and costly simulations. The optimization problem adopted in this study is heuristic-based that requires repetitive evaluation for the objective function, which is computationally expensive. Therefore, surrogate models are built and used to emulate complex functions' responses predefined by the designer. In order to evaluate the objective function through real-time simulation will be very time-consuming and will not be computationally affordable if a more significant number of population or generations for the genetic algorithm is used. Surrogate models have been proven to be a reliable solution to design optimization problems against wind loads (Bernardini, Spence, Wei, et al., 2015; Cid Montoya et al., 2018; Elshaer, Bitsuamlak, & El-Damatty, 2017; Elshaer & Bitsuamlak, 2018; Noormohamadian & Salajegheh, 2021; Qiu et al., 2021). ANN is used in this study as a surrogate model due to its proven efficiency in capturing complex functions (Ahmad et al., 2020; Elshaer & Bitsuamlak, 2018; Jia & Wu, 2021; Kotsovou

et al., 2020; Lagaros & Plevris, 2022; Nguyen et al., 2021; Papadrakakis & Lagaros, 2002; Pizarro & Massone, 2021a). ANN is a regression model that consists of inputs, hidden layers and outputs. The quality of the neural network outputs (i.e., objective function and constraints) relies on the training process effectiveness through various training sample models that can cover most of the search space required in the optimization problem. As shown in Fig. 2-4, building the adopted surrogate model starts by generating a random sample of training models. A total of 2000 samples of random configurations of shear wall segments are prepared using MATLAB code that automates the process of building models and extracting results on ETABS through the Open Application Programming Interface (OAPI). This code also generates columns' locations based on the predefined locations and avoids any overriding or intersections with the generated shear walls. This prepared Finite Element Models (FEM) database will be used to train ANN models to act as objective and constraint functions, as shown in the upcoming paragraphs.

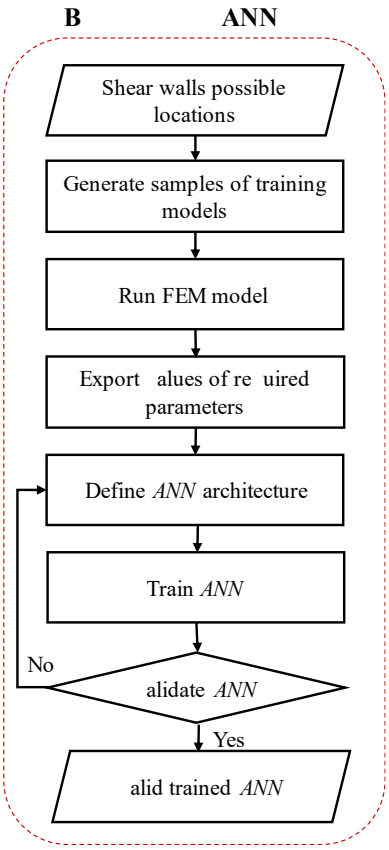

Fig. 2-4 Surrogate model building flowchart

A forward-propagation neural network is used to determine the output of a group of functions as follows: the critical inter-story drift in both X and Y directions, the distance between the center of mass (C_M), the center of rigidity (C_R), the standard deviation of shear walls' base moments (σ_M), the total number of piers (N_P), and groups of shear walls acting as one unit (i.e., piers). Bayesian regularization backpropagation algorithm was adopted to update the weight and bias values according to Levenberg-Marquardt optimization. It minimizes a combination of squared errors and weights, and then determines the correct combination to produce a generalized network. A more detailed explanation of each function and how their ANN models are built is presented in sections 2.3.2.1, 2.3.2.2, 2.3.2.3 and 2.3.2.4. These outputs are based on an input of shear wall locations. As shown in Fig. 2-5, the input layer is one layer of size equal to 170 neurons that accept binary values (i.e., 0 "absent" or 1 "exist"), while the output layer size is one neuron representing the constraint value required. In the input layer, these neurons represent possible locations of shear

wall segments. Each shear wall segment, S_i, is assigned an order value i from 1 to 170. The ANN input nodes order is based on the sequencing that took place by preparing the FEM training database used to build the ANN. The number of hidden layers and their sizes are identified separately based on the complexity of each function. Firstly, the training sample size is defined; it is a crucial parameter affecting the regression coefficient, the generalization of the ANN and ANN training duration. Thus, for quality check, a sensitivity analysis is carried out on a sample size of range [100:2000] of 100 samples increment as shown in Fig. 2-6. The regression coefficient, R, indicates the proportionate amount of variation in the response variable, $y_{predicted}$, by the actual values, y_{actual}, as shown in equation (2-1), where SSR is the sum of squared residuals and SST is the total of sum of squared . For instance, this figure shows the sensitivity analysis of the σ_M ANN as it is found to be the most complex. It can be noticed that with the increase in sample size, the regression coefficient of the ANN increases almost by 25% from 100 samples to 1000 samples. Then, a plateau can be noticed with a slight fluctuation that could be explained as a result of the generalization of the ANN. The more samples introduced to the ANN training, the harder it can be generalized. However, the final regression coefficient that could be reached for this ANN is 0.97, which is a sufficient representation of a complex function like the (σ_M). For each ANN, different training-to-test ratios have been used based on the complexity of the parameters. For instance, the interstorey drift ANN is trained using 1400 samples, representing 70% of the 2000 samples, and 600 samples are used for testing. While for eccentricity, $e_{C_M C_R}$, and standard deviation of base moments, σ_M, the training-to-testing ratio increased to be 80% : 20%.

$$
\begin{aligned}
&R = \sqrt{1 - \frac{SSR}{SST}}, \\
&SSR = \sum_{i=1}^{n} \left(y_{predicted,i} - y_{actual,i} \right)^2, \\
&SST = \sum_{i=1}^{n} \left(y_{actual,i} - mean(y_{actual}) \right)^2
\end{aligned}
\tag{2-1}
$$

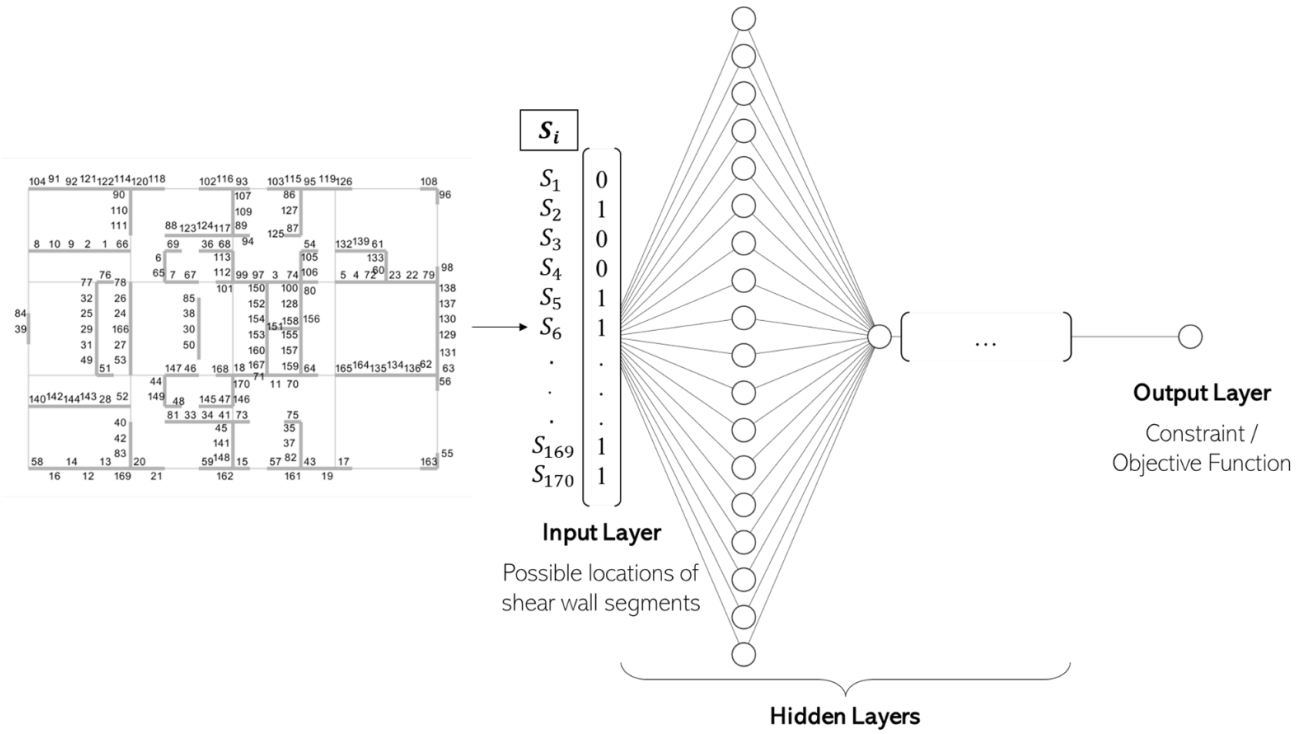

Fig. 2-5 Schematic diagram for general ANN architecture

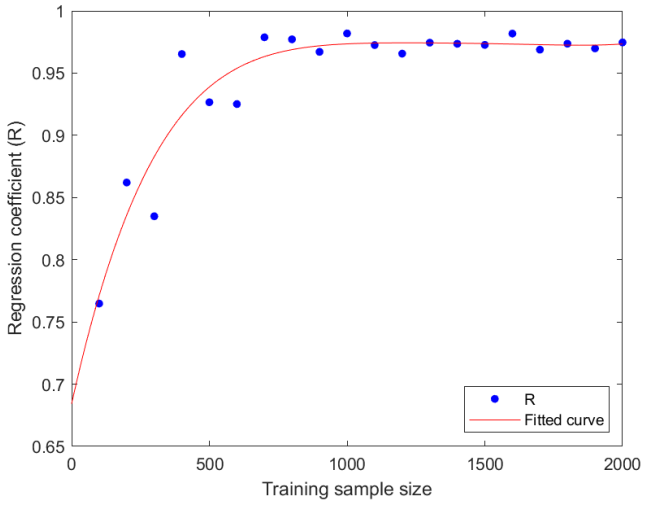

Fig. 2-6 Change of regression coefficient with the training sample (training of the σ_M)

2.3.2.1.Interstory drift

Based on article 4.1.3.5. in the (*National Building Code of Canada*, 2015), the total drift per storey under service wind and gravity loads shall not exceed 1/500 of the storey height. So, interstory drift constraints in both X (δ_x) and Y (δ_y) directions should be less than or equal to 0.2%. ANN

architecture building process is a trial-and-error procedure that does not follow a specific technique that will work for all problems. So, in this study, we relied on an exhaustive search algorithm to build the architecture of each constraint function. Through this algorithm, we start systematically investigating the number of hidden layers, the number of neurons for each hidden layer, the transfer function responsible for adjusting the weights and the training algorithm. The Drift function turns out to be a simple one. Only two hidden layers are sufficient for a correlation regression coefficient (R) of 0.99.

Regarding the size of the hidden layers, the second hidden layer is recommended to be of weight equal to the output layer, which is one neuron. For the first hidden layer, sensitivity analysis is done for testing a various numbers of neurons from 10 to 50 neurons, as shown in Fig. 2-7. It is found that 18 neurons with a hyperbolic tangent sigmoid transfer function that transfers inputs into values belonging to [-1, 1], for both hidden layers achieved 0.993 correlation regression coefficient. After using 70% of the samples in training and 30% in testing and validation, the correlation coefficient between the FEM database and the ANN model is 0.99 for δ_y while 0.98 for δ_x, as shown in Fig. 2-8. In addition, An error histogram is presented in Fig. 2-9 to show how the error % is distributed in the whole testing samples, as shown in equation (2-2). It was noted that 95% of the samples produced an error of less than 4%, which reflects the accuracy of the ANN surrogate model in mapping complex relations between inputs and outputs.

$$error\ \% = \frac{ANN\ ouptut - FEM\ values}{FEM\ values} \times 100 \tag{2-2}$$

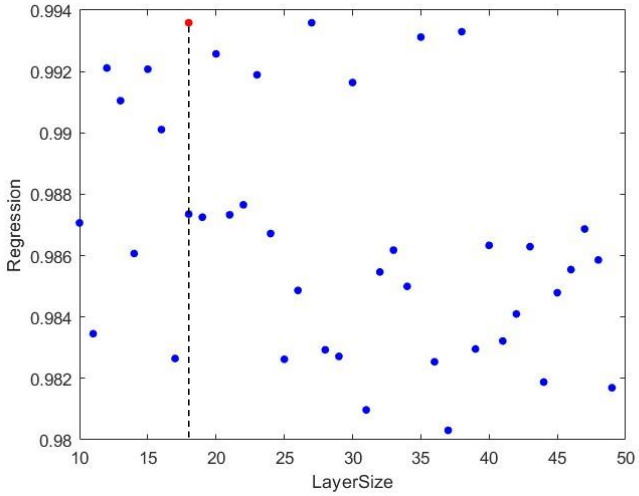

Fig. 2-7 Sensitivity analysis for the interstorey drift ANN hidden layer size

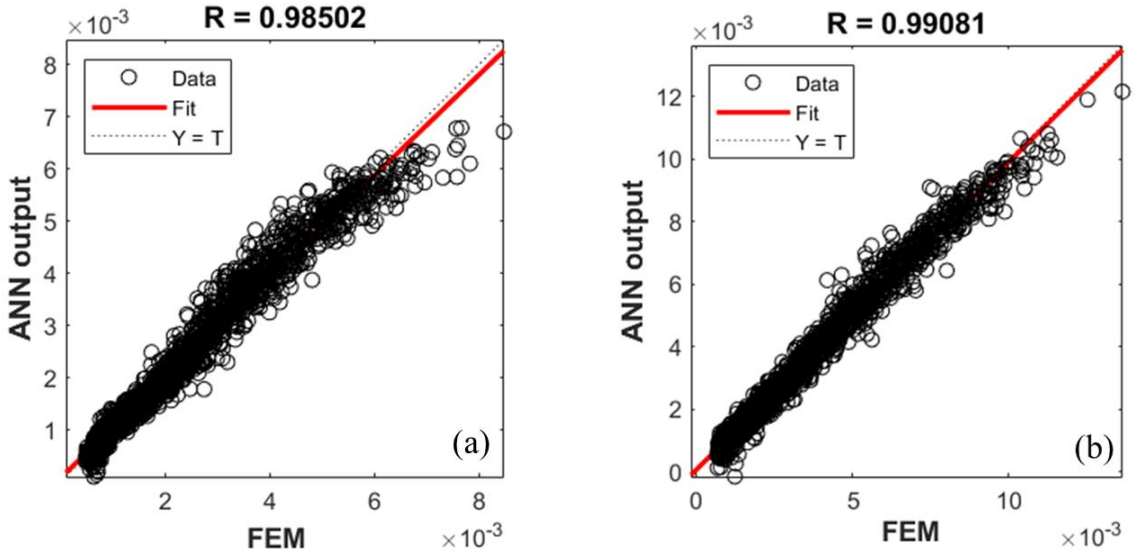

Fig. 2-8 Regression coefficient for intersorey drift ANN in (a) Y-direction and (b) X-direction

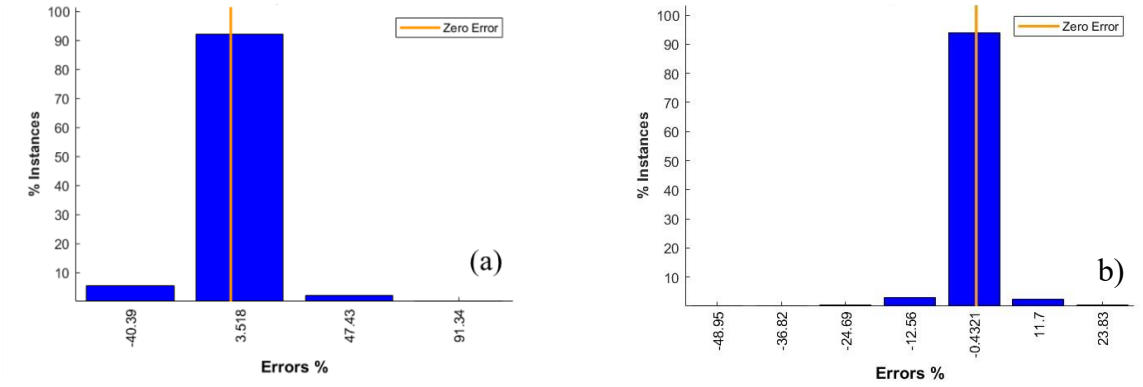

Fig. 2-9 Error Histogram for interstorey drift ANN in (a) Y-direction and (b) X-direction

2.3.2.2.Torsional effect (eccentricity)

Tall buildings are sensitive to torsional moments, and failure due to torsion can be considered one of the severest failures that should be avoided through the design process. Many reasons might cause torsional moment (e.g., layout irregularity, unequal mass distribution, openings in the floor slabs). In this case study, the distance between the center of mass (C_M) and center of rigidity (C_R) is adopted as an indication of structure torsion, and it is noted as eccentricity ($e_{C_M C_R}$), and it is calculated using equation (2-3). The NBCC indicated the accidental eccentricity ratio included in the wind load cases of 0.15, a ratio of the distance between C_M and C_R and the wind exposure depth. Consequently, ($e_{C_M C_R}$) limit is typically assigned by the designer. In the current study, $1000\ mm$ is set as the maximum allowed value used to assure minimum eccentricity between the applied lateral load and center of mass. The trained sample values range between 0.1 and 7 m, covering a large portion of the problem's search space. The adopted exhaustive search algorithm led to three hidden layers of sizes 23, 44 and 1, respectively. After using 80% of the samples in training and 20% in testing and validation, the correlation coefficient between the FEM database and the ANN model is 0.95 for $e_{C_M C_R}$. Also, 98.85% of the samples produced an error of less than 6%.

$$e_{C_M C_R} = \sqrt{\left(X_{C_R} - X_{C_M}\right)^2 + \left(Y_{C_R} - Y_{C_M}\right)^2} \tag{2-3}$$

2.3.2.3.The standard deviation of shear walls base moments (σ_M)

Through previous studies, the flexural capacity of shear walls was either predefined or missing due to the computational complexity of calculating the shear wall capacity for each candidate. In the current study, an indirect methodology is adopted to control the distribution of bending

moments on the resulting shear wall segments. The standard deviation of the base moment per shear wall segment is used as a constraint in this study. It was found in previous studies (Alanani & Elshaer, 2021) that the lower the standard deviation, the more consistent the distribution of moments on the segments and the less variation in the required reinforcement ratios. Lowering the standard deviation, σ_M, will either lump shear wall segments or disperse segments. It will also reduce the possible exceedance of the demand-to-capacity ratio for the used segments with their predefined reinforcement ratio. It is calculated by Equation (2-4), where x_i is the value of the critical base moment of segment i. μ_M is the mean critical moment of all segments. $\Sigma\, S_i$ is the total number of shear wall segments used in this layout. Same exhaustive search algorithm is used to find the ANN architecture. Due to the complexity of calculating the standard deviation of moments, four hidden layers are required to build its ANN with sizes of 20, 15, 7 and 1, respectively. The ANN-based constraint function evaluation error does not exceed 3.26% in 95.7% of the samples used. The regression coefficient between the ANN predicted objective function and the FEM database is found to be 0.9702.

$$\sigma_M = \sqrt{\frac{\Sigma\,(x_i - \mu_M)^2}{\Sigma\, S_i}} \tag{2-4}$$

2.3.2.4.Number of grouped segments (piers) (N_P)

The constructability of generated shear wall segments is an essential factor to be taken into consideration. Several factors can impact their constructability, including materials and equipment availability, wall layout and design, foundation design, coordination with other trades, construction sequencing, and quality control and safety measures. The lateral surface area of shear walls, which is part of the layout and design, can also impact constructability, as in some cases where the lateral load-resisting system is distributed throughout the building and not concentrated in a specific area,

increasing the number of lumped shear walls can reduce the overall lateral surface area and increase stiffness at the same time. It depends on the possible layouts generated from SWOF that can satisfy the objective function and serviceability limitations but may or may not be an economical solution for construction. The addition of constructability as a constraint or an objective function can be done in different forms. In some cases where the lateral load-resisting system is distributed throughout the building and not concentrated in a specific area, increasing the number of lumped shear walls can reduce the overall lateral surface area and increase stiffness at the same time. In this chapter, the focus will be on the number of piers formulated N_P, where piers are a group of shear wall segments lumped together. In order to force the standard deviation constraint to lump shear wall segments instead of dispersing them, N_P can be defined as a constraint or as a minimization objective function. Defining N_P as an objective function is expected to be more computationally economic than being a constraint, as it was found that the number of shear wall segments is directly proportional to the number of piers. Minimizing the number of piers may also reduce the number of shear wall segments, which will be presented in section 2.4.4. For this parameter, a function was developed to calculate the total number of formulated piers to avoid building a FEM database and increase the number of training samples that can cover a broader range of the search space. The training sample of formulated piers ranges from 10 to 55 piers of 3000 samples. Three hidden layers of ANN of sizes 19, 25, and 1 yielded a 0.997 regression coefficient, and 94% of total samples produced an error of less than 1.

2.4. Optimization problems description and results

This section explains four different optimization problems, discussing the effect of assigning different constraint(s) and objective function(s). The results of each optimization problem will be presented and discussed within each sub-section. A summary of the proposed optimization

problems is presented in Table 2-1. Additional constraints will be added to different optimization problems to show the effect of introducing various constraints. Finally, all constraints will be assigned in one optimization problem (Problem-4). It is worth noting that for Problem-2 and Problem-3, it is not possible to define $e_{C_M C_R}$ and σ_M separately within the optimization problem as they will yield a zero number of shear wall segments. As a result, these constraints are coupled with the drift constraints to avoid these undesirable solutions.

Table 2-1 Optimization problems matrix for objective function and constraints

Optimization Problem ID	Objective Function	Constraints (C_{Total})			
		δ_y	δ_x	$e_{C_M C_R}$	σ_M
Problem-1-1	$\sum_{i=1}^{N} S_i$	✓	×	×	×
Problem-1-2		×	✓	×	×
Problem-1-3		✓	✓	×	×
Problem-2		✓	✓	✓	×
Problem-3		✓	✓	×	✓
Problem-4	N_P	✓	✓	✓	✓

Where S_i is a set of design variables of the optimization problems that represent each shear wall segment. C_{Total} Indicate all constraints for each optimization problem. While δ_y and δ_x denote the maximum interstorey drift in the Y-direction and X-direction, respectively. $e_{C_M C_R}$ is the eccentricity of the center of rigidity C_R from the center of mass C_M. σ_M represents the standard deviation of shear walls base moments while N_P represents a number of formulated piers.

2.4.1. Optimization Problem-1 (Drift constraints)

This sub-section will include three optimization sub-problems based on the adopted constraint(s). The first constraint that is induced in the optimization problem is drift. First, drift in the Y-direction only (Problem-1-1) is used to check the framework's efficiency in understanding the building's behaviour and the wind load's direction. Then, drift in the X-direction is applied (Problem-1-2). Finally, both drift constraints are used (Problem-1-3), as presented in Table 2-2.

Table 2-2 GA parameters of the optimization Problem-1

Optimization Problem ID	Population size	Number of generations	Mutation function	Crossover ratio	Constraints (C_{Total})			
					δ_y	δ_x	$e_{C_M C_R}$	σ_M
Problem-1-1	4000	1800	"Mutationpower"	0.8	0.2%	×	×	×
Problem-1-2	4000	2000	"Mutationpower"	0.8	×	0.2%	×	×
Problem-1-3	500	1400	"Mutationpower"	0.8	0.2%	0.2%	×	×

2.4.1.1.Optimization Problem-1-1 (Drift in Y-direction)

Equation (2-5) defines optimization Problem-1-1, where S is a set of all design variables that represent the shear wall segments layout. While all variables are subjected to total constraints indicated as C_{Total} stating that δ_y should not exceed 0.2% based on the NBCC 2015 (*National Building Code of Canada*, 2015). SWOF produced an optimal shear wall layout against drift in the Y-direction constraint, as shown in Fig. 2-10. It can be noticed that almost 80% of the generated shear wall segments are oriented towards the Y-direction. This shows how the SWOF is capable of recognizing the inertia concept without explicitly defining it through the developed code. N is the total number of shear wall segments resulting from the discretization process. As shown in Fig. 2-11 (a), the population size of 4000 converges to the most optimal number of shear wall segments, which is 50, based on GA parameters defined in Table 2-2. As discussed before, at the verification stage, the results of the optimal layout are compared to verify the structural behaviour improvement achieved throughout the SWOF, as presented in Table 2-3. 17.5% is the maximum error achieved for the interstorey drift. The main reason for this error is the absence of the constraint for the drift in the X-direction, which can not be found in a real design scenario. It is also the reason for the drift limitation violation in the X-direction, as presented in Fig. 2-11 (b).

$$find\ S = (S_1, S_2, S_3, \dots, S_N)$$
$$minimize \sum_{i=1}^{N} S_i \qquad (2\text{-}5)$$
$$Subjected\ to: C_{Total} = \delta_y \leq 0.2\%$$
$$Where\ S_i \in \{0,1\}\ (i = 1,2,\dots,N), N = 170$$

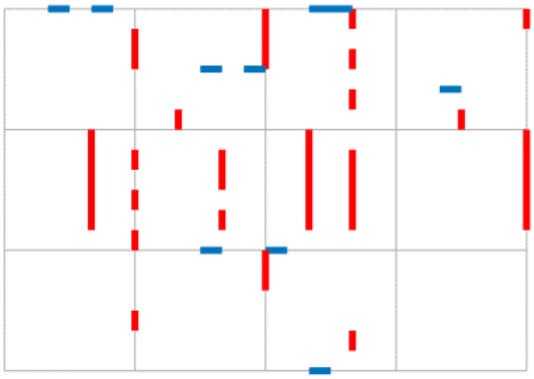

Fig. 2-10 Optimal shear wall layout of optimization Problem-1-1

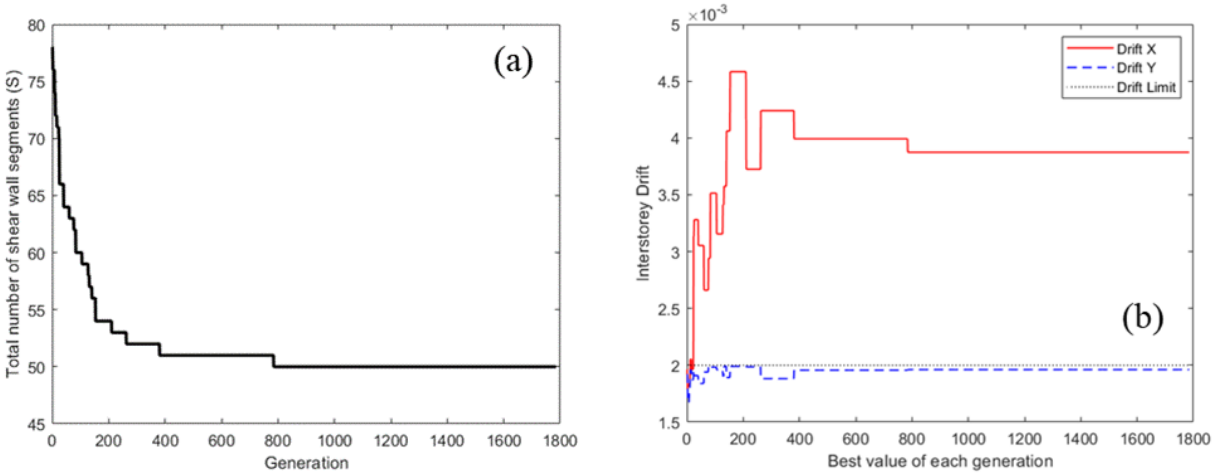

Fig. 2-11 (a) Interstorey drift of optimization Problem-1-1 (b) Interstorey drift of optimization Problem-1-1

Table 2-3 Validation results of optimization Problem-1

Constraint	ANN	FEM	Error%
Drift Y	0.00198	0.0024	17.5%
Drift X	0.0039	0.0049	20%

2.4.1.2.Optimization Problem-1-2 (Drift in X-direction)

When assigning the drift constraint to only the X-direction, as shown in equation (2-6), the SWOF is now able to understand that the priority is to resist loads from the X-direction, as shown in Fig. 2-12. The fitness curve in Fig. 2-13 (a) shows that SWOF converged to 48 shear wall segments, with 78% of the segments being oriented towards the X-direction. Due to the absence of a constraint on the Y-direction, the violation of the drift limit occurred in the δ_y as shown in Fig. 2-13 (b), which is in contract to the results of Problem-1-1.

$$
\begin{aligned}
&find\ S = (S_1, S_2, S_3, \dots, S_N) \\
&minimize \sum_{i=1}^{N} S_i \\
&Subjected\ to: C_{Total} = \delta_x \leq 0.2\% \\
&Where\ S_i \in \{0,1\}\ (i = 1,2, \dots, N\ ), N = 170
\end{aligned}
\tag{2-6}
$$

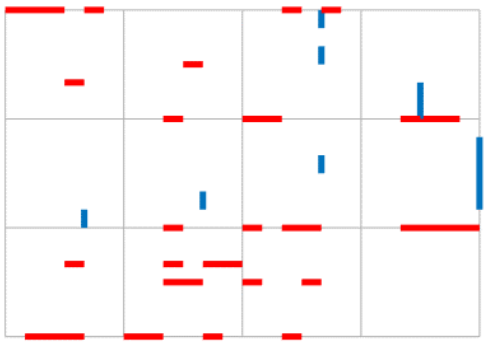

Fig. 2-12 Optimal shear wall layout of optimization Problem-1-2

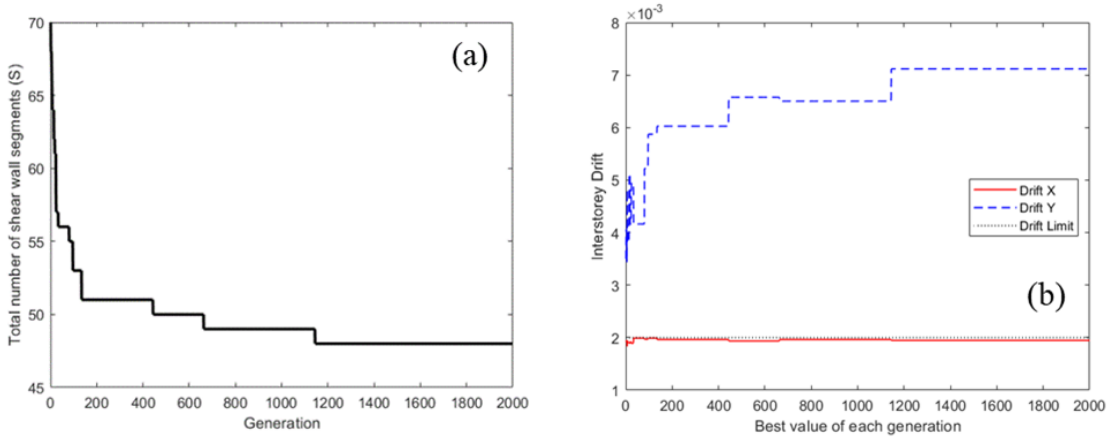

Fig. 2-13 (a) Fitness curve for the total number of shear wall segments of optimization Problem-1-2, (b) Interstorey drift of optimization Problem-1-2

2.4.1.3.Optimization Problem-1-3 (Drift in Y and X-directions)

Based on the previous two optimization sub-problems, SWOF showed efficiency in capturing the target behaviour and achieving the required output. For forming a more reasonable optimization problem, the drift limitation constraint is defined for both δ_y and δ_x as shown in equation (2-7). Four different sizes of the initial population are chosen to check the adequate population sample, as shown in Fig. 2-14 (a). It can be noticed that the increase in the population size requires more time to converge to an optimal solution. The reason behind that is multiple possible optimal solutions that can satisfy the drift constraints (i.e., multiple global minima). Consequently, more constraints are defined in the following sections: 2.4.2 to 2.4.4. Also, it can be concluded that a population size of 500 is computationally affordable and sufficient to converge to the most optimal configuration of shear wall segments to get the least number of shear wall segments, which were found to be segments without violating the defined constraints as shown Fig. 2-14 (b), with drift values of 0.19% and 0.17% in X and Y, respectively. SWOF is able to find a combination of shear wall segments that is slightly higher in number but with higher stiffness that can resist load from both directions. Yet, SWOF is sensitive enough to form shear 57 wall piers with inertia relative to the magnitude of the load subjected to it, as shown in Fig. 2-15. As a result, 53% of shear wall segments are oriented towards the Y-direction of the bigger width that can capture more wind loads.

$$
\begin{aligned}
&find\ S = (S_1, S_2, S_3, \dots, S_N) \\
&minimize \sum_{i=1}^{N} S_i \\
&Subjected\ to: C_{Total} = (\delta_y \leq 0.2\%, \delta_x \leq 0.2\%) \\
&Where\ S_i \in \{0,1\}\ (i = 1,2, \dots, N), N = 170
\end{aligned}
\tag{2-7}
$$

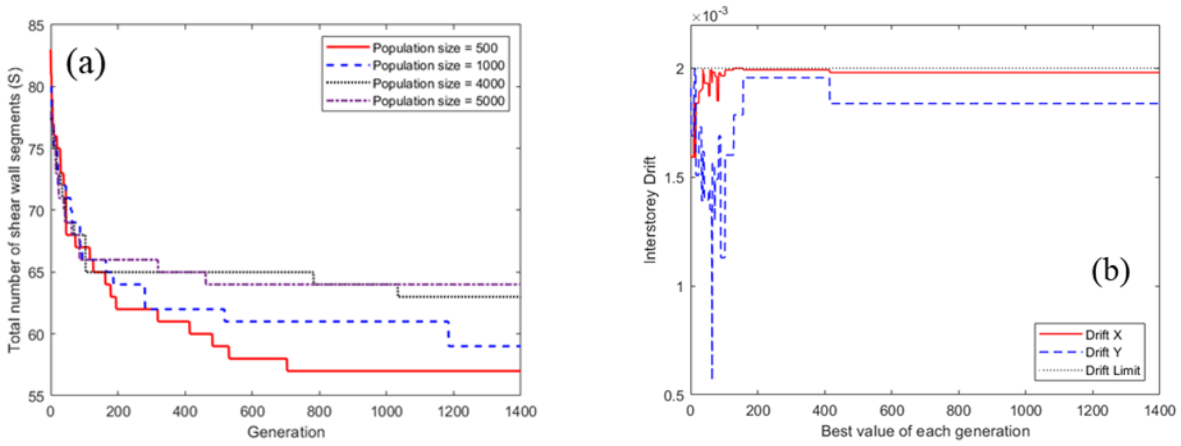

Fig. 2-14 (a) Various population size fitness curves of optimization Problem-1-3, (b) Interstorey drift of optimization Problem-1-3

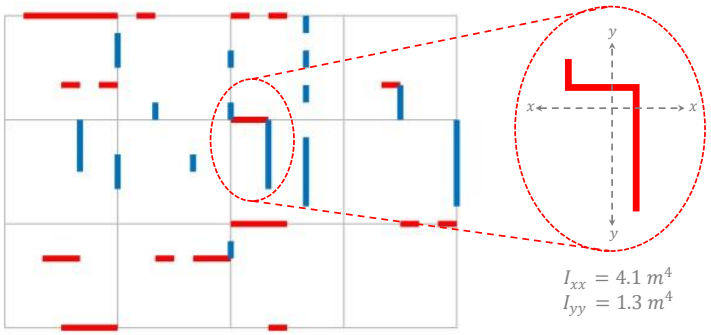

Fig. 2-15 Optimal shear wall layout optimization Problem-1-3

2.4.2. Optimization problem 2 (Eccentricity constraint)

As presented in section 2.4.1, the SWOF outputs with drift constraints are randomly scattered shear wall segments that might induce torsional loads on shear walls due to the eccentricity of the applied lateral load. Accordingly, the SWOF will aim to limit the torsional effect using eccentricity constraint in this section. Equation (2-8) shows how the eccentricity constraint is added to the drift constraints with a distance limitation of 0.5 m between C_M and C_R. Since there is no limitation value mentioned in NBCC for eccentricity, a ratio of the distance between C_M and C_R and the wind exposure depth, this value can be determined by the designer based on the project requirement. Using GA parameters mentioned in Table 2-4, SWOF converged to 68 shear wall segments based on the fitness curve in Fig. 2-16 (a). The number of shear wall segments resulting is higher

compared to the optimization Problem-1 as SWOF added more segments in order to satisfy the constraint limits provided as presented in Fig. 2-17. It yielded a balanced distribution of shear wall segments, as shown in Fig. 2-16 (b). In Table 2-5, the FEM validation for the resulting layout shows how efficient the SWOF and the surrogate models to capture the behaviour of the building with an acceptable error.

$$
\begin{aligned}
&find\ S = (S_1, S_2, S_3, \dots, S_N) \\
&minimize \sum_{i=1}^{N} S_i \\
&Subjected\ to: C_{Total} = \left(\delta_y \leq 0.2\%, \delta_x \leq 0.2\%, e_{C_M C_R} \leq 0.5\ m \right) \\
&Where\ S_i \in \{0,1\}\ (i = 1,2, \dots, N\ ), N = 170
\end{aligned}
\tag{2-8}
$$

Table 2-4 GA parameters of optimization Problem-2

Population size	Number of generations	Mutation function	Crossover ratio	Constraints (C_{Total})		
				δ_y	δ_x	$e_{C_M C_R}$
1000	2000	"Mutationpower"	0.8	0.2%	0.2%	0.5 m

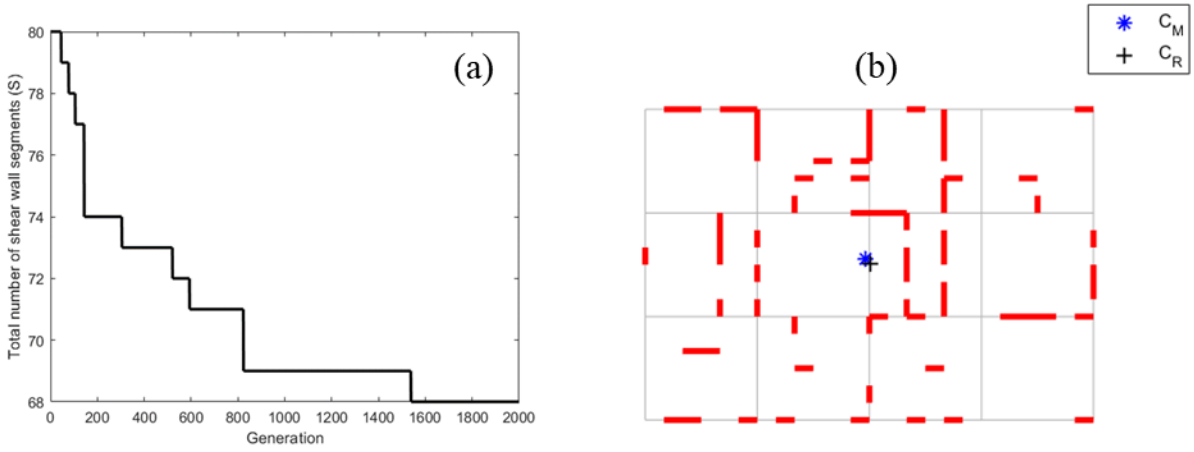

Fig. 2-16 (a) Fitness curve for the total number of shear wall segments of optimization Problem-2, (b) Optimal shear wall layout of optimization Problem-2

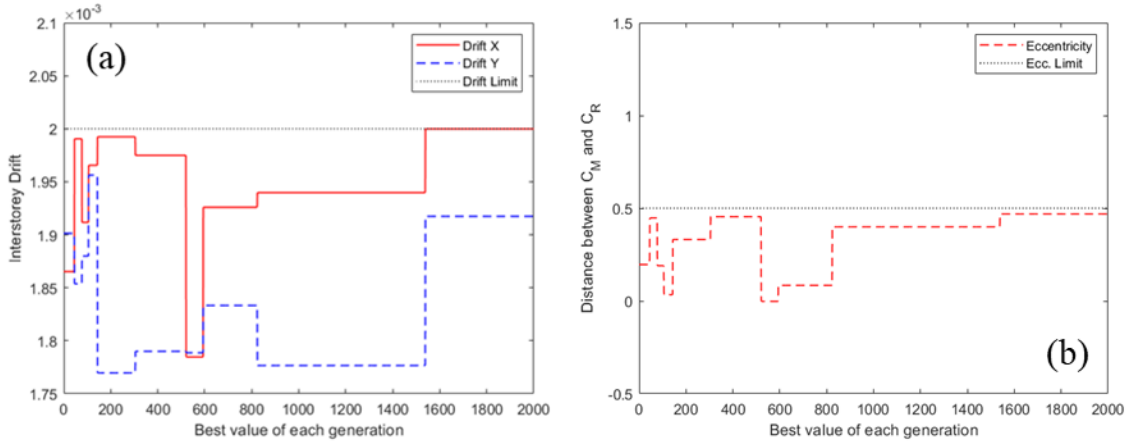

Fig. 2-17 (a) Interstorey drift, and (b) distance between the center of mass and center of rigidity of the best fitness candidate in each generation of optimization Problem-2

Table 2-5 Validation results of optimization Problem-2

Constraint	ANN	FEM	Error%
Drift Y ($\boldsymbol{\delta_y}$)	0.002	0.002	0%
Drift X ($\boldsymbol{\delta_x}$)	0.00192	0.00196	2%
Eccentricity ($\boldsymbol{e_{C_M C_R}}$)	0.46 m	0.39 m	-15.27%

2.4.3. Optimization problem 3 (Base moment standard deviation constraint)

With the increase in the number of shear wall segments resulting from SWOF in optimization Problem-2, a noticeable range of different pier stiffnesses is formed. As a result, the induced base moments on each pier will vary significantly. This might require various groups of reinforcement rebars that will result in a non-economic design. So, the standard deviation constraint for base moments is introduced in equations (2-9). This constraint, as explained in section 2.3.2, represents the amount of variation in the base moments. Similar to the $e_{C_M C_R}$ constraint, the value can vary from project to another based on the designer's targets. In this problem, SWOF con e rged to 68 shear wall segments, as presented in Fig. 2-18 (a), using GA parameters mentioned in Table 2-6. By lowering the limit, as shown in equation (2-9), to $100\ t.m$, SWOF will try to either lumb shear

wall segments or to create more dispersed segments. It also pushed the drift in Y and X-directions to their limits to satisfy the standard deviation constraint σ_M as shown in Fig. 2-19. As shown in the resulting output in Fig. 2-18 (b), around 65% of shear wall segments are lumped into 16 piers. The built surrogate model mainly derives SWOF towards a specific trend based on the constraint value; however, the accuracy of SWOF in this section is not the goal. Through the validation, as shown in Table 2-7, SWOF shows acceptable performance with high accuracy in drift values compared to the standard deviation values due to the complexity of the standard deviation constraints and the multiple load cases that this surrogate model represents. In addition, this constraint plays a vital role in reducing the induced base moments, as shown in Fig. 2-20. The optimal solution layout, which consists of 68 shear wall segments, has yielded a maximum moment per segment of 235 t.m, as shown in Fig. 2-21. Meanwhile, the other layout alternatives (i.e., Non-optimal 1 and Non-optimal 2) produced a maximum moment per segment of 800 and 1200, respectively. However, the non-optimal solutions have a lower number of segments, but the value of generated moments will increase the cost of the structure as more reinforcement is required.

$$
\begin{aligned}
&find\ S = (S_1, S_2, S_3, \dots, S_N) \\
&minimize \sum_{i=1}^{N} S_i \\
&Subjected\ to: C_{Total} = \left(\delta_y \le 0.2\%, \delta_x \le 0.2\%, \sigma_M \le 100 \right) \\
&Where\ S_i \in \{0,1\}\ (i = 1,2, \dots, N\ ), N = 170
\end{aligned}
\tag{2-9}
$$

Table 2-6 GA parameters of optimization Problem-3

Population size	Number of generations	Mutation function	Crossover ratio	Constraints (C_{Total})			
				δ_y	δ_x	$e_{C_M C_R}$	σ_M
1000	1800	"Mutationpower"	0.8	0.2%	0.2%	×	100 t.m

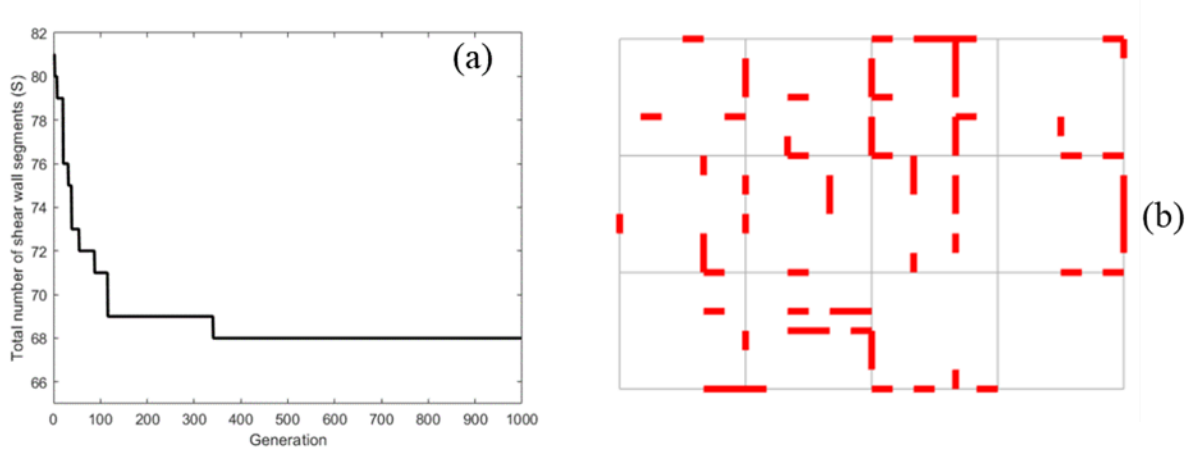

Fig. 2-18 (a) Fitness curve for the total number of shear wall segments of optimization Problem-3, and (b) optimal shear wall layout of optimization Problem-3

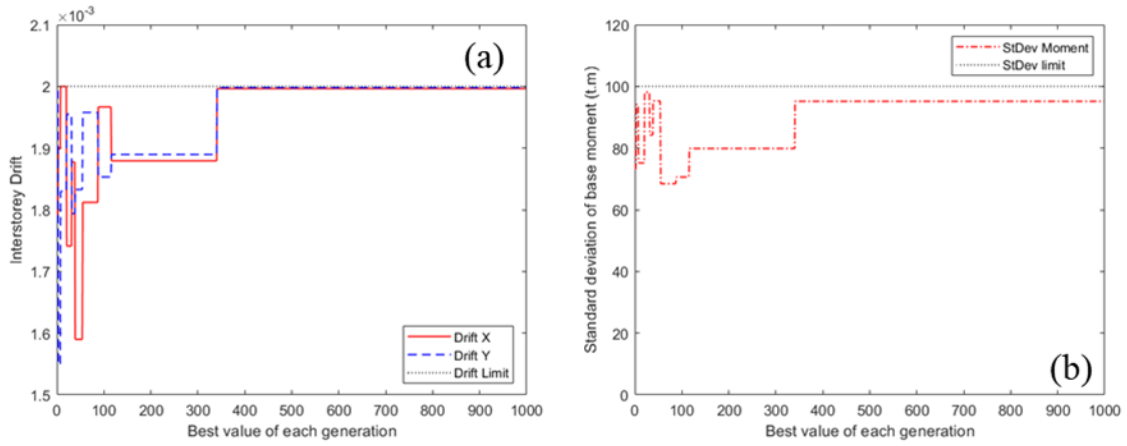

Fig. 2-19 (a) Interstorey drift, and (b) standard deviation of base moments of optimization Problem-3

Table 2-7 Validation results of optimization Problem-3

Constraint	ANN	FEM	Error%
Drift Y ($\boldsymbol{\delta_y}$)	0.002	0.0021	5%
Drift X ($\boldsymbol{\delta_x}$)	0.002	0.0022	10%
Standard deviation ($\boldsymbol{\sigma_M}$)	92.18 t.m	69.79 t.m	-24%

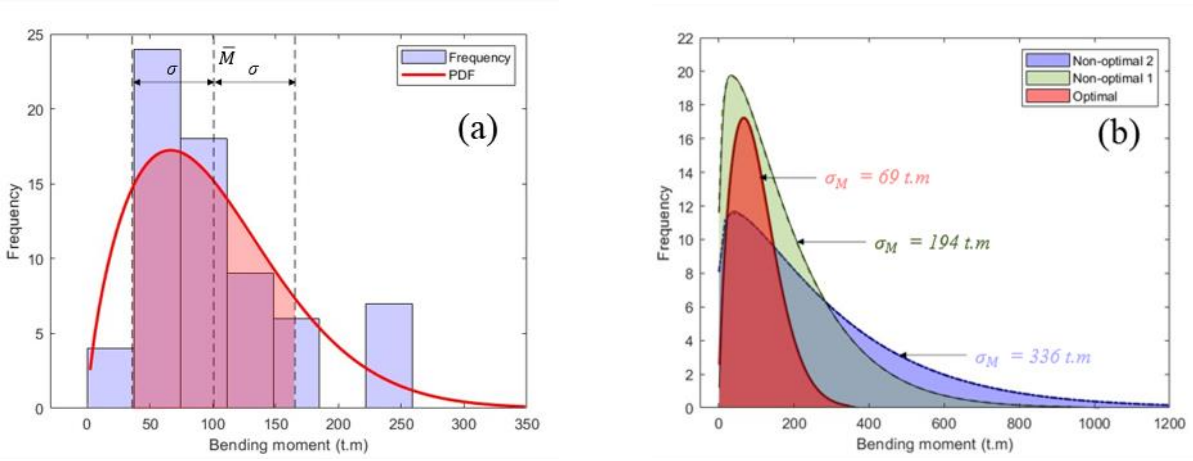

Fig. 2-20 (a) Histogram for base maximum bending moment of optimization Problem-3, and (b) probability distribution function for three different generated layouts

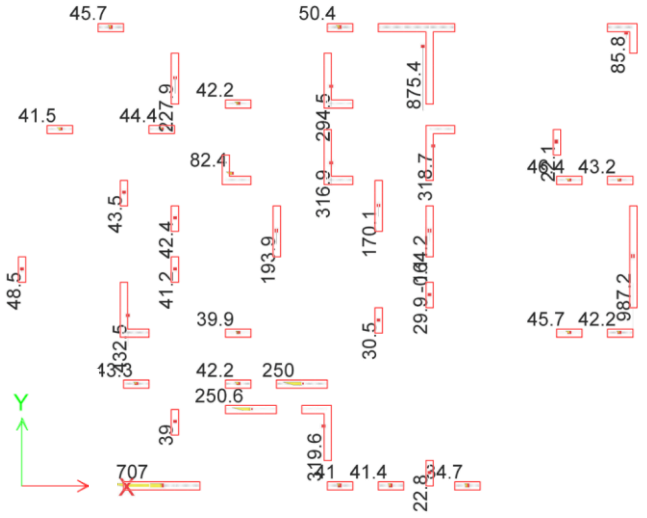

Fig. 2-21 Maximum bending moment around the local perpendicular axis of piers

2.4.4. Optimization problem 4 (All constraints)

Based on the earlier results, it was noticed that SWOF outputs produce scattered single shear wall segments that might reduce the constructability efficiency and might affect the total construction cost. So, all constraints are grouped together in one optimization problem for more rational results, as defined in equation (2-10). Noting that introducing a number of piers N_P as a constraint will increase the computational cost of the optimization process tremendously, and it might not

converge to the required number of grouped shear walls. However, changing the objective function to minimize the number of piers will reduce the number of shear wall segments as well. As shown in Fig. 2-22, SWOF converged to 19 piers, coupled with a reduction in the number of shear wall segments as predicted while satisfying all other constraints' limitations. In this problem, SWOF starts to lump shear wall segments to reduce the formulated piers. As shown in Fig. 2-23, ~98% of shear wall segments are grouped in piers, and only two shear wall segments are not lumped into any group. In order to assure SWOF efficiency, a three-dimensional FEM analysis is conducted using the resulting optimal layout presented in Fig. 2-24 (a). By investigating the demand-to-capacity ratio (D/C ratio) for all piers based on the initial reinforcement presented in Fig. 2-24 (b), only one pier is considered unsafe, with only 2%. A slight increase in reinforcement ratio for that pier will end up satisfying the limit state design requirements. It is also noticed that most piers experienced a D/C ratio of less than 70%. Consequently, decreasing the reinforcement ratio in those piers will increase the material efficiency and generate more economical solutions. As shown in Fig. 2-25, all constraints are satisfied. However, some constraints, like the drift, have a noticeable error compared to the FEM results; they are still not violating their limitations, as shown in Table 2-9. This confirms that the optimization process is robust, and the error does not have a significant impact on it. Yet, the propagation of the error and the trend of the results of the evaluated samples through generations is of concern to yield an optimal solution, as shown in Fig. 2-26. The main concern in the optimization procedure is to have an efficient objective function capable of deriving the optimization algorithm to an optimal solution within the constraints' limits and the design variables' boundaries. Using an ANN surrogate model made it possible to investigate thousands of possible solutions (i.e., candidates) through multiple generations within a few minutes. As a result, all generated errors are within the optimization algorithm's acceptable

tolerance limits since a preliminary exploration for large portions of the search space can first be explored and then validated with FEM.

$$
\begin{aligned}
&find\ S = (S_1, S_2, S_3, \dots, S_N)\\
&minimize\ (N_P)\\
&Subjected\ to:\\
&C_{Total} = \big(\ \delta_y \le 0.2\%, \delta_x \le 0.2\%,\ e_{C_M C_R} \le 1\ m, \sigma_M \\
&\qquad\qquad \le 150\ t.m\big)\\
&Where\ S_i \in \{0,1\}\ (i = 1,2, \dots, N\ ), N = 170
\end{aligned}
\tag{2-10}
$$

Table 2-8 GA parameters of optimization Problem-4

Population size	Number of generations	Mutation function	Crossover ratio	Constraints (C_{Total})			
				δ_y	δ_x	$e_{C_M C_R}$	σ_M
10000	1745	"Mutationpower"	0.8	0.2%	0.2%	1 m	150 t.m

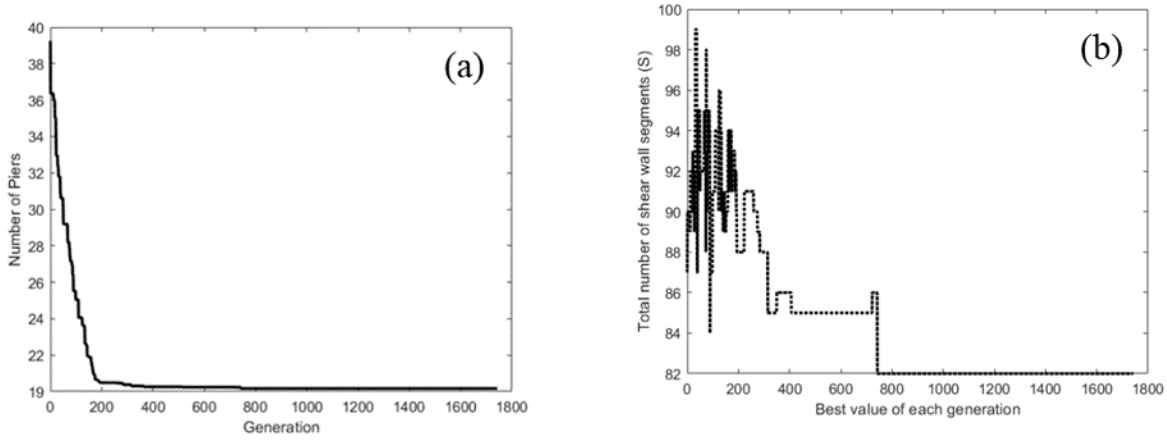

Fig. 2-22 Fitness curve for (a) the total number of piers and (b) the number of shear wall segments of optimization Problem-4

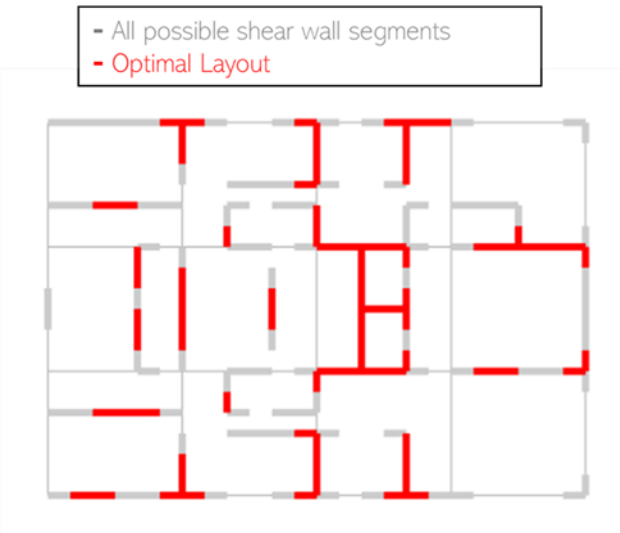

Fig. 2-23 Optimal shear wall layout of optimization Problem-4

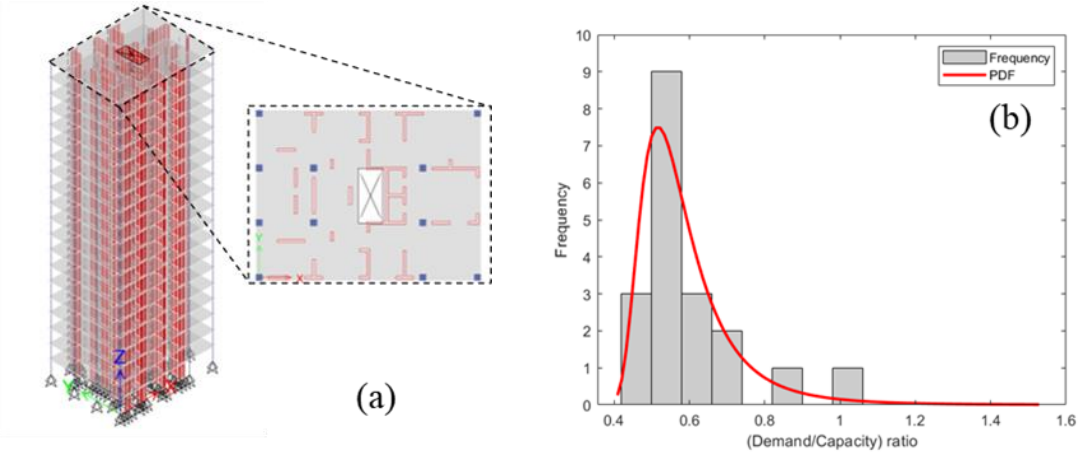

Fig. 2-24 (a) Three-dimensional FEM model for the optimal layout of optimization Problem-4, and (b) Demand/capacity ratio histogram and probability distribution function for all piers of the optimization Problem-4

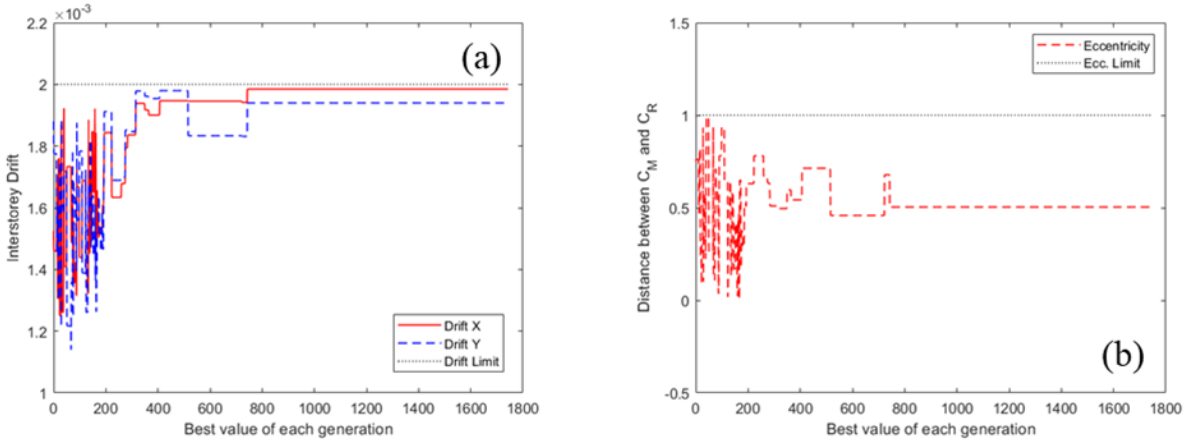

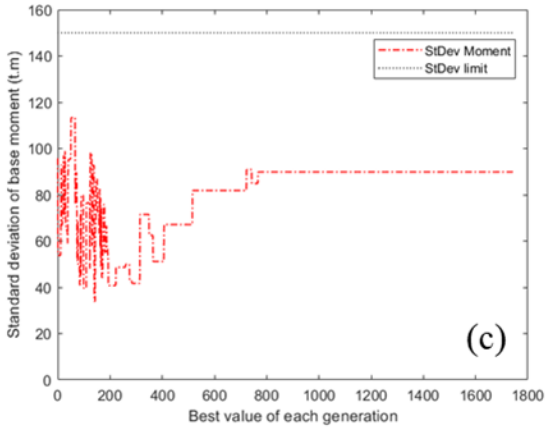

Fig. 2-25 (a) Interstorey drift, (b) distance between the center of mass and center of rigidity, and (c) standard deviation of the base moment.

Table 2-9 Validation results of optimization Problem-4

Constraint	ANN	FEM	Error%
Drift Y ($\boldsymbol{\delta_y}$)	0.0019	0.0016	-21%
Drift X ($\boldsymbol{\delta_x}$)	0.00186	0.00155	-17%
Eccentricity ($\boldsymbol{e_{C_M C_R}}$)	0.51m	0.567 m	11%
Standard deviation ($\boldsymbol{\sigma_M}$)	90 t.m	113.78 t.m	20%

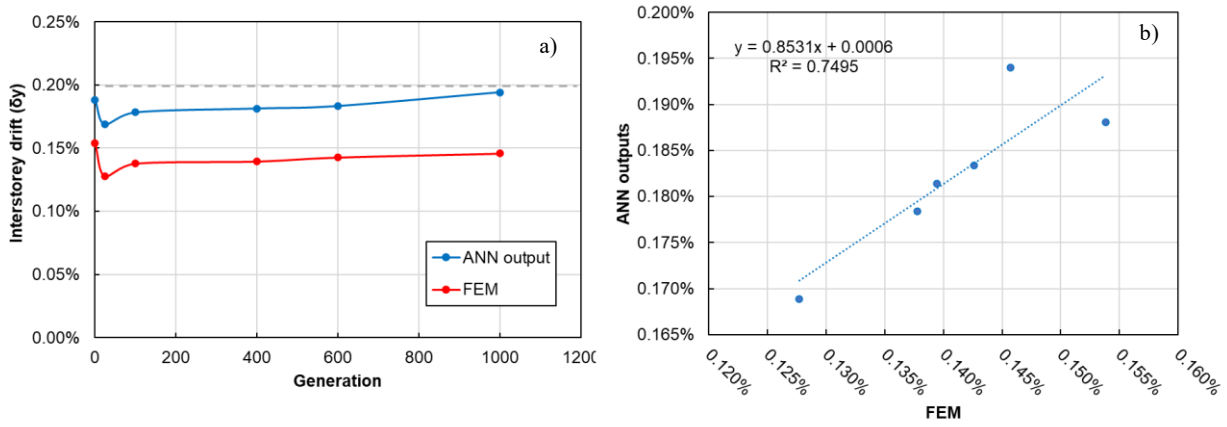

Fig. 2-26 (a) FEM and ANN outputs for interstorey drift, (b) Regression coefficient for Intersotrey drift of optimization Problem-4

2.5. Conclusion

In this study, a robust automated Structural Wind Optimization Framework (SWOF) is developed to find the optimal layout for tall buildings' Lateral load resisting system, taking into consideration multiple load cases and architectural constraints. SWOF is a genetic algorithm-based optimization

framework that uses Artificial Neural Network (ANN) as a surrogate model to evaluate its constraints and objective function. These surrogate models rely on a training dataset prepared using the Finite Element Method (FEM) and automated by an OAPI MATLAB code. This study focuses on the shear wall layout; however, SWOF is capable of incorporating different materials, constraints, or lateral load resisting systems. The main purpose of the SWOF in this study is to minimize the total weight of the structural system by reducing the number of used shear wall segments within the predefined layout to enhance the structure's wind performance without violating architectural and serviceability constraints. A typical 70 m tall building is adopted as a case study to apply the SWOF and check its validity against interstorey drift, torsional effect, and base moment distribution. SWOF introduced a column distribution process to minimize slab design changes, avoid structural weight changes, and avoid overlapping between vertical structural elements. The complexity of calculating the flexural capacity through the optimization procedure is mitigated by limiting the variation of induced base moments on shear wall segments through the standard deviation constraint. Also, the constructability of shear walls is taken into consideration by reducing the number of formulated shear wall groups, known as piers. In this study, the possible location of shear walls is discretized into 170 finite shear wall segments. Four main optimization problems were discussed to show the effect of assigning different constraint(s) and objective function(s). By defining the maximum interstorey drift as a constraint in Problem-1, it was noticed that SWOF was capable of identifying wind direction as presented in Problem-1-1 and Problem-1-2. Also, SWOF recognized the concept of inertia without explicitly defining it through the developed code, as shown in the formulated shear walls. In Problem-2, adding the eccentricity constraint to the drift constraint reduced the distance between the center of mass and the center of rigidity. While in Problem-3, the addition of the standard deviation of base bending moments to

the drift constraint pushed SWOF to distribute shear wall segments in a manner that can limit the variation of induced base moments on each shear wall segment. In Problem-4, where all constraints were defined, it was found that assigning the objective function to be the number of piers has led to a consequent reduction in the total number of segments, which will result in a more economical design. It also managed to enhance the constructability of the generated layout. Through the four optimization problems, it was found that the more constraints are assigned to the problem, the more shear wall segments are generated. This can be related to the increase in problem complexity to satisfy all provided limitations. Thanks to the built surrogate models with a correlation coefficient of 0.95, SWOF was able to identify critical load cases to generate layouts that only require slight modifications in reinforcement ratio to satisfy the Demand-to-Capacity ratio of shear walls based on the chosen design code.

2.6. References

Ahmad, A., Cotso os, D. M., & La garos, N. D. 2020). Framework for the de e lopment of artificial neural networks for predicting the load carrying capacity of RC members. *SN Applied Sciences*, *2* 4), 1–21. https://doi.org/10.1007/s42452-020-2353-8

Alanani, M., & Elshaer, A. 2021). Impro ing wi nd performance of structural systems of tall buildings using topology modifications. *The Canadian Society of Civil Engineering Annual Conference 2021*, *244* May), 1–9. https://doi.org/10.1007/978-981-19-0656-5_41

Aly, A. M., & Abburu, S. 2015). On the design of high-rise buildings for multihazard: Fundamental differences between wind and earth ua ke demand. *Shock and Vibration*, *2015*. https://doi.org/10.1155/2015/148681

Baldock, R., Shea, K., & Eley, D. 2005). E ol i ng optimized braced steel frameworks for tall buildings using modified pattern search. *Proceedings of the 2005 ASCE International Conference on Computing in Civil Engineering*, 631–642. https://doi.org/10.1061/40794 179)60

Behmanesh, I. 2018). Design Optimization of Shear Wall High-Rise Building Structures. *Structures Congress 2018*, 222–232. https://doi.org/10.1061/9780784481325.024

Bernardini, E., Spence, S. M. J., Wei, D., & Kareem, A. 2015). Aerodynamic shape optimization of ci i l structures: A CFD-enabled Kriging-based approach. *Journal of Wind Engineering and Industrial Aerodynamics*, *144*, 154–164.

Bobby, S., Spence, S. M. J., Bernardini, E., & Kareem, A. 2014). Performance-based topology optimization for wind-excited tall buildings: A framework. *Engineering Structures*, *74*, 242–255. https://doi.org/10.1016/j.engstruct.2014.05.043

Chan, C. M., & Wong, K. M. 2008). Structural topology and element sizing design optimisation of tall steel frameworks using a hybrid OC-GA method. *Structural and Multidisciplinary Optimization*, *35* 5), 473–488. https://doi.org/10.1007/s00158-007-0151-1

Cid Montoya, M., Nieto, F., Hernández, S., Kusano, I., Ál a rez, A. J., & Jurado, J. 2018). CFD-based aeroelastic characterization of streamlined bridge deck cross-sections subject to shape modifications using surrogate models. *Journal of Wind Engineering and Industrial Aerodynamics*, *177* January), 405–428. https://doi.org/10.1016/j.jweia.2018.01.014

CSA. 2019). *Design of concrete structures* A23.3:19). CSA Group.

CSI. 2018). *ETABS building analysis and design* 2018.1.1). Computers and Structures, Inc. www.csiamerica.com

Elshaer, A., & Bitsuamlak, G. 2018). Multiobjecti e Aerodynamic Optimization of Tall Building Openings for Wind-Induced Load Reduction. *Journal of Structural Engineering*, *144* 10), 4018198. https://doi.org/10.1061/ ASCE)ST.1943-541X.0002199

Elshaer, A., Bitsuamlak, G., & El-Damatty, A. 2017). Enhancing wind performance of tall buildings using corner aerodynamic optimization. *Engineering Structures*, *136*, 133–148. https://doi.org/10.1016/j.engstruct.2017.01.019

Forrester, A. I. J., Sóbester, A., & Keane, A. J. 2008). Engineering Design ia Surrogate Modelling. In *Engineering Design via Surrogate Modelling*. Wiley. https://doi.org/10.1002/9780470770801

Jia, D.-W., & Wu, Z.-Y. 2021). Seismic fragility analysis of RC frame-shear wall structure under multidimensional performance limit state based on ensemble neural network. *Engineering Structures*, *246* March), 112975. https://doi.org/10.1016/j.engstruct.2021.112975

Kotso ou, G. M., Ahma d, A., Cotso os, D. M., & Lagaros, N. D. 2020). Reappraisal of methods for calculating flexural capacity of reinforced concrete members. In *Proceedings of the Institution of Civil Engineers: Structures and Buildings* ol. 173, Issue 4). https://doi.org/10.1680/jstbu.18.00110

Lagaros, N. D., & Ple r is, . 2022) . Artificial Intelligence AI) Applied in Ci i l Engineering. *Applied Sciences*, *12* 15), 7595. https://doi.org/10.3390/app12157595

Lou, H., Gao, B., Jin, F., Wan, Y., & Wang, Y. 2021). Shear wall layout optimization strategy for high-rise buildings based on conceptual design and data-dri e n tabu search. *Computers & Structures*, *250*, 106546. https://doi.org/10.1016/j.compstruc.2021.106546

Lou, H. P., Ye, J., Jin, F. L., Gao, B. Q., Wan, Y. Y., & Quan, G. 2021). A practical shear wall layout optimization framework for the design of high-rise buildings. *Structures*, *34* September), 3172–3195. https://doi.org/10.1016/j.istruc.2021.09.038

Lu, H., Gilbert, M., & Tyas, A. 2019). Layout optimization of building frames subject to gra it y and lateral load cases. *Structural and Multidisciplinary Optimization*, *60* 4), 1561–1570. https://doi.org/10.1007/s00158-019-02283-x

Luo, X., Suksuwan, A., Spence, S. M. J., & Kareem, A. 2017). Topology Optimization and Performance-Based Design of Tall Buildings: A Spatial Framework. *Structures Congress 2017*, 447–458. https://doi.org/10.1061/9780784480410.037

Ministry of Housing and Urban-Rural De e lopment of the People's Republic of China. 2010). *Technical Specification for Concrete Structures of Tall Building (JGJ 3-2010).* https://www.chinesestandard.net/PDF/BOOK.aspx/JGJ3-2010

National Building Code of Canada. 2015). Canadian Commission on Building and Fire Codes National Research Council of Canada.

Nguyen, H. D., Dao, N. D., & Shin, M. 2021). Prediction of seismic drift responses of planar steel moment frames using artificial neural network and extreme gradient boosting. *Engineering Structures*, *242*, 112518. https://doi.org/10.1016/J.ENGSTRUCT.2021.112518

Noormohamadian, M., & Salajegheh, E. 2021). E a luation and minimization of moment coefficient of tall buildings with trilateral cross-section ia a surrogate model. *SN Applied Sciences*, *3* 2). https://doi.org/10.1007/s42452-020-04128-5

Papadrakakis, M., & Lagaros, N. D. 2002). Reliability-based structural optimization using neural networks and Monte Carlo simulation. *Computer Methods in Applied Mechanics and Engineering*, *191* 32), 3491–3507. https://doi.org/10.1016/S0045-7825 02)00287-6

Pizarro, P. N., & Massone, L. M. 2021). Structural design of reinforced concrete buildings based on deep neural networks. *Engineering Structures*, *241* July 2020), 112377. https://doi.org/10.1016/j.engstruct.2021.112377

Qiu, Y., San, B., He, H., & Zhao, Y. 2021). Surrogate-based aerodynamic optimization for enhancing the shelter effect of porous fences on a triangular prism. *Atmospheric Environment*, *244* September 2020). https://doi.org/10.1016/j.atmosen .2020.117922

Talatahari, S., & Rabiei, M. 2020). Shear wall layout optimization of tall buildings using Quantum Charged System Search. *Frontiers of Structural and Civil Engineering*, *14* 5), 1131–1151. https://doi.org/10.1007/s11709-020-0660-1

Zhang, Y., & Mueller, C. 2017). Shear wall layout optimization for conceptual design of tall buildings. *Engineering Structures*, *140*, 225–240. https://doi.org/10.1016/j.engstruct.2017.02.059

CHAPTER 3

3. MULTI-OBJECTI E STRUCTURAL LAYOUT OPTIMIZATION OF TALL BUILDINGS SUBJECTED TO DYNAMIC WIND LOADS

3.1. Introduction

Tall buildings are growing taller, and the need to provide more tall buildings is increasing. In 2019, a new record was accomplished by having a total of 126 tall buildings of +200 meters were constructed, including 26 supertall buildings exceeding 300 meters (CTBUH, 2019). Tall buildings are one of the solutions that meet the goals of providing sufficient housing while minimizing the environmental impact. Utilizing taller buildings to solve the housing shortage has the advantages of using relatively smaller footprints with fewer infrastructure requirements, as well as maximizing its affordability (Roser et al., 2019). They are sensitive to dynamic lateral loads, especially wind, that might cause excessive vibration or even damage to either structural or non-structural elements (Cui & Caracoglia, 2020). Structural designers' main concern is to satisfy the safety and serviceability requirements. This design process typically goes through a time-consuming iterative procedure to ensure the cost efficiency of the proposed structural system. Therefore, structural optimization frameworks have been developed to minimize the cost of proposed structural systems, especially the lateral load resisting systems (LLRS) that provide tall buildings with adequate stiffness to withstand critical load cases generated by wind and seismic loads. Structural designers follow two main optimization philosophies when designing tall buildings to withstand such loads. The first is by reducing captured wind loads by altering the shape of the building (i.e., outer shape optimization) (Bernardini, Spence, Wei, et al., 2015; Elshaer, Bitsuamlak, & El-Damatty, 2017; Elshaer & Bitsuamlak, 2018; Kareem et al., 1999, 2013a; Tanaka et al., 2012, 2019). The second philosophy is to optimize the lateral load resistance system performance (LLRS) (i.e., structure optimization). The latter, which is the focus of this study, aims to find the optimal system and layout configuration (e.g., shear walls, cores, bracing systems) to achieve the objective performance of the building with the least cost and/or improve the structural

performance. Structure optimization of tall buildings can be categorized in several ways, such as problem definition (e.g., size, shape or topology optimization), lateral load (e.g., wind or seismic), load time-dependency (e.g., static or dynamic), and structural analysis technique (e.g., eigenvalue analysis or time-history analysis).

Considering lateral loads in structural optimization problems started with applying equivalent deterministic static loads as a simplification. As presented in the sizing optimization problem by (C.-M. Chan et al., 1995), wind load was defined as horizontal point loads in both X and Y directions based on American standards. They used the optimality criteria algorithm to find the optimal size of structural elements based on a predefined layout. In a previous study by (Zakian & Kaveh, 2020), they employed the optimality criteria algorithm to formulate a continuous topology optimization framework for shear walls. The objective was to minimize structural compliance under equivalent static seismic load combinations, following the guidelines provided by the (ASCE, 2017) code. A number of researchers tackled the LLRS optimization problem through Structural Topology Optimization (STO) techniques, where the optimal distribution of materials required to be found in a specific design domain (Bendsøe & Sigmund, 2004). STO can be applied to a two-dimensional structural system to find the optimal layout, taking into consideration wind loads. These two-dimensional problems most probably focus on the vertical elevation layout of the LLRS as presented by (Baldock et al., 2005; Baldock & Shea, 2006), in which a pattern search algorithm has been used to find the optimal steel bracing layout of a tall building subjected to equivalent static wind loads. Moreover, (Lu et al. 2019) considered different load cases of wind loads to find the optimal bracing system layout for pre-existing frame structures through plastic analysis. Not only the vertical layout but also the horizontal plan layout was investigated. (H. P. Lou et al., 2021; Y. Zhang & Mueller, 2017) developed shear wall layout optimization frameworks of tall buildings subjected to wind loads.

The aforementioned research simplified the lateral load behaviour into equivalent deterministic static loads. However, lateral loads have stochastic dynamic behaviours that affect the structural vibrational modes. Therefore, these simplifications might not yield the most economical solution as they rely on the determination of an equivalent static load, which probably results in a less economical structural solution. Based on the (*National Building Code of Canada*, 2015), the specified wind loads for a building and its components can be determined using three procedures: static, dynamic or wind tunnel procedure. The choice of the appropriate procedures depends on the structure's dynamic characteristics, whether it's classified as dynamically insensitive, sensitive, or very sensitive. Tall buildings with a height of more than $60\,m$, are considered dynamic, sensitive structures. In some cases, tall buildings, whose lowest natural frequency is less than $0.25\ Hz$, or whose height-to-width ratio is more than $6\ m$, are classified as very sensitive dynamic structures due to its slenderness. Those dynamically sensitive structures are considered a multi-degrees of freedom dynamic problem that can be presented in the form of the general equation of motion as shown in equation (3-1). Where M is the mass matrix, K is the stiffness matrix for linear systems or $f_s(u)$ for an inelastic system as force-deformation relations, C is the damping matrix, and the dynamic excitation, which may be external forces (e.g., wind loads) $P(t)$ or ground acceleration (e.g., earthquake) $\ddot{u}_g(t)$.

$$M\ddot{u} + C\dot{u} + Ku = P(t) \tag{3-1}$$

These coupled differential equations can be solved using time-domain or frequency-domain analysis, depending on the way the system is defined as either linear or nonlinear. For nonlinear systems like tall buildings, numerical analysis is the most convenient approach to finding structural responses (Chopra, 2012). This motivated researchers to consider the dynamic representation of dynamically sensitive structures in optimization problems, especially topology optimization

problems. It was found that maximization of the fundamental eigenvalue will result in an optimized structure that can work well for static loads. Some researchers have considered stochastic topology optimization for structures subjected to seismic excitation using time history analysis, such as (Sotiropoulos & Lagaros, 2022). In comparison, eigenvalue analysis is most common for STO problems of structures subjected to seismic loads due to its computational affordability compared to time-history analysis (Fragiadakis & Lagaros, 2011; Gholizadeh & Ebadijalal, 2018; Joyner et al., 2022; Martin & Deierlein, 2020; X. Zhou et al., 2022). For instance, (Chun et al., 2016) used random vibration theories in topology optimization to satisfy probabilistic constraints defined in terms of stochastic responses. Also, (Gomez et al., 2020) developed a gradient-based optimization framework in which stochastic ground excitation is modelled as a zero-mean filtered white noise; an augmented state space representation is formed by combining the equation of motion for the structure with the excitation filter. Filtering the white noise introduces specific frequency characteristics, potentially mimicking the filtering effect of the ground itself on the earthquake waves. By combining the governing equation of motion for the structure with the mathematical model of the excitation filter into a single state-space representation, the analysis can simultaneously consider the interaction between the structural dynamics and the filtered ground motion.

Wind loads are also considered dynamic due to the turbulent flow and variance in time and space. Some researchers considered wind loads for topology optimization. For example, (Bobby et al., 2014) used Monte Carlo simulations to develop a performance-based topology optimization framework for tall buildings. This framework relies on an approximate static subproblem for the 2D vertical layout of the bracing system. Afterwards, (Luo et al., 2017) expanded this framework to consider 3D performance-based topology optimization problems using dynamic wind loads extracted from boundary layer wind tunnel tests. (Gomez et al., 2021) used the equation of motion within the topology optimization algorithm against dynamic wind loads correlated to known

stationary wind power spectral densities, where dynamic loads were employed in sizing optimization problems. (Deng et al., 2019) developed a framework of performance-based wind-resistant optimization design based on the concept of structural reliability. Meanwhile, most of this research focused on the vertical layout of the LLRS. However, a limited contribution was found to consider the dynamic wind load for the horizontal layout of the LLRS, noting that the dynamic loads for some layouts show lower responses compared to the correlated NBCC static loads (Alanani & Elshaer, 2022).

In this chapter, a multi-objective LLRS (i.e., shear walls) layout optimization framework is provided for dynamically sensitive tall buildings subjected to stochastic wind load. In previous studies, it has been shown that different parameters, rather than the weight, can tremendously affect the layout of the LLRS. For instance, (Alanani & Elshaer, 2023) have investigated the effect of different constraints and objective functions on finding an optimal layout. It was found that better results were generated by only changing the objective function. While the single objective function was efficient in deriving the optimization algorithm, this limits decision-making flexibility in investigating other options that could be adequate for particular projects. The importance of applying multiple objective functions for providing a Pareto optimal set, from which the decision maker can choose the perfect compromise, is shown by (Zou et al., 2007), where the life-cycle cost and the future damage loss were adopted as objective functions for finding the optimal structural member sizes using a weighted genetic algorithm. In this study, a Non-Dominated Sorting Genetic Algorithm (NSGA-II) is adopted to avoid predefined weighted objective functions and utilizes the Pareto dominance to compare and rank solutions, resulting in a diverse set of Pareto optimal solutions instead of one single solution. To the best of the authors' knowledge, this study is the first to address more than two objective functions in a preliminary design stage optimization. In this study, a CFD model is adopted to generate the wind load time history required to be applied to the study building. Adopting a time history analysis is considered challenging through the

optimization process due to the cumbersome analysis that involves simplification of the structural system as presented in the literature. The developed framework in this chapter relies on an ANN-surrogate model for constraints and objective function evaluation. That makes it possible to overcome the simplification of the structural system and make it applicable in real-case scenarios. The adopted surrogate model is built based on an automated FEM-generated database using ETABS (CSI, 2018) and (MATLAB, 2023) code. The usage of the surrogate model will reduce the computational time needed for the optimization process. This integration of dynamic response analysis and surrogate modelling is a significant contribution that enables more accurate and efficient design optimization, which was previously lacking in the literature. A non-gradient optimization algorithm is adopted due to the complexity of modelling the governing equations for such structures. A genetic algorithm is used to identify the optimal shear wall layout against dynamic wind load and gravity loads provided by the (*National Building Code of Canada*, 2015). Finally, suitable column locations will be chosen based on the generated locations of shear walls. The chapter is organized into five sections.

Section 3.1 (this section) presents an introduction and literature review on the optimization of tall buildings. Section 3.2 provides a description of the developed Structural Wind Optimization Framework (SWOF). Section 3.3 presents the optimization application on a case study building, focusing on minimizing the number of shear wall segments used while considering architectural and structural constraints and the CFD model validation. Section 3.4 presents the results and discusses the optimization problem. Finally, Section 3.5 presents the conclusions and findings of the developed SWOF.

3.2. Structural-Wind Optimization Framework (SWOF)

The developed Structural Wind Optimization Framework (SWOF) has been previously used for optimizing tall buildings subjected to static wind load (Alanani & Elshaer, 2023). In this study, SWOF is expanded to include multiple objective functions to enhance the quality of the produced

optimal layout and provide varieties for structural designers to choose from. In addition, the dynamic behaviour of wind loads is also included within SWOF to capture more accurate structural behaviour that could not be achieved using static wind loads. As shown in section 3.3.1, Applying dynamic wind load generated via CFD on a specific layout results in a lower structural response than the load applied based on the (*National Building Code of Canada*, 2015) using the same mean wind velocity. It was also noticed that considering dynamic wind load will yield a lower number of shear wall segments, which can result in avoiding the overdesign of LLRS.

Although this study will focus on the shear wall layout, SWOF is developed generically to incorporate different materials and structural systems. As shown in Fig. 3-1, a flowchart represents the procedure of structural wind optimization. The procedure starts with defining the optimization problem, which includes identifying the objective functions (i.e., fitness functions). The optimization algorithm adopts four main objective functions in SWOF for evaluating generated random samples. Also, SWOF targets minimizing selected structural responses controlled by the objective functions defined in Table 3-1.

For this problem, design variables are the possible location and orientation of the shear walls. Due to architectural requirements, the design variables cannot be located anywhere within the plan boundaries; they are considered constrained (or bounded) binary variables based on a predefined domain. They have been chosen to be binary (i.e., 0 or 1) to indicate the availability or absence of the shear wall segment. This domain went through a preprocessing phase where it got discretized into smaller elements (shear wall segments) based on the accuracy required. The last part of problem definitions is the constraints, where design code limitations are also included as constraints in addition to architectural constraints and any supplementary parameters required by the designer. In this chapter, interstorey drift is considered a constraint in both X-direction (δ_x) and Y-direction $\left(\delta_y \right)$.

Table 3-1. Objective functions definition

Objective Function	Notation
Total number of shear wall segments	$\sum_{i=1}^{N} S_i$
Total number of piers	N_P
Torsional effect (Eccentricity)	$e_{C_M C_R} = \sqrt{\left(X_{C_R} - X_{C_M}\right)^2 + \left(Y_{C_R} - Y_{C_M}\right)^2}$
The standard deviation of shear wall base moments	$\sigma_M = \sqrt{\frac{\Sigma\,(x_i - \mu_M)^2}{\Sigma\, S_i}}$

Once the optimization problem is defined, an optimization algorithm can be used to start looking for the group of optimal layout solutions. An evolutionary algorithm called nondominated sorting genetic algorithm II (NSGA-II) is chosen to tackle it. NSGA-II relies on numerous objective function evaluations by altering design variables systematically using mutation and crossover operators until a group of optimal solutions are found called the "Pareto Front". This Pareto Front is found through sorting procedures based on non-dominated ranking and crowd distance sorting (Deb et al., 2002a).

SWOF relies on surrogate models to represent its objective functions. The evaluation process of generated models through FEM directly is computationally costly as numerous outputs are calculated precisely in addition to the number of iterations required to evaluate various objective functions. Therefore, surrogate models are considered an adequate and computationally efficient solution to be used within the evaluation process. These surrogate models require a group of random training samples to be built. ANN-based surrogate model is used in this study due to its proven efficiency in capturing complex functions (Elshaer & Bitsuamlak, 2018; Lagaros & Plevris, 2022; Papadrakakis & Lagaros, 2002; Pizarro & Massone, 2021a). The required training samples were prepared using linear FEM time history analysis subjected to dynamic wind load generated using LES CFD. A detailed explanation of the LES CFD is included in section 3.3.1. After building the surrogate model, it will be used to represent these constraints and objective functions.

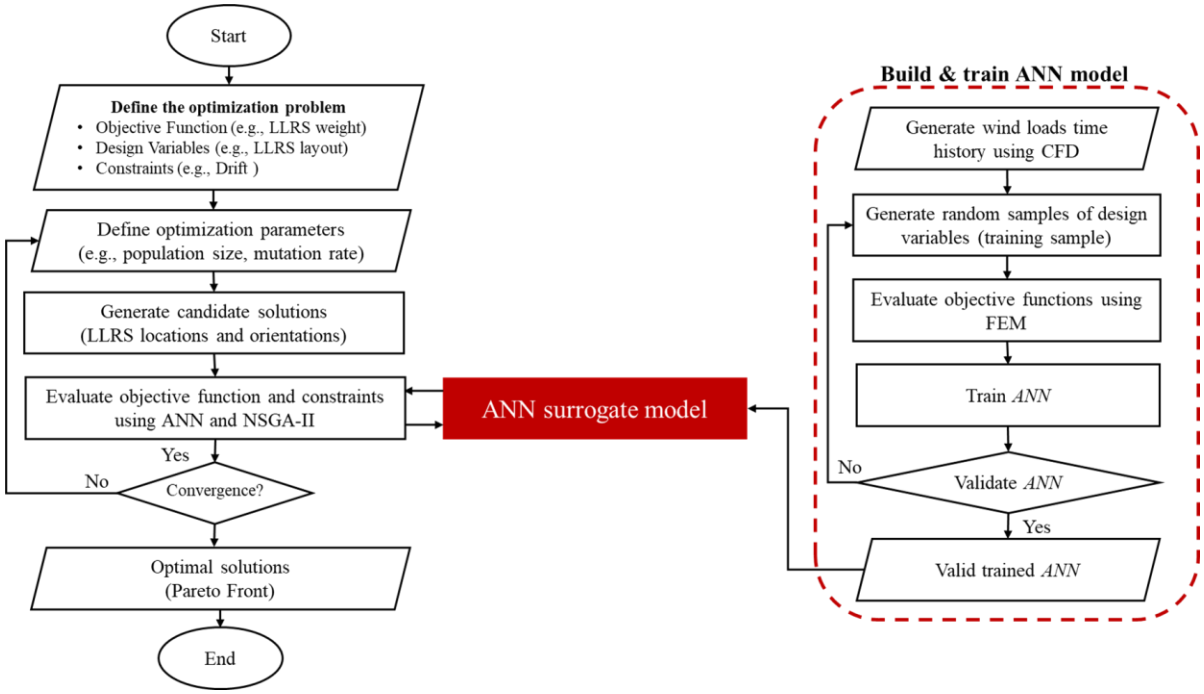

Fig. 3-1. Structure wind optimization framework (SWOF) flowchart

3.2.1. Non-dominant Sorting Genetic Algorithm (NSGA-II)

The Non-dominated Sorting Genetic Algorithm II (NSGA-II) is a popular and widely used multi-objective optimization algorithm that ensures all objective functions are minimized without any dominance of one objective over the other. It is designed to find a set of solutions that represents the trade-off among multiple conflicting objectives. The NSGA-II algorithm operates based on the concept of Pareto dominance. It maintains a population of candidate solutions, where each solution represents a possible design or solution to the optimization problem. The algorithm iteratively evolves the population through selection, crossover, and mutation operations, mimicking the principles of natural evolution, as shown in Fig. 3-2. The resulting generation will then be combined with the parents to provoke elitism. The elitist selection mechanism is a key feature of NSGA-II, which ensures that the best solutions survive from generation to generation. The algorithm maintains multiple fronts, where each front consists of non-dominated solutions that are not dominated by any other solution in the population. This helps to preserve diversity and explore

different trade-off solutions. The NSGA-II algorithm also incorporates a crowding distance mechanism to maintain diversity within each front. The crowding distance measures the density of solutions in the objective space, favouring solutions that are located in less crowded regions. This encourages the algorithm to explore different areas of the Pareto front and avoid premature convergence to a single solution. Overall, the NSGA-II algorithm is known for its ability to effectively handle multiple conflicting objectives and provide a diverse set of solutions on the Pareto front. Its implementation involves a combination of selection, crossover, mutation, and diversity maintenance techniques. By iteratively improving the population, NSGA-II guides the search toward optimal trade-off solutions, enabling decision-makers to make informed choices based on their preferences and requirements.

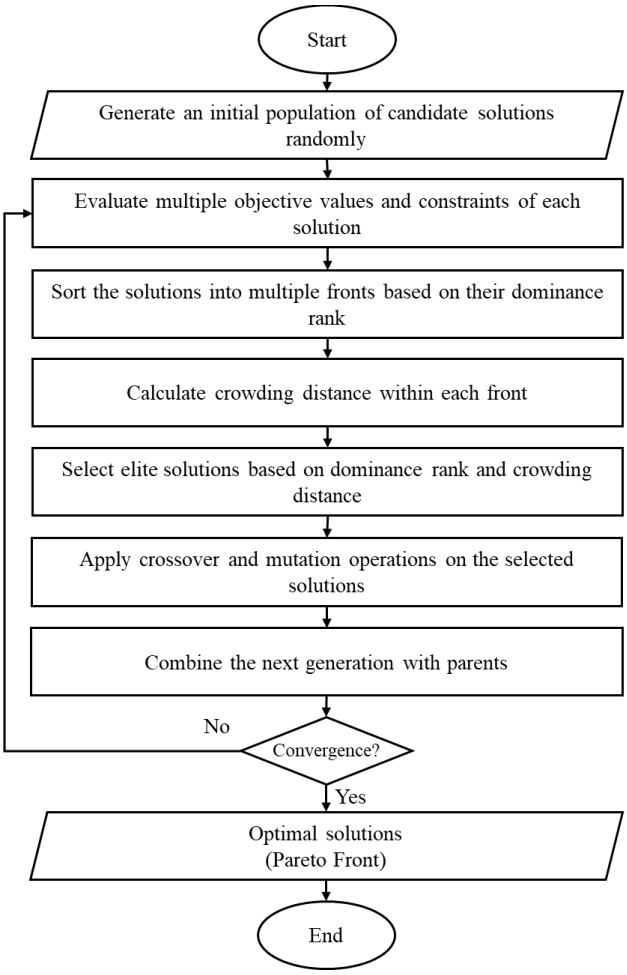

Fig. 3-2 Non-dominant Sorting Genetic Algorithm (NSGA-II) flowchart

3.2.2. Artificial Neural Network (ANN) model

In this section, we provide a detailed overview of the ANN architecture, hyperparameters, input and output configuration, training process, training termination condition, and data preparation steps employed in our research. ANN is a regression model that consists of inputs, hidden layers and outputs. The quality of the neural network outputs (i.e., objective function and constraints) relies on the training process effectiveness through various training sample models that can cover most of the search space required in the optimization problem. As shown in Fig. 3-2, building the adopted surrogate model starts first by generating a random sample of training models. A total of 5000 samples of random configurations of shear wall segments are prepared using MATLAB code that automates the process of building models and extracting results on ETABS through the Open

Application Programming Interface (OAPI). This code also generates columns' locations based on the predefined locations and avoids any overriding or intersections with the generated shear walls. This prepared Finite Element Models (FEM) database will be used to train ANN models to act as objective and constraint functions. A sensitivity analysis of the number of samples has been conducted to ensure the convergence of the built ANN. As shown in Fig. 3-3, Increasing the number of training samples will improve the regression coefficient of the trained model. Yet increasing the number of samples will be computationally costly and will stretch the training process significantly. A forward-propagation deep neural network is used to determine the output of a group of functions, including the critical inter-story drift in both X-direction (δ_x) and Y-direction (δ_y), the distance between the center of mass (C_M), the center of rigidity (C_R), and the standard deviation of shear walls' critical base moments (σ_M).

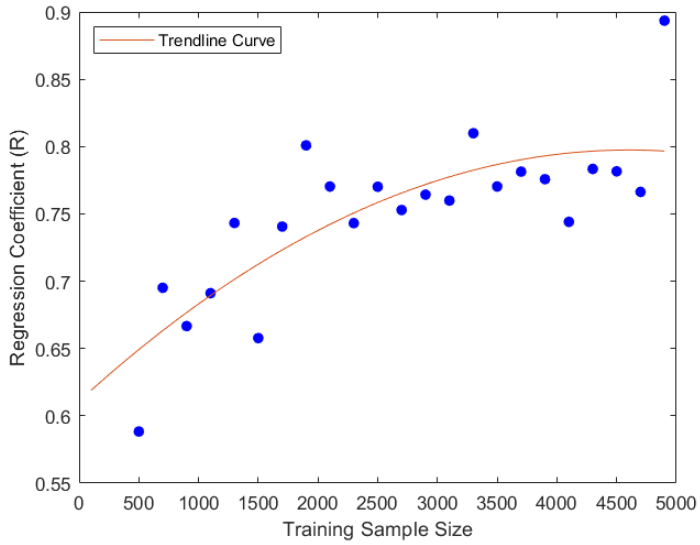

Fig. 3-3 Sensitivity analysis for the training sample size of $(e_{C_M C_R})$

Regarding the ANN architecture, we have incorporated a fully connected feedforward neural network with three hidden layers of 23, 44 and 10 nodes, respectively, that have been determined based on an exhaustive search. The input layer size is set to accommodate the 170 binary variables,

and the output layer size corresponds to the output parameters of interest. For the hyperparameters, we have utilized a Bayesian regularization backpropagation algorithm for training (MacKay, 1992) . The training process involves using Levenberg-Marquardt optimization to update the network weights. To ensure convergence and prevent overfitting, we have implemented early stopping with a validation set, terminating the training process when the validation error fails to improve after 30 consecutive epochs. Regarding data preparation, we have preprocessed the dataset by performing normalization to outputs and standardizing them to have zero mean and unit variance. Additionally, we have split the dataset into training, validation, and testing sets with a ratio of 70:15:15, respectively, to facilitate model evaluation and generalization.

As shown in Fig. 3-4, all trained ANNs showed a satisfactory regression coefficient that is adequate to drive the optimization problem toward the required optimal layouts. The structural response parameters vary in complexity, and the ANN was able to capture the interstorey drift with a regression coefficient of 98%. In comparison, the eccentricity was more complex to be captured, with a regression coefficient of ~90%. Meanwhile, the error histogram presented in Fig. 3-5 displays the count of errors within predefined intervals. By examining the shape and spread of the error distribution, it can be deduced that 70 to 80 % of samples result in errors of less than 20 %. With deeper investigation, it was found that the majority of those samples lie in the lower value region of our structural response parameters, which is the target of the minimization problem. That can indicate the efficiency of the model and its accuracy in predicting the targeted outputs of interest. Additionally, those outliers will not impact the model's performance as they are away from the region of interest.

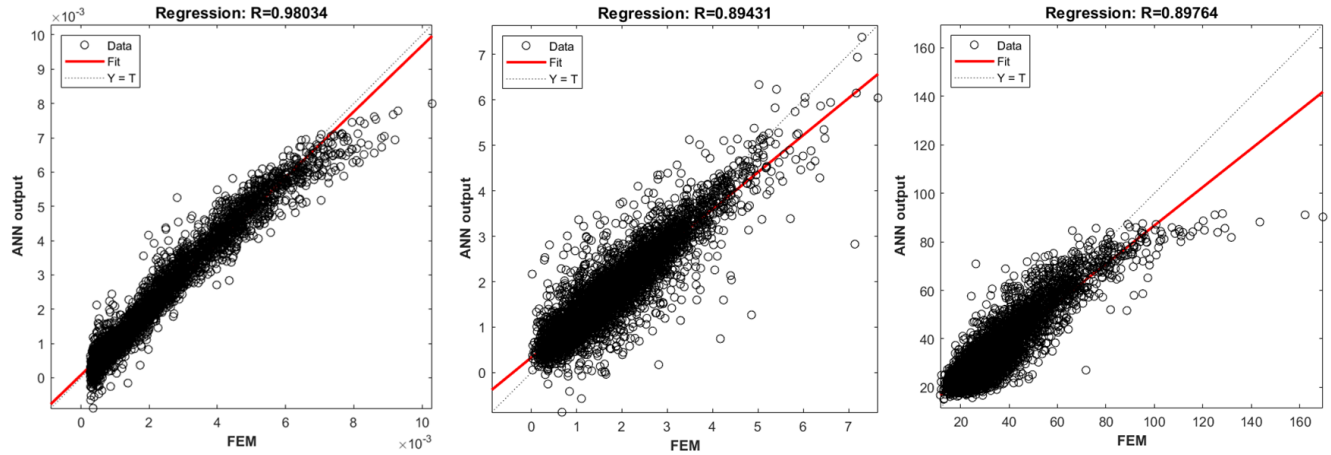

Fig. 3-4. Regression coefficient of (a) interstorey drift in the Y-direction (δ_y), (b) eccentricity ($e_{C_M C_R}$), and (c) standard deviation of the base moment (σ_M).

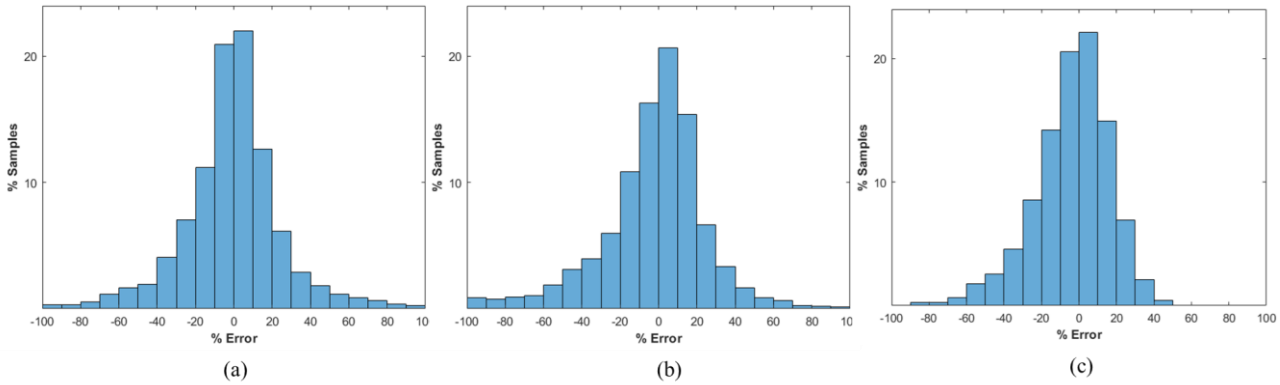

Fig. 3-5 Error Histogram of (a) interstorey drift in the Y-direction (δ_y), (b) eccentricity ($e_{C_M C_R}$), and (c) standard deviation of the base moment (σ_M).

The performance of the ANN model was evaluated using several commonly used metrics, including Root Mean Squared Error (RMSE), Mean Absolute Error (MAE), and the coefficient of determination (R^2). The RMSE is an estimate of the standard deviation of the errors, defined in (2-1), that shows the deviation from the actual values and is a scale-dependent metric. This explains the variation in RMSE values among the different parameters considered due to the different magnitude of orders. Also, MAE was calculated using equation (3-3), which is a scale-

dependent value that represents the average absolute difference between predicted and actual values. In contrast, R^2, in equation (3-4), describes the predictability of variance in the surrogate model. Overall, the ANN model exhibits a satisfactory performance that can be used to derive the optimization algorithm.

$$RMSE = \sqrt{\frac{1}{n}\sum_{i=1}^{n}\left(y_{predicted\,i} - y_{actual\,i}\right)^2} \tag{3-2}$$

$$MAE = \frac{1}{n}\sum_{i=1}^{n}\left|y_{predicted\,i} - y_{actual\,i}\right| \tag{3-3}$$

$$\begin{aligned} &R = \sqrt{1 - \frac{SSR}{SST}}, \\ &SSR = \sum_{i=1}^{n}\left(y_{predicted\,i} - y_{actual\,i}\right)^2, \\ &SST = \sum_{i=1}^{n}\left(y_{actual\,i} - \bar{y}_{actual}\right)^2 \end{aligned} \tag{3-4}$$

Table 3-2 ANN regression performance metrics

ANN model	RMSE	MAE	$\boldsymbol{R^2}$
$\boldsymbol{\delta_y}$	3.5×10^{-4}	2.4×10^{-4}	0.96
$\boldsymbol{\delta_x}$	1.9×10^{-4}	1.3×10^{-4}	0.92
$\boldsymbol{e_{C_M C_R}}$	0.46	0.32	0.80
$\boldsymbol{\sigma_M}$	7.11	5.13	0.81

3.3. Optimization problem definition

3.3.1. Computational Fluid Dynamic model

3.3.1.1. Validation

For wind load time-history generation, a validation model for an experimental wind tunnel test is conducted on a selected tall building. This step provides a validated computational domain that can be used later in the adopted case study. A well-established standard tall building, known as the Commonwealth Advisory Aeronautical Research Council (CAARC) building (Melbourne, 1980), with dimensions shown in Fig. 3-6, is adopted in the validation process.

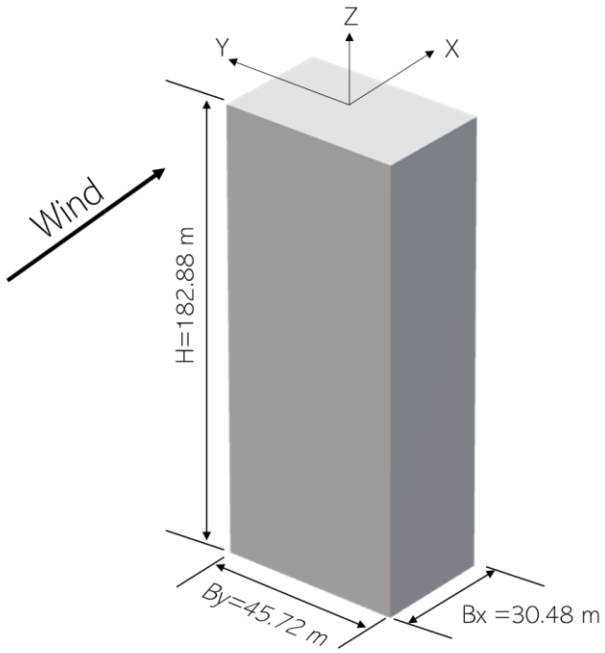

Fig. 3-6. CAARC standard full-scale dimensions

This building has been extensively studied either through boundary layer wind tunnel (BLWT) tests (Dragoiescu et al., 2006; Melbourne, 1980) and numerical CFD simulations (Braun & Awruch, 2009; Dagnew & Bitsuamlak, 2010; S. Huang et al., 2007; Thordal et al., 2020). For the sake of validation, the mean pressure coefficient ($mean\ C_p$) and root mean square of the pressure coefficient ($RMS\ C_p$) will be compared to two main BLWT tests on the CAARC building presented in (Melbourne, 1980), where the pressure coefficient is calculated using equation (3-5). These BLWT tests are held at Monash University and the National Physics Laboratory (NPL). Large Eddy Simulation (LES) is conducted for a scaled model of the CAARC building similar to the BLWT. Based on (Elshaer et al., 2016) study, the time scale and length scale are 1:100 and 1:400, respectively. The building and Computational domain full-scale dimensions are provided in Table 3-3. Three zones are used for grid discretization with different base mesh sizes: zone 1, zone 2, and zone 3 grid sizes are H/5, H/10 and H/25, respectively, producing a total number of ~1,730,000 cells, as shown in Fig. 3-7. In addition, 10 prism layers are used around wall regions

with a stretching factor of 1.30. In order to generate a turbulent inflow, the consistent discrete random flow generation (CDRFG) (Aboshosha et al., 2015) technique is utilized with a mean wind speed of 10 m/s at the building's height. Turbulent intensity, turbulence length scale and velocity profile regression coefficients are used as per (Elshaer et al., 2016) as shown in Fig. 3-8. To represent the wind power spectral density (PSD), a range of frequencies from 1.0 to 3500 Hz is utilized. The spatial discretization of the domain can be seen in Fig. 3-9, where the fine hexahedral mesh appropriately captures the buildings' dimensions. The Velocity streamlines in Fig. 3-10 show a very reasonable behaviour with a velocity magnitude similar to what is conducted by (Elshaer et al., 2016). As shown in Fig. 3-11, $mean\ C_P$ and $RMS\ C_P$ are compared against Monash University and NPL results, and they showed a good agreement with a maximum variation of less than 6% in both parameters and mean average error of less than 0.045.

$$C_P = \frac{P - P_o}{\frac{1}{2}\rho v_H^2} \tag{3-5}$$

where v_H is the reference velocity at the building height, $(P - P_o)$ is the dynamic pressure head, ρ is the air density, and H is the height of the study building.

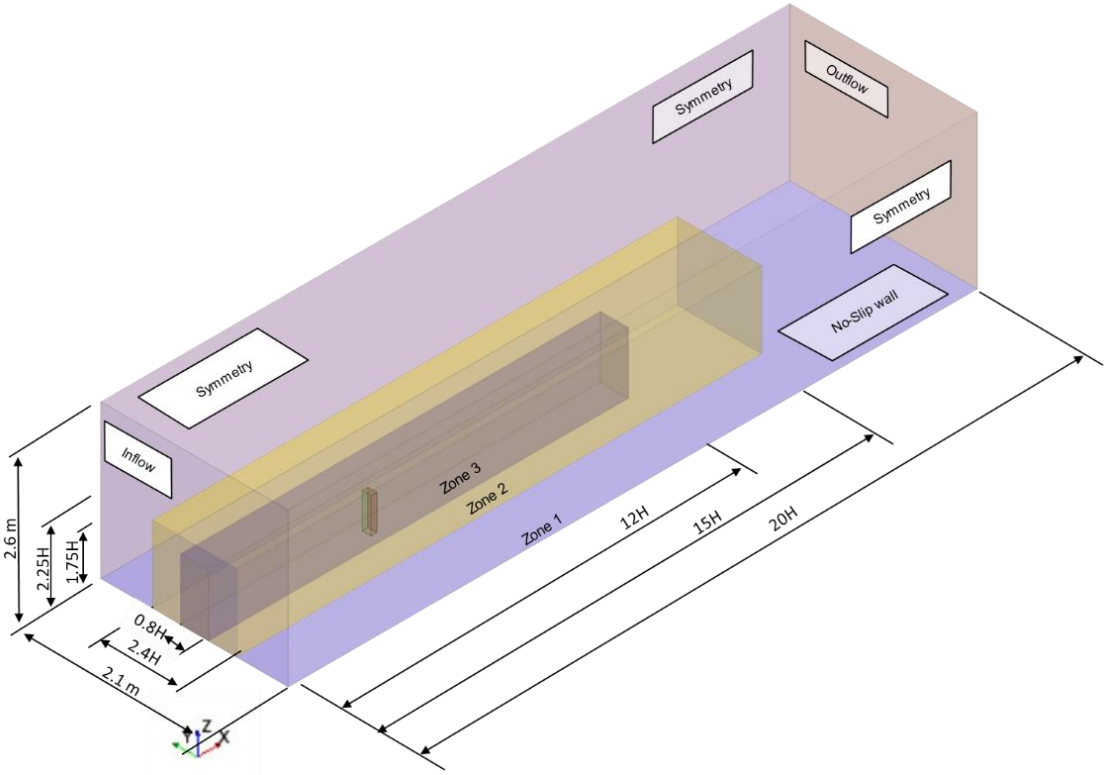

Fig. 3-7. Computational domain details and boundary conditions

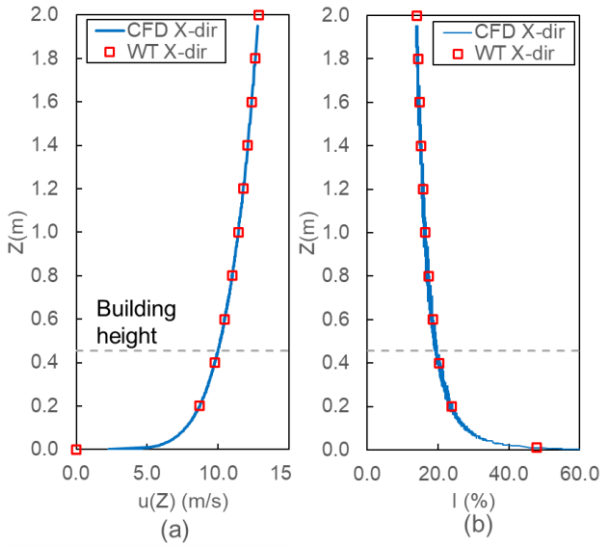

Fig. 3-8. (a) mean wind velocity and (b) turbulence intensity profiles used for the inflow boundary condition (Elshaer et al., 2016)

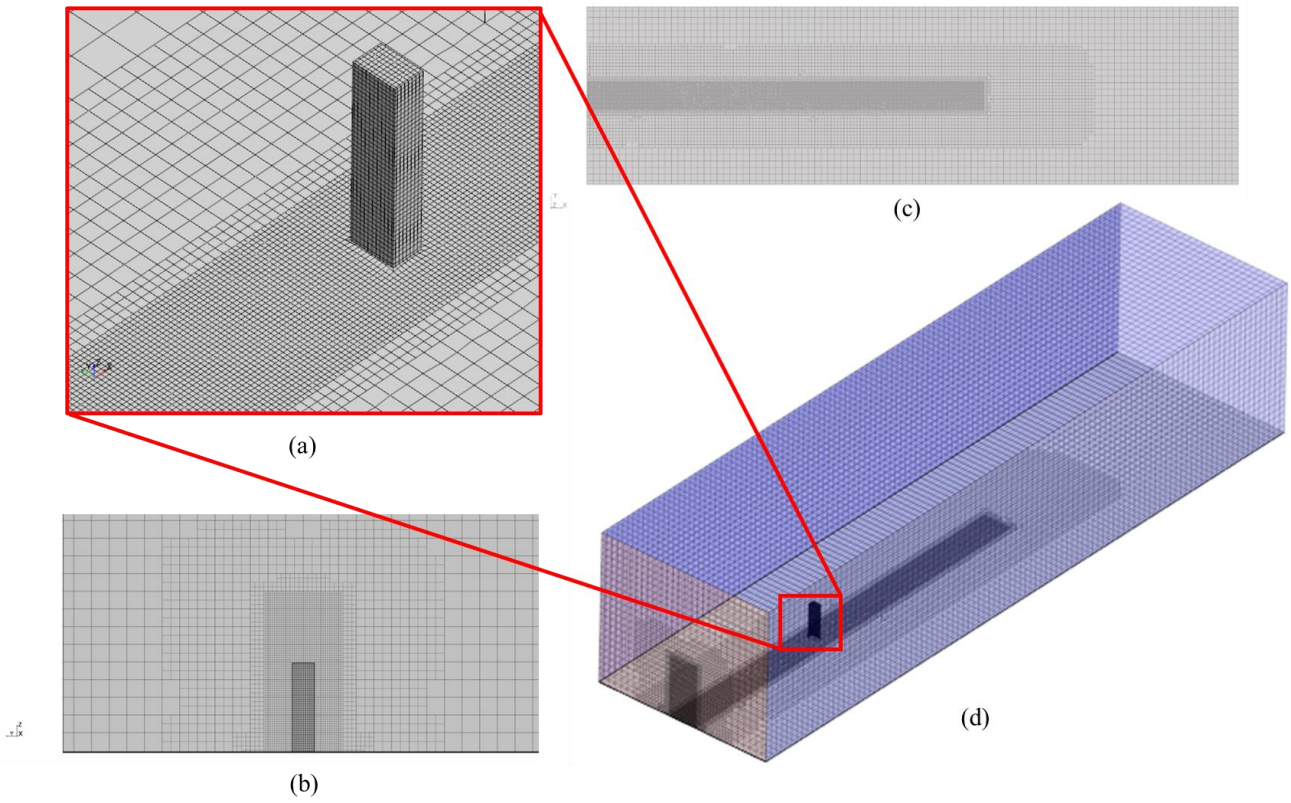

Fig. 3-9 Computational grid (a) near target buildings, (b) inlet, (c) ground and (c) 3d view for the computational domain.

Table 3-3. Building and computational domain dimensions

	Length (X-direction)	Width (Y-direction)	Height (Z-direction)
Building	30.5 m	45.7 m	182.5 m
Zone 1	20 H	wind tunnel width (2.1 m)	wind tunnel height (2.6 m)
Zone 2	15 H	2.4 H	2.25 H
Zone 3	12 H	0.8 H	1.75 H

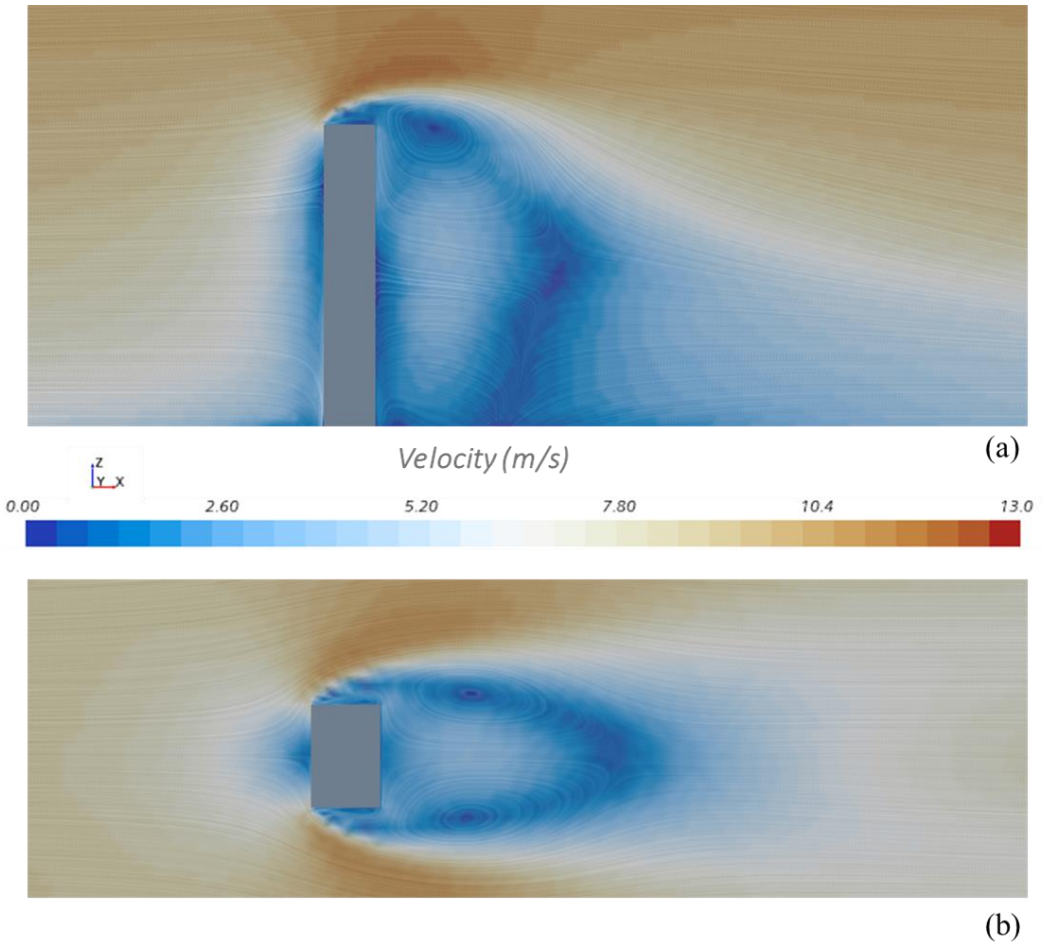

Fig. 3-10 Mean velocity magnitude with flow streamlines

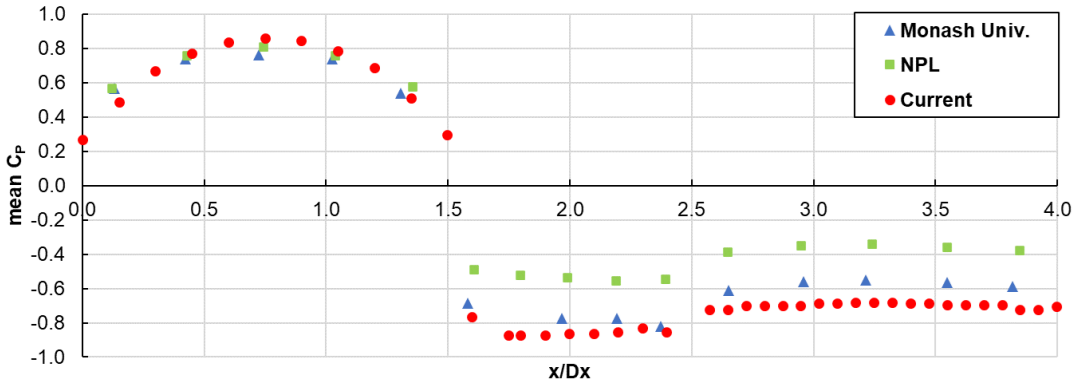

(a)

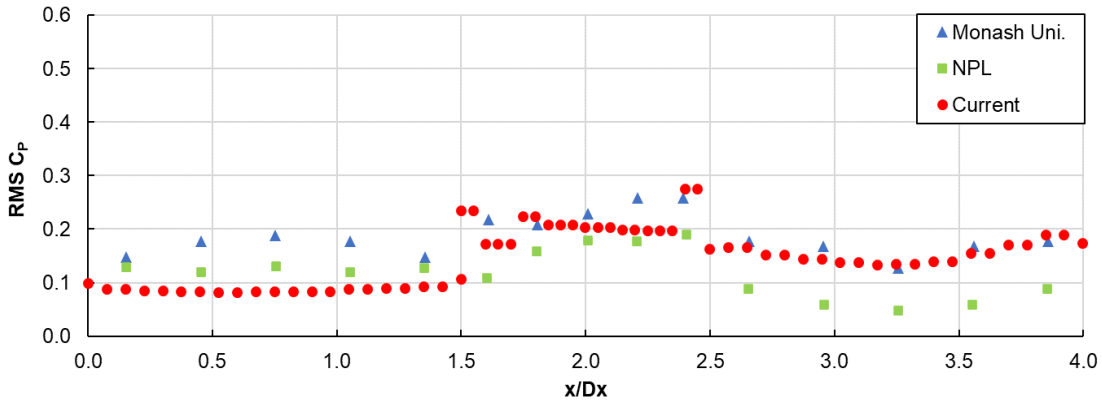

(b)

Fig. 3-11. (a) *mean* C_P (b) *RMS* C_P distribution over the horizontal section of the building at 2/3 H against BLWT test results

3.3.1.2. Wind load's time history *generation*

The previously validated computational domain and boundary conditions are used to investigate the aerodynamic performance of the selected building. The chosen case study building replaces the CAARC building bluff body with dimensions described in section 3.3.2. The building is discretized into 20 derived surfaces representing the tributary area of each storey in the building. These surfaces are responsible for integrating forces over time in the x and y directions. As shown in Fig. 3-12, a sample of wind load time history at the 10^{th} floor is generated for longitudinal direction (Y-axis) and across direction (x-axis). Then, the generated time histories for wind loads are defined in the FEM model as time history functions and applied at each storey's center of gravity in both directions.

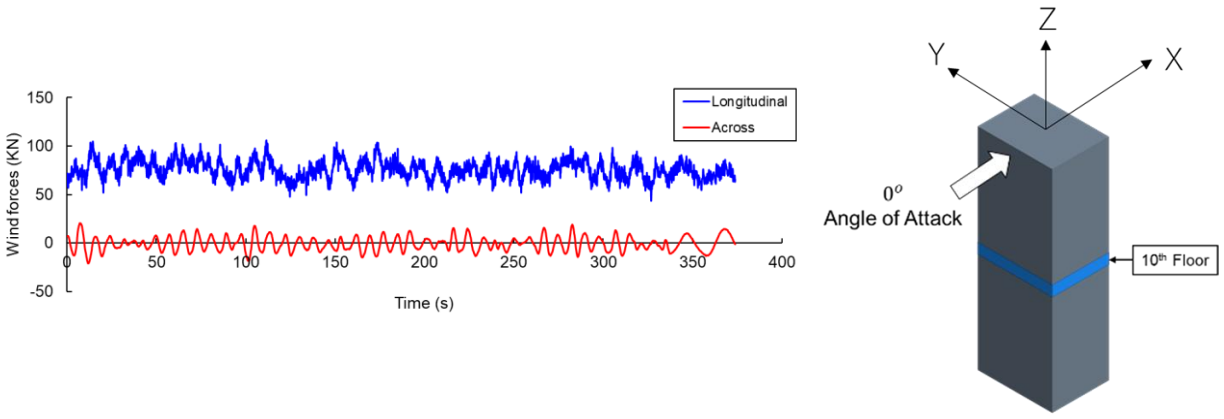

(a) (b)

Fig. 3-12. (a) Longitudinal and across wind forces time history at 10th floor, (b) Highlighted derived surface for the 10th floor

3.3.2. Structural details of the Case study

The adopted building is a multistorey residential building of 20 floors, with a storey height of 3.5 m, which follows (Alanani & Elshaer, 2023; Y. Zhang & Mueller, 2017). It is considered a single symmetric layout of rectangular-shaped beamless slabs with dimensions of 24.75 $m \times$ 18.75 m. Since the selected building height is 70 m, it is classified as a dynamically sensitive structure based on the (*National Building Code of Canada*, 2015). A superimposed dead load of 5 kN/m^2 and a live load of 1.9 $kN/m^2$are applied to all slabs. The objective of structural design is to identify the layout, dimensions (length and thickness) and reinforcement ratio for all structural elements. The column dimensions and shear wall thicknesses are set to be fixed. On the other hand, the layout and the length of reinforced concrete shear wall elements are determined using the SWOF. Finally, the reinforcement ratio can be adjusted by structural designers for the produced optimal layouts based on the project requirements. Initial values of structural elements are implemented (i.e., column cross-section and shear wall segments), as shown in Fig. 3-13. The layout shown in Fig. 3-13 is designed according to the CSA 23.3-14 (CSA (Canadian Standards Association), 2019) using concrete of $f_c' = 35\ MPa$ and steel reinforcement ASTM992 of grade 50. The ultimate limit state and serviceability limit load combinations are used for designing structural elements. An architectural layout is proposed for two apartments per storey, as shown

in Fig. 3-14 (a). Based on the proposed architectural layout, possible locations for shear walls are identified to fulfill architectural objectives as illustrated in Fig. 3-14 (b). A preprocessing stage is implemented to prepare the optimization problem that will be described in detail in the following sections. The dark grey lines in the Fig. 3-14 (b) is considered the domain for shear walls. To identify the length and the shape of shear walls, a discretization of this domain is performed based on a rectangular mesh of a predefined base size of one meter. As a result of this process, the domain will be divided into 170 one-meter segments of shear walls. For each model, different locations of columns will be identified to avoid overlapping between shear wall segments and columns. Column distribution is based on a rectangular mesh of a $6\ m$ span.

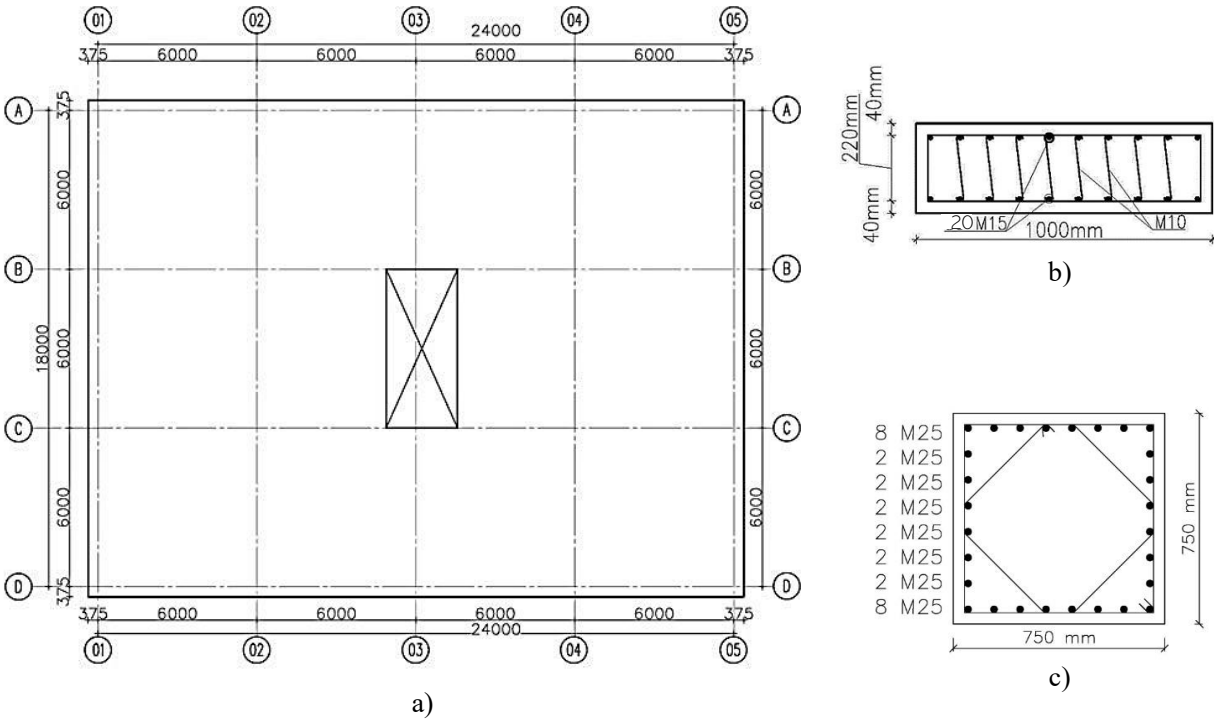

Fig. 3-13 (a) Slab plan layout, (b) shear wall segment and (c) column cross-section

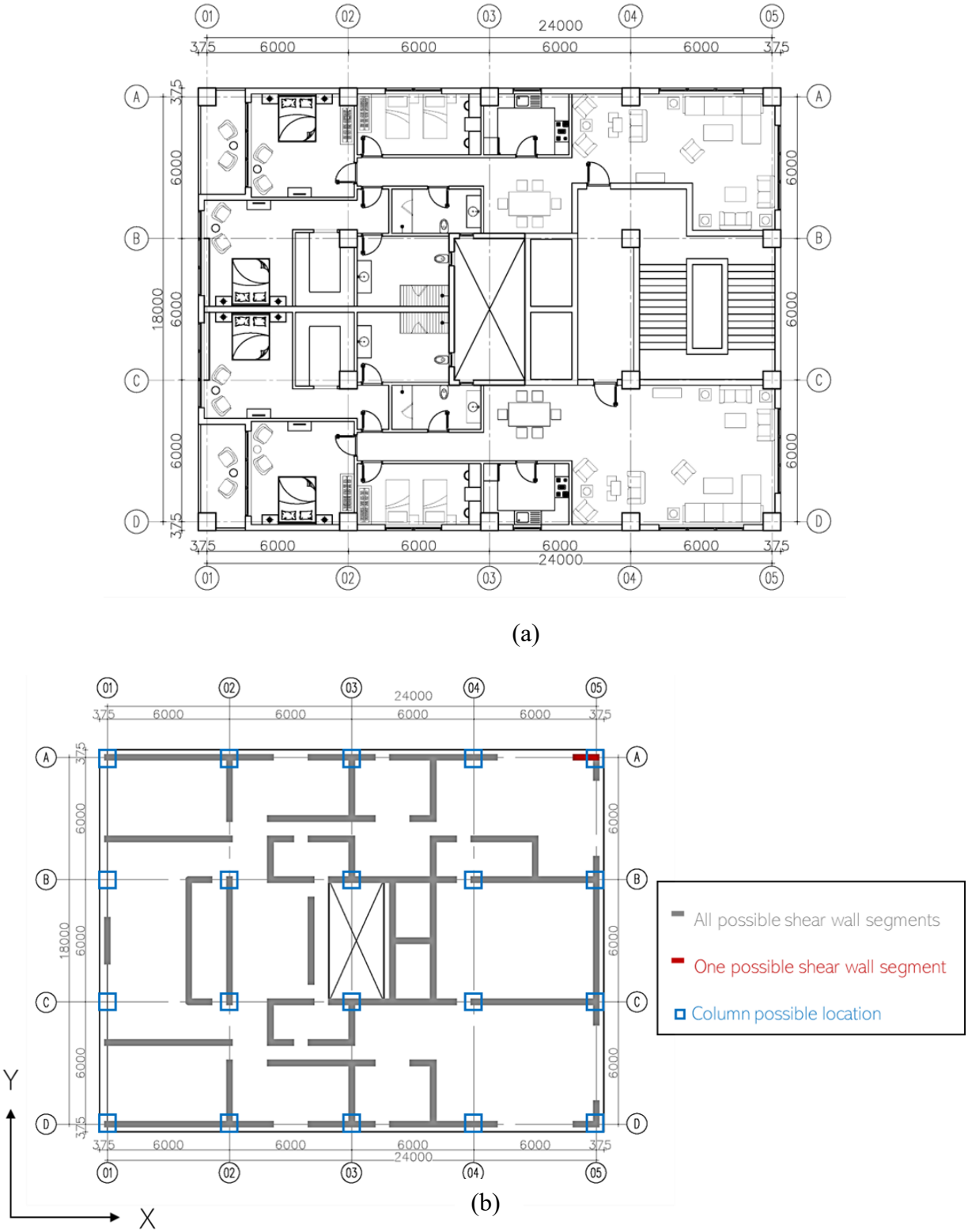

(a)

(b)

Fig. 3-14. (a) Architectural plan view and (b) possible shear wall locations

3.3.3. Finite Element Method model

3.3.3.1.FEM validation

A validation of the full-scale CAARC structure is adopted in this chapter based on (Brown et al., 2024). CAARC's dimensions are 180 m tall with a rectangular base of 30 m by 45 m long, respectively. It consists of 45 similar storeys, each of 4 m in height, with a 10-bay by 15-bay, as seen in Fig. 3-15 (a). Each bay is considered to be 3 m wide. The steel size members of the chosen CAARC structure are based on analysis by (C. M. Chan et al., 2009; M. Huang, 2017), and they were created based on an initial strength check following the AISC steel code (2001) to precisely duplicate the verified model. As indicated in Table 3-4, the steel columns and beams are chosen according to the W14 and W30 sizes, respectively. A fixed base support is considered to give the overall building a rigid floor connection. To get the dynamic drift responses, the structure serves as a moment-resisting frame with a modal damping ratio of 2%. The steel density is 7850 kg/m3, with a Young's Modulus and Poison's ratio of 200,000 MPa and 0.25, respectively. The first, second and third modes are found to be at 0.198, 0.281, and 0.361 Hz, respectively. Table 3-5 presents the design along-wind and across-wind base shear forces, the torsional base torque from the wind-induced structural loads at a velocity of 40 m/s. The overall applied wind loading was acquired using the numerical LES analysis and then applied to the FEM model to compare the structural response of the structure under a 0° wind angle of attack, as shown in Fig. 3-15 (a), (b) and (c) show a comparison of the lateral deflection and inter-storey drift along the x-direction at the most critical instant, respectively.

Table 3-4: Steel sections for the examined structures at a mean wind velocity of 40 m/s (Brown et al., 2024)

Storey levels	Beam size	Column size at
1 - 9	W30 x 357	W14 x 550
10 - 18	W30 x 326	W14 x 500
19 - 27	W30 x 292	W14 x 370
28 - 36	W30 x 261	W14 x 257
37 - 45	W30 x 211	W14 x 159

Table 3-5: Design wind loads for Building 1 subjected to a design mean wind velocity of 40 m/s (Brown et al., 2024)

Structure height (m)	Along-wind base shear (kN)	Across-wind base shear (kN)	Torsional base torque (kN.m)
180 (CAARC)	18826	28238	688307

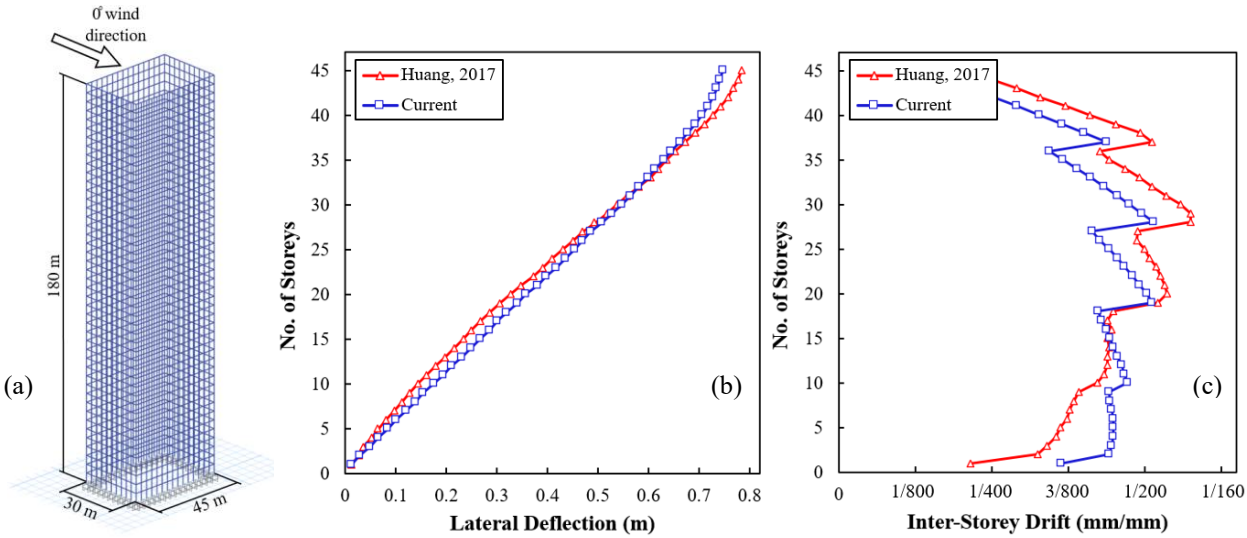

Fig. 3-15 (a) FEM CAARC model dimensions, (b) maximum deflection of storeys, and (c) maximum inter-storey drift in the along-wind direction (Brown et al., 2024)

3.3.3.2.Case study FEM model

A 3D linear Finite Element Model of the previously described structure is modelled in ETABS, a Finite Element Method (FEM) commercial software extensively used for designing tall buildings. Different FEM elements are adopted to capture a satisfactory performance of the structural elements. The most vital elements in this study are the shear wall segments modelled as shell-thin elements, which allow the capture of bending stresses and in-plane stresses. Slabs are modelled as shell-thin as well. Each slab, with all the attached elements, is assigned to a diaphragm to ensure

the transfer of lateral loads and unify the lateral displacement at any point all over the slab. On the other hand, the frame element is used for columns since the beam-column formulation is included to attain the effects of biaxial bending, torsion, axial deformation and biaxial shear deformation. Regarding load application, all generated wind load time histories are added to the centre of gravity of each story.

Since the dynamic response is the main focus of this study, a linear time history analysis is adopted, while the modal analysis is used to solve the general dynamic equilibrium equation shown in equation (3-1). A number of 30 mode shapes are predefined to be used for capturing more than 90% of the total dynamic mass participation ratio. In order to build up the training database, the maximum value of each parameter for all time steps is selected so the surrogate model can be built on those data, as explained in section 3.2. For instance, Fig. 3-16 shows a sample of the structural response resulting from the linear time history analysis from which the maximum value of displacement of each storey is exported and then used for the training process of the ANN surrogate model.

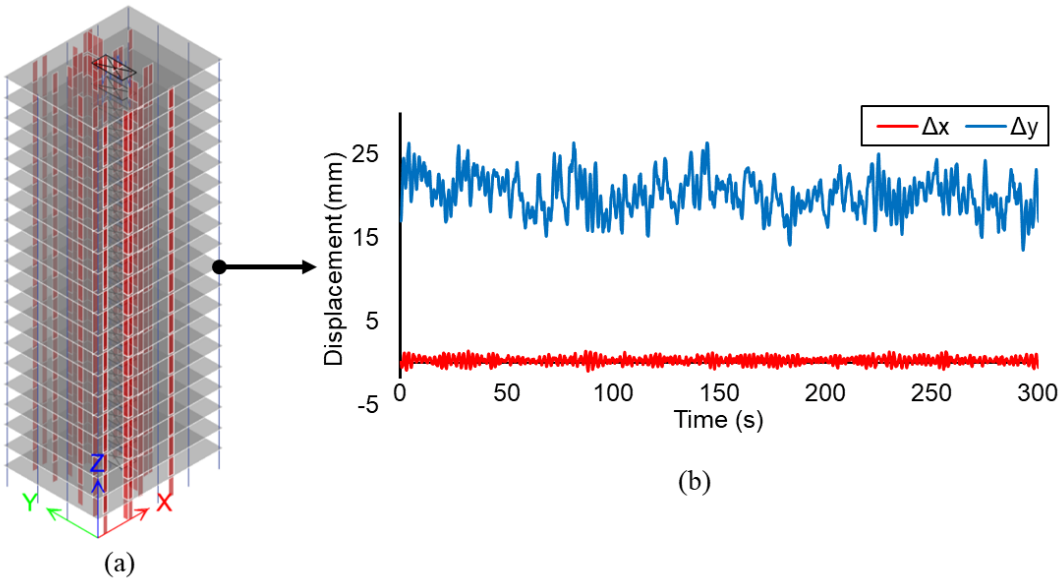

Fig. 3-16 (a) 3D Finite Element model and (b) 10th story displacement

3.4. Optimization problem description and results

In this section, a multi-objective optimization problem is presented. In order to exploit the potential of the developed optimization algorithm, all parameters (i.e., the total number of shear wall segments, the total number of piers, the eccentricity, and the standard deviation of base moments) are defined as objective functions except the drift, as it is defined as a constraint equivalent to the code limitation in clause 4.1.8.13 (*National Building Code of Canada*, 2015) for drift in both directions, as shown in equation (3-6). Then, a postprocessing Pareto pruning methodology using the "Direct selection method" is applied to the generated solutions to select a single layout based on an ordered prioritization of each objective function solution.

The mathematical formulation of the optimization problem is shown in (3-6), where S_i is a set of design variables of the optimization problems that represent each shear wall segment. C_{Total} indicates all constraints for each optimization problem. While δ_y and δ_x denote the maximum interstorey drift in the Y-direction and X-direction, respectively. $e_{C_M C_R}$ is the eccentricity of the center of rigidity, C_R, from the center of mass, C_M. σ_M represents the standard deviation of shear walls' base moments while N_P represents a number of formulated piers.

$$
\begin{aligned}
&find\ S = (S_1, S_2, S_3, \dots, S_N) \\
&minimize\ (\sum_{i=1}^{N} S_i\ , N_{\mathrm{P}}, e_{C_M C_R}, \sigma_M) \\
&Subjected\ to: C_{Total} = \left(\ \delta_y \leq 0.2\%, \delta_x \leq 0.2\%\right) \\
&Where\ S_i \in \{0,1\}\ (i = 1,2, \dots, N\ ), N = 170
\end{aligned}
\tag{3-6}
$$

In this optimization problem, A total of 700 solutions were generated by SWOF as optimal solutions on the Pareto Front based on the defined NSGA-II parameters shown in Table 3-6

Table 3-6. NSGA-II parameters of the optimization problem

Population size	Number of generations	Mutation function	Crossover ratio	Constraints (C_{Total})	
				δ_y	δ_x
2000	1000	"Mutation power"	0.8	0.2%	0.2%

Multiple runs have been conducted by altering the NSGA-II parameters to guarantee that SWOF will converge to the same optimal group of solutions. A total of 700 optimal solutions are located on the Pareto Front. It was noticed that multiple optimal solutions could get the same objective function values. For example, two layouts might have the same number of shear wall segments and the same number of piers formulated. Still, the configuration and the arrangement of those

segments can vary, resulting in different eccentricity values. A proper pruning algorithm can be applied in order to reduce the search scope among limited choices. Since (Alanani & Elshaer, 2023) have shown the priority of some parameters over others, the adopted pruning algorithm will seek extreme values for each parameter (i.e., objective function), as shown in Fig. 3-17. This selection process consists of two main steps: prioritizing and sorting. Prioritizing is a ranking process where objective functions are given ranks based on their priority to the designer. As presented in Fig. 3-17, The four objective functions are ranked based on their priorities, where the number of shear wall segments (S) is ranked first, and the standard deviation of the base moments is ranked last. The algorithm will sort the optimal solutions based on the minimum number of shear segments. As explained before, multiple solutions on the Pareto Front might yield the same number of shear wall segments. Therefore, the algorithm will sort those equivalents based on the minimum number of piers formulated (P). Then, if they happen to be equal, layouts can be arranged based on the eccentricity of the center of mass and the center of rigidity (E), then the standard deviation of base moments (M). The resulting layout of this process can be labelled as (S-P-E-M). With four objective functions, the number of all possible optimal layouts will be minimized to 24 out of 700 solutions, where each objective function can be set to be the 1st priority, and then permutations can be applied. As shown in Fig. 3-18, four layouts are selected using the previously described algorithm to show the structural response based on the prioritization of each objective function.

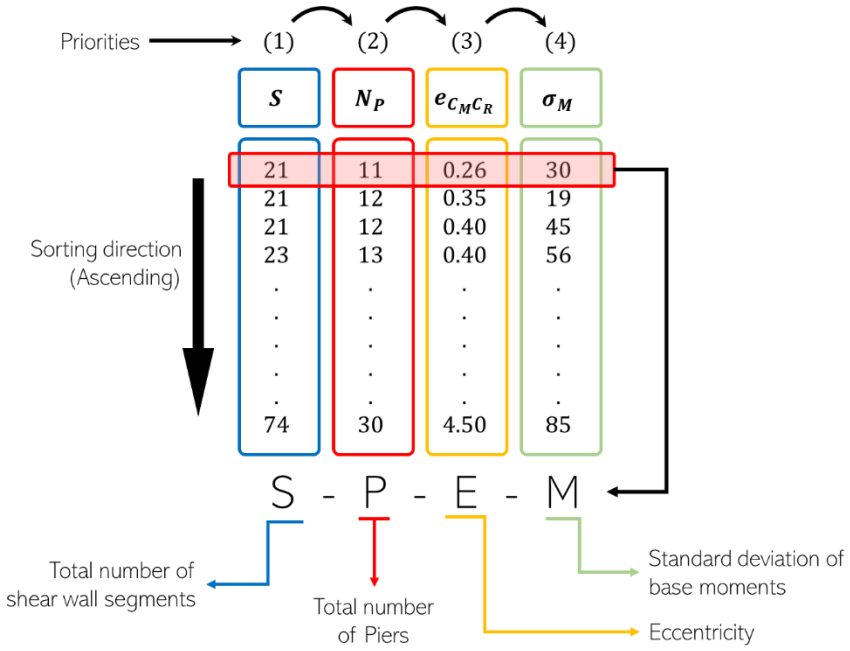

Fig. 3-17. Selection of optimal solutions on the Pareto Front

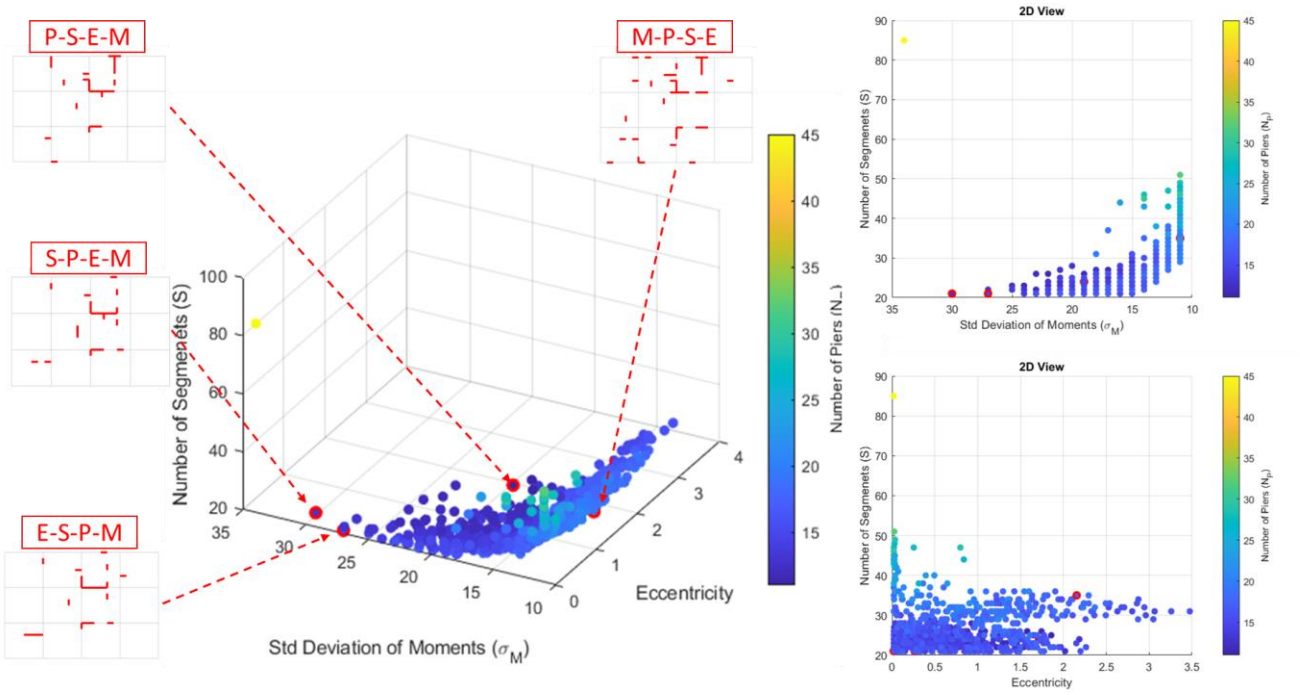

Fig. 3-18 Pareto Front optimal layouts and corresponding objective function values.

In Fig. 3-19, a comparison is made between the four selected optimal layouts to show how prioritizing objective functions can affect the layout of shear walls. As shown in S-P-E-M, the

least number of shear wall segments can be achieved by prioritizing (S). For P-S-E-M, it can be noticed that the number of piers is reduced from 11 to 10. The change in the number of piers is not tremendous, as the number of piers and segments are expected to be correlated. However, there is a noticeable change in the eccentricity and standard deviation of moment values. Through prioritizing the eccentricity (E) in E-S-P-M, it was found that it has the same number of shear wall segments and piers similar to S-P-E-M. Yet, the difference in priorities pushed SWOF to obtain various configurations of shear wall segments that affected the eccentricity and the distribution of base moments over piers. Putting the standard deviation of base moments (M) as 1st rank in M-P-S-E made SWOF increase the number of shear wall segments and piers to maintain the least variance in the moments' distribution over shear wall segments. Moreover, it was noticed that most of the generated solutions pushed the constraint values to the limit due to the inversely proportional relationship between the number of shear wall segments and the drift. The increase in shear wall segments will increase the structural stiffness and reduce the drift, accordingly, as shown in Fig. 3-20.

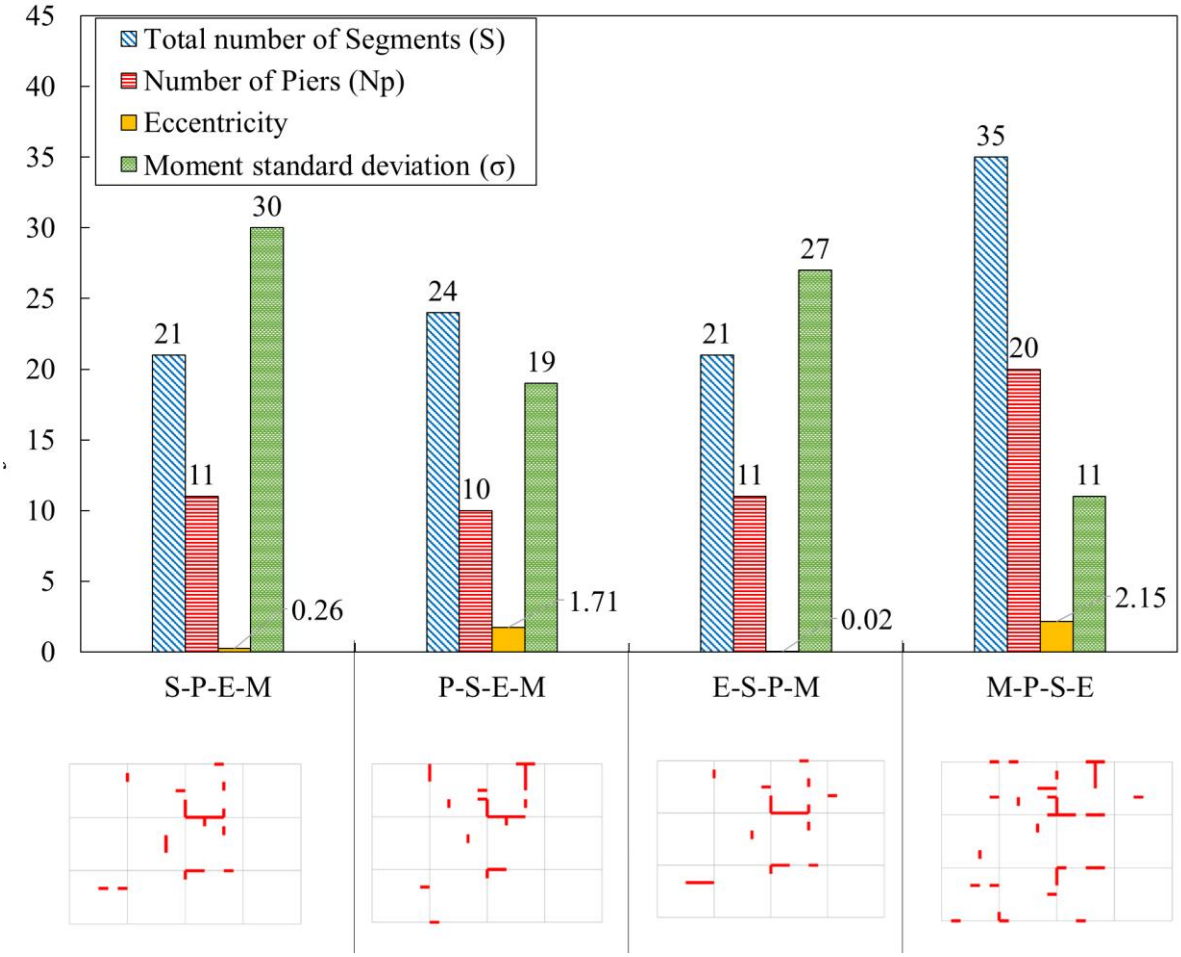

Fig. 3-19 Values of objective functions for a sample of optimal solutions on the Pareto Front

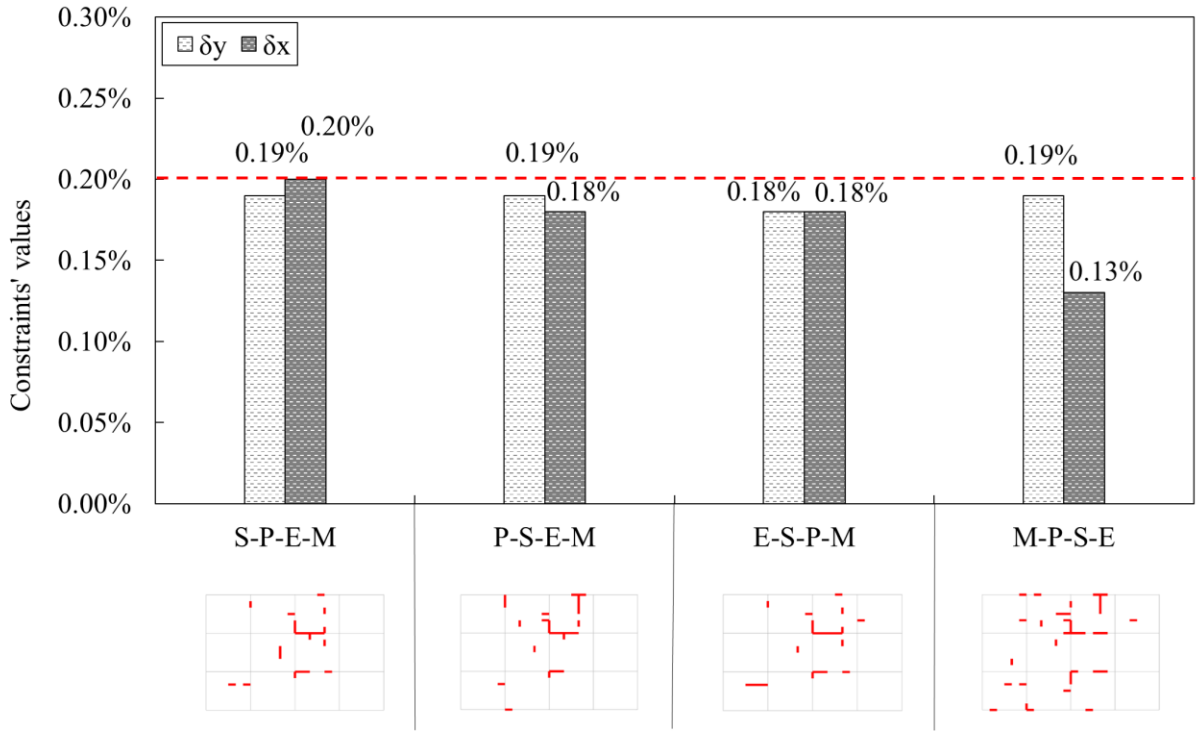

Fig. 3-20. Drift constraint values for a sample of optimal solutions on the Pareto Front

Regarding the limit state design, it was tackled indirectly in this study through the σ_M objective function. For Instance, in Fig. 3-21, Comparing the frequency of occurrence of the demand-to-capacity ratio of each formulated pier within the four selected solutions shows that Prioritizing the σ_M as in M-P-S-E, resulted in 89% of piers satisfying the demand-to-capacity ratio based on the (*National Building Code of Canada*, 2015), while only two piers will require slight modification in the reinforcement ratio, which will yield a safe design, as presented in Fig. 3-21. Comparing the M-P-S-E solution with other optimal layouts with lower rank for σ_M shows an exceedance in the demand-to-capacity ratio that requires more adjustment in the final design to satisfy the allowable demand-to-capacity ratio. This selection process requires a compromising decision based on the designers' objectives to either use more shear wall segments with an appropriate moment distribution or to alter the reinforcement ratio to withstand the generated moment, as shown in Fig. 3-22.

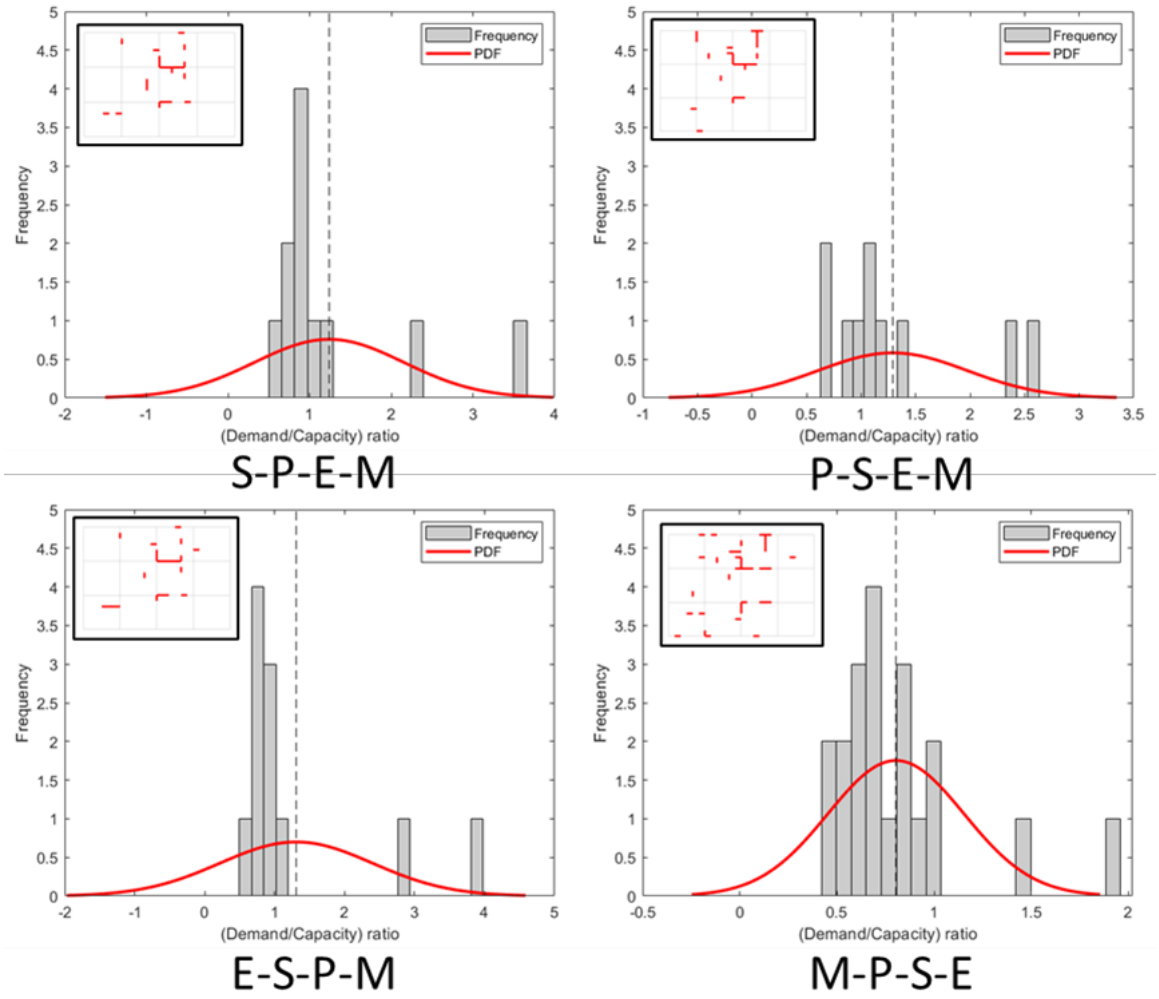

Fig. 3-21. Demand/capacity ratio histogram and probability distribution function for all piers for a sample of optimal solutions on the Pareto Front.

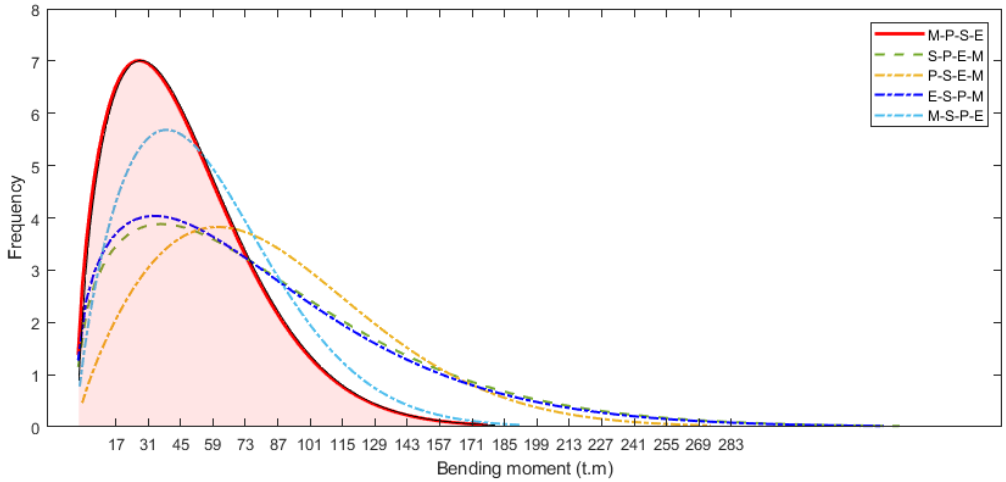

Fig. 3-22. Probability distribution function for 5 optimal solutions on the Pareto Front

3.5. Conclusion

In the current study, a novel multi-objective LLRS (i.e., shear walls) layout optimization framework is presented for dynamically sensitive tall buildings subjected to stochastic wind load. SWOF is developed to find the optimal layout for the Lateral Load Resisting System (LLRS) of tall buildings subjected to wind loads. It couples the genetic algorithm (GA), artificial neural network (ANN) models, and large eddy simulation (LES). The ANN model estimates the objective function values (e.g., eccentricity) and constraint values (e.g., drift) after being trained using a FEM-based database of different combinations of design variables (i.e., shear wall layouts) and the corresponding objective function and constraint values. NSGA-II is adopted as a multi-objective optimization algorithm to form a Pareto Front of optimal solutions based on the defined objective functions and constraints. Four objective functions are used to control the structural response of tall buildings based on the shear walls' layout, including the total number of shear wall segments ($\sum S_i$), the total number of formulated piers (N_P), the eccentricity ($e_{C_M C_R}$) of the center of rigidity (C_R) from the center of mass (C_M), and the standard deviation of shear walls' base moments (σ_M). In addition to the architectural constraints, two constraints are adopted, which are the maximum interstorey drift in Y-direction (δ_y) and X-direction (δ_x). In order to reduce the number of optimal layout solutions on the Pareto Front, a pruning algorithm is used to limit the optimal solutions to 24 layouts. This will enable designers to use the direct selection method to choose an appropriate layout that fits the project's objectives. It was noted that prioritizing the standard deviation of base moments yielded six layouts that required slight modifications in the reinforcement ratio for less than 10% of shear wall segments to satisfy the required demand-to-capacity ratio. Moreover, using ANN as a surrogate model proved its efficiency in capturing complex variations in objective functions and constraints with a correlation coefficient that ranges

between 90% to 98%. In addition, it enables SWOF to become capable of exploring numerous possible layouts in an affordable computational time.

3.6. References

Aboshosha, H., Elshaer, A., Bitsuamlak, G. T., & El Damatty, A. (2015). Consistent inflow turbulence generator for LES evaluation of wind-induced responses for tall buildings. *Journal of Wind Engineering and Industrial Aerodynamics*, *142*, 198–216. https://doi.org/10.1016/J.JWEIA.2015.04.004

Alanani, M., & Elshaer, A. (2022). Structural Layout Optimization of Tall Buildings Against Wind Load. *Proceedings of the Canadian Society of Civil Engineering Annual Conference 2022*. https://www.researchgate.net/publication/361756060_Structural_Layout_Optimization_of_Tall_Buildings_Against_Wind_Load

Alanani, M., & Elshaer, A. (2023). ANN-based optimization framework for the design of wind load resisting system of tall buildings. *Engineering Structures*, *285*, 116032. https://doi.org/10.1016/j.engstruct.2023.116032

ASCE. (2017). Minimum Design Loads for Buildings and Other Structures. In *ANSI/ASCE Standard* (Issue 7 98). American Society of Civil Engineers. https://doi.org/10.1061/9780872629042

Baldock, R., & Shea, K. (2006). Structural topology optimization of braced steel frameworks using genetic programming. *Lecture Notes in Computer Science (Including Subseries Lecture Notes in Artificial Intelligence and Lecture Notes in Bioinformatics)*, *4200 LNAI*, 54–61. https://doi.org/10.1007/11888598_6

Baldock, R., Shea, K., & Eley, D. (2005). Evolving optimized braced steel frameworks for tall buildings using modified pattern search. *Proceedings of the 2005 ASCE International Conference on Computing in Civil Engineering*, 631–642. https://doi.org/10.1061/40794(179)60

Bendsøe, M. P., & Sigmund, O. (2004). Topology Optimization. In *Topology Optimization*. Springer Berlin Heidelberg. https://doi.org/10.1007/978-3-662-05086-6

Bernardini, E., Spence, S. M. J., Wei, D., & Kareem, A. (2015). Aerodynamic shape optimization of civil structures: A CFD-enabled Kriging-based approach. *Journal of Wind Engineering and Industrial Aerodynamics*, *144*, 154–164.

Bobby, S., Spence, S. M. J., Bernardini, E., & Kareem, A. (2014). Performance-based topology optimization for wind-excited tall buildings: A framework. *Engineering Structures*, *74*, 242–255. https://doi.org/10.1016/j.engstruct.2014.05.043

Braun, A. L., & Awruch, A. M. (2009). Aerodynamic and aeroelastic analyses on the CAARC standard tall building model using numerical simulation. *Computers & Structures*, *87*(9), 564–581.

Brown, T., Alanani, M., Elshaer, A., & Issa, A. (2024). Formulation of Separation Distance to Mitigate Wind-Induced Pounding of Tall Buildings. *Buildings*, *14*(2), 479. https://doi.org/10.3390/buildings14020479

Chan, C.-M., Grierson, D. E., & Sherbourne, A. N. (1995). Automatic Optimal Design of Tall

Steel Building Frameworks. *Journal of Structural Engineering*, *121*(5), 838–847. https://doi.org/10.1061/(asce)0733-9445(1995)121:5(838)

Chan, C. M., Chui, J. K. L., & Huang, M. F. (2009). Integrated aerodynamic load determination and stiffness design optimization of tall buildings. *Structural Design of Tall and Special Buildings*, *18*(1), 59–80. https://doi.org/10.1002/tal.397

Chopra, A. K. (2012). *Dynamics of structures : theory and applications to earthquake engineering, 4/E*. https://www.pearson.com/us/higher-education/product/Chopra-Dynamics-of-Structures-4th-Edition/9780132858038.html

Chun, J., Song, J., & Paulino, G. H. (2016). Structural topology optimization under constraints on instantaneous failure probability. *Structural and Multidisciplinary Optimization*, *53*(4), 773–799. https://doi.org/10.1007/s00158-015-1296

CSA (Canadian Standards Association). (2019). *CSA (2019) Design of concrete structures. Standard CAN/CSA A23.3:19* (A23.3:19).

CSI. (2018). *ETABS building analysis and design* (2018.1.1). Computers and Structures, Inc. www.csiamerica.com

CTBUH. (2019). Council on Tall Buildings and Urban Habitat. In *Damping Technologies for Tall Buildings* (Vol. 1, Issue 1, pp. v–vi). Elsevier. https://doi.org/10.1016/B978-0-12-815963-7.00022-1

Cui, W., & Caracoglia, L. (2020). Performance-Based Wind Engineering of Tall Buildings Examining Life-Cycle Downtime and Multisource Wind Damage. *Journal of Structural Engineering*, *146*(1), 1–12. https://doi.org/10.1061/(ASCE)ST.1943-541X.0002479

Dagnew, A. K., & Bitsuamlak, G. T. (2010). LES evaluation of wind pressures on a standard tall building with and without a neighboring building. *The Fifth International Symosium on Computational Wind Engineering (CWE2010) Chapel Hill, North Carolina, USA*, *2007*.

Deb, K., Pratap, A., Agarwal, S., & Meyarivan, T. (2002). A fast and elitist multiobjective genetic algorithm: NSGA-II. *IEEE Transactions on Evolutionary Computation*, *6*(2), 182–197. https://doi.org/10.1109/4235.996017

Deng, T., Fu, J., Zheng, Q., Wu, J., & Pi, Y. (2019). Performance-Based Wind-Resistant Optimization Design for Tall Building Structures. *Journal of Structural Engineering*, *145*(10). https://doi.org/10.1061/(ASCE)ST.1943-541X.0002383

Dragoiescu, C., Garber, J., & Kumar, K. S. (2006). A comparison of force balance and pressure integration techniques for predicting wind-induced responses of tall buildings. *Structures Congress 2006: Structural Engineering and Public Safety*, 1–10.

Elshaer, A., Aboshosha, H., Bitsuamlak, G., El Damatty, A., & Dagnew, A. (2016). LES evaluation of wind-induced responses for an isolated and a surrounded tall building. *Engineering Structures*, *115*, 179–195. https://doi.org/10.1016/j.engstruct.2016.02.026

Elshaer, A., & Bitsuamlak, G. (2018). Multiobjective Aerodynamic Optimization of Tall Building Openings for Wind-Induced Load Reduction. *Journal of Structural Engineering*,

144(10), 4018198. https://doi.org/10.1061/(ASCE)ST.1943-541X.0002199

Elshaer, A., Bitsuamlak, G., El-Damatty, A., & El Damatty, A. (2017). Enhancing wind performance of tall buildings using corner aerodynamic optimization. *Engineering Structures*, *136*, 133–148. https://doi.org/10.1016/j.engstruct.2017.01.019

Fragiadakis, M., & Lagaros, N. D. (2011). An overview to structural seismic design optimisation frameworks. *Computers & Structures*, *89*(11–12), 1155–1165. https://doi.org/10.1016/j.compstruc.2010.10.021

Gholizadeh, S., & Ebadijalal, M. (2018). Performance based discrete topology optimization of steel braced frames by a new metaheuristic. *Advances in Engineering Software*, *123*(June), 77–92. https://doi.org/10.1016/j.advengsoft.2018.06.002

Gomez, F., Spencer, B. F., & Carrion, J. (2020). Topology optimization of buildings subjected to stochastic base excitation. *Engineering Structures*, *223*(February), 111111. https://doi.org/10.1016/j.engstruct.2020.111111

Gomez, F., Spencer, B. F., & Carrion, J. (2021). Topology optimization of buildings subjected to stochastic wind loads. *Probabilistic Engineering Mechanics*, *64*(July 2020), 103127. https://doi.org/10.1016/j.probengmech.2021.103127

Huang, M. (2017). High-Rise Buildings under Multi-Hazard Environment. In *High-Rise Buildings under Multi-Hazard Environment*. Springer Singapore. https://doi.org/10.1007/978-981-10-1744-5

Huang, S., Li, Q. S., & Xu, S. (2007). Numerical evaluation of wind effects on a tall steel building by CFD. *Journal of Constructional Steel Research*, *63*(5), 612–627. https://doi.org/10.1016/j.jcsr.2006.06.033

Joyner, M. D., Puentes, B., Gardner, C., Steinberg, S., & Sasani, M. (2022). Multiobjective Optimization of Building Seismic Design for Resilience. *Journal of Structural Engineering*, *148*(4), 1–13. https://doi.org/10.1061/(ASCE)ST.1943-541X.0003286

Kareem, A., Kijewski, T., & Tamura, Y. (1999). Mitigation of motions of tall buildings with specific examples of recent applications. *Wind and Structures*, *2*(3), 201–251. https://doi.org/10.12989/was.1999.2.3.201

Kareem, A., Spence, S., Bernardini, E., Bobby, S., & Wei, D. (2013). Using Computational Fluid Dynamics to Optimize Tall Building Design. *International Journal on Tall Buildings and Urban Habitat*, *CTBUH Journal 2013 Issue III*.

Lagaros, N. D., & Plevris, V. (2022). Artificial Intelligence (AI) Applied in Civil Engineering. *Applied Sciences*, *12*(15), 7595. https://doi.org/10.3390/app12157595

Lou, H. P., Ye, J., Jin, F. L., Gao, B. Q., Wan, Y. Y., & Quan, G. (2021). A practical shear wall layout optimization framework for the design of high-rise buildings. *Structures*, *34*(September), 3172–3195. https://doi.org/10.1016/j.istruc.2021.09.038

Luo, X., Suksuwan, A., Spence, S. M. J., & Kareem, A. (2017). Topology Optimization and Performance-Based Design of Tall Buildings: A Spatial Framework. *Structures Congress*

2017, 447–458. https://doi.org/10.1061/9780784480410.037

MacKay, D. J. C. (1992). Bayesian Interpolation. *Neural Computation*, *4*(3), 415–447. https://doi.org/10.1162/neco.1992.4.3.415

Martin, A., & Deierlein, G. G. (2020). Structural topology optimization of tall buildings for dynamic seismic excitation using modal decomposition. *Engineering Structures*, *216*(April), 110717. https://doi.org/10.1016/j.engstruct.2020.110717

MATLAB. (2023). *MATLAB and Statistics Toolbox Release 2023b* (9.10). The MathWorks Inc.

Melbourne, W. H. (1980). Comparison of measurements on the CAARC standard tall building model in simulated model wind flows. *Journal of Wind Engineering and Industrial Aerodynamics*, *6*(1–2), 73–88. https://doi.org/10.1016/0167-6105(80)90023-9

National Building Code of Canada. (2015). Canadian Commission on Building and Fire Codes National Research Council of Canada.

Papadrakakis, M., & Lagaros, N. D. (2002). Reliability-based structural optimization using neural networks and Monte Carlo simulation. *Computer Methods in Applied Mechanics and Engineering*, *191*(32), 3491–3507. https://doi.org/10.1016/S0045-7825(02)00287-6

Pizarro, P. N., & Massone, L. M. (2021). Structural design of reinforced concrete buildings based on deep neural networks. *Engineering Structures*, *241*(July 2020), 112377. https://doi.org/10.1016/j.engstruct.2021.112377

Roser, M., Ritchie, H., & Ortiz-Ospina, E. (2019). *World Population Growth - Our World in Data*. https://ourworldindata.org/world-population-growth

Sotiropoulos, S., & Lagaros, N. D. (2022). Optimum topological bracing design of tall steel frames subjected to dynamic loading. *Computers and Structures*, *259*(January). https://doi.org/10.1016/j.compstruc.2021.106705

Tanaka, H., Matsuoka, Y., Kawakami, T., Azegami, Y., Yamamoto, M., Ohtake, K., & Sone, T. (2019). Optimization calculations and machine learning aimedat reduction of wind forces acting on tall buildingsand mitigation of wind environment. *International Journal of High-Rise Buildings*, *8*(4), 291–302. https://doi.org/10.21022/IJHRB.2019.8.4.291

Tanaka, H., Tamura, Y., Ohtake, K., Nakai, M., Chul Kim, Y., Chul, Y., & Chul Kim, Y. (2012). Experimental investigation of aerodynamic forces and wind pressures acting on tall buildings with various unconventional configurations. *Journal of Wind Engineering and Industrial Aerodynamics*, *107–108*, 179–191. https://doi.org/10.1016/j.jweia.2012.04.014

Thordal, M. S., Bennetsen, J. C., Capra, S., & Koss, H. H. H. (2020). Towards a standard CFD setup for wind load assessment of high-rise buildings: Part 1 – Benchmark of the CAARC building. *Journal of Wind Engineering and Industrial Aerodynamics*, *205*(January), 104283. https://doi.org/10.1016/j.jweia.2020.104283

Zakian, P., & Kaveh, A. (2020). Topology optimization of shear wall structures under seismic loading. *Earthquake Engineering and Engineering Vibration*, *19*(1), 105–116. https://doi.org/10.1007/s11803-020-0550-5

Zhang, Y., & Mueller, C. (2017). Shear wall layout optimization for conceptual design of tall buildings. *Engineering Structures*, *140*, 225–240. https://doi.org/10.1016/j.engstruct.2017.02.059

Zhou, X., Wang, L., Liu, J., Cheng, G., Chen, D., & Yu, P. (2022). Automated structural design of shear wall structures based on modified genetic algorithm and prior knowledge. *Automation in Construction*, *139*(April), 104318. https://doi.org/10.1016/j.autcon.2022.104318

Zou, X. K., Chan, C. M., Li, G., & Wang, Q. (2007). Multiobjective Optimization for Performance-Based Design of Reinforced Concrete Frames. *Journal of Structural Engineering*, *133*(10), 1462–1474. https://doi.org/10.1061/(asce)0733-9445(2007)133:10(1462)

CHAPTER 4

4. PERFORMANCE-BASED LAYOUT OPTIMIZATION FRAMEWORK OF TALL BUILDINGS SUBJECTED TO DYNAMIC WIND LOAD

4.1. Introduction

The whole world is approaching a critical threshold of global warming, reaching a $1.5^{o}C$ increase in the global average temperature will change the inhabitant life dramatically (IPCC, 2023). As global warming and environmental concerns continue to escalate, the construction industry faces growing concerns about its significant contribution to greenhouse gas emissions, with a total of 39% energy related CO_2 emissions. Among the various sectors, building construction is a major contributor to embodied carbon emissions, which represent the greenhouse gases emitted during the entire life cycle of a building, from material extraction to construction and demolition. The embodied carbon emissions only contribute to 11% of the global carbon emissions (Adams et al., 2019). Consequently, reducing the carbon footprint of buildings has become a crucial requirement in the pursuit of sustainable and environmentally responsible practices. In the context of addressing climate change and environmental impacts, the structural design of buildings plays a pivotal role. During the design stage, careful consideration of structural choices can significantly influence the embodied carbon emissions of the building (Cerè et al., 2022; Lagaros et al., 2009). By optimizing the design and material selection, engineers can reduce overall structural materials consumption through innovative design methodologies that reduce embodied carbon emissions. Performance-Based Design (PBD) offers a promising approach to address these challenges. By focusing on the performance of buildings under various environmental loads, such as wind and seismic forces, PBD seeks to design structures that are not only safe and reliable but also more sustainable (Mokarram & Banan, 2018). In the last few decades, Performance-based design (PBD) has grasped the attention of stakeholders and municipalities toward having a quantitative approach that can

predict buildings' performance through catastrophic events (e.g., extreme wind speeds, tornados, floods). These privileges provided by PBD make it more favourable compared to the deterministic-design approach, which lacks the ability to consider the stochastic nature of loads and relies on conservative factors of safety to include the uncertainties of loads, materials and construction. These perspective guidelines will most probably result in noneconomic and inefficient designs, especially when lateral loads are considered for tall buildings. The temporal and spatial dynamic nature of lateral loads (e.g., wind and earthquakes) require an advanced simulation to capture tall buildings' dynamic behaviour accurately. In general, PBD methods provide specific performance objectives that should be met. Moreover, reliability analysis included within PBD, either explicitly or implicitly, offers a thorough consideration of all uncertainties within the design (Valdebenito & Schuëller, 2010; Wen, 2001). The need to assess the standing buildings to identify their capacity for rehabilitation, especially after severe earthquakes, led to the development of the Performance-Based Seismic Design (PBSD) approach. PBSD emerged as a response to the limitations of traditional deterministic provisions for seismic design. The 1990s marked the initial development of PBSD when significant economic losses and functional disruptions occurred during the Loma Prieta and Northridge earthquakes (Petrini & Ciampoli, 2012). The need for resilient communities encourages organizations like the Applied Technology Council (ATC), funded by FEMA, to develop procedures for implementing PBSD. The publication of the NEHRP Guidelines and Commentary for Seismic Rehabilitation of Buildings in 1997 marked the foundation of the first generation of PBSD methods (Federal Emergency Management Agency (FEMA), 1997). These guidelines introduced key concepts that underpin the philosophy of PBSD and serve as the basis for applying the principles of Performance-Based Design (PBD) to other natural and man-made hazards. Other influential reports, such as ATC-32, ATC-40, and FEMA 356 ((FEMA) & (ASCE),

2000; Applied Technology Council, 1996a, 1996b), also contributed to the development of PBSD during this period. The developed PBSD allowed for exploring various lateral load resisting systems not included in the code provisions and making exceptions to code exact wordings. The main concept introduced through these reports is the performance objectives, which consist of specific design events and performance levels. Standard performance levels were established with performance-oriented descriptions, such as fully operational, functional (Immediate Occupation), life safety, and near collapse (Collapse Prevention). These performance levels quantified both structural and non-structural damages using response parameters and limitations like inter-story drifts, inelastic member deformations, and member forces. In the first generation of PBSD procedures, a building meets the requirements if the member forces and deformations on each element satisfy the predefined limits (e.g., drift limitations). This approach aimed to move beyond simply achieving life safety and avoidance of collapse, acknowledging that these implicit performance targets could not reliably be met using traditional prescriptive approaches.

However, several limitations were identified, including the focus on component-level damage assessment. To address these shortcomings, FEMA's recently published P-58 volumes outlined a seismic performance assessment methodology that explicitly considers uncertainties in response prediction and communicates performance through system-level measures (FEMA P58-6, 2018). It is important to note that the Pacific Earthquake Engineering Research (PEER) center's framework, while developed for PBSD, is adaptable and can be applied to other natural hazards (S. M. J. J. Spence & Arunachalam, 2022). This flexibility enables the framework to be used in various decision models, extending the application of PBD principles to achieve resilient designs for mitigating the effects of different natural hazards. Since the core of PBD is allowing a wide spectrum of alternative solutions relying on four main stages of analysis: from hazard analysis to

structural analysis and damage analysis and ending up with a loss analysis for decision making. Building upon these principles and methodologies of PBSD, similar concepts and approaches can be extended to Performance-Based Wind Design (PBWD) to enhance the understanding and resilience of structures subjected to wind loads through quantifying the intensity of wind events and reducing loss analysis.

Various studies proposed formulations, approaches and frameworks of PBWD to provide a guideline that engineers can follow and fulfill the stakeholders' objectives (Abdelwahab et al., 2023; Bernardini, Spence, Kwon, et al., 2015; Bezabeh et al., 2020; Jeong et al., 2021; Preetha Hareendran et al., 2022). (ASCE, 2019) is considered the first PBWD official guidelines that provide an alternative for the (ASCE, 2017; IBC, 2021) with three different design processes are prescribed to allow for linear elastic analysis and Nonlinear Time History Analysis (NLTHA) that would enable limited inelastic deformations in MWFRS. As a result, complex computational models are used to adopt reliability/probability analysis, and typical trial and error will be inefficient in maintaining the required goals of PBD (Methods et al., 2008). Consequently, it is recommended to couple the PBD procedure with an optimization algorithm that can handle the cumbersome design procedure (S. M. J. Spence & Kareem, 2014). PBD can be considered a form of reliability-based design through which uncertainties are quantitatively represented using probabilities of failure and expected values.

Throughout the literature, multiple philosophies are introduced to tackle this problem. One of the extensively used approaches is decoupling. In traditional reliability-based design optimization (RBDO), the optimization and reliability analysis are nested, leading to computationally intensive iterations, especially for complex systems with uncertainties. The decoupling approach separates the reliability analysis from the optimization loop by defining approximate subproblems. These

subproblems retain essential characteristics of the original nested problem but are formulated for more efficient solutions in a deterministic, approachable way. These functions represent reliability terms, capturing essential engineering demand parameters while avoiding computationally intensive probabilistic evaluations. By iteratively solving these subproblems, engineers efficiently explore the design space and find reliable solutions with reduced computational effort, striking a balance between efficiency and accuracy in the presence of uncertainties. For instance, (M. F. Huang et al., 2012) developed an RBDO method for wind-induced tall buildings subjected to wind loads extracted from a wind tunnel. For a fixed geometric shape of the building, the wind-induced acceleration was the main building's response that is assessed through the developed method using a decoupling approach by introducing an intermediate design parameter like the mean value of modal frequency that helps decouple the problem into two subproblems. The first subproblem is a probabilistic optimization using an inverse reliability algorithm to find the optimal mean value of modal frequency. The second subproblem is a deterministic optimization to find the minimum size of design members for the optimal mean value of modal frequency using the optimality criteria algorithm. PBDO approaches often face challenges in comprehensively addressing system-level constraints that stakeholders can easily understand. To address this, (Suksuwan & Spence, 2019) propose a robust framework that handles constraints in the form of loss metrics. Their approach incorporates a stochastic wind load generation technique using wind tunnel data and fragility and consequences databases to establish the loss model. Stochastic simulation is utilized within the subproblems after decoupling. While several studies have explored the application of the decoupling approach in the context of fixed geometry buildings, few studies can be found tackling the initial/preliminary design stages where the building's layout should be identified. For example, (Bobby et al., 2014) proposed a framework that includes model idealization with time-variant wind

loads on slender structures. The framework is also based on a decoupling strategy through which a reliability analysis for the current design point is applied to form an approximate optimization problem that can be fully solved to produce a new design point. A fragility-based quasi-static load is formulated to equalize the peak response of a dynamically excited system using the concepts of the Monte Carlo algorithm to yield a static topology optimization problem that can be solved using a gradient-based algorithm. The approximate representation of the limit state functions associated with failure events has proven efficient since it allows for more affordable computations. Yet, applying such approaches in the early design stage is still questionable.

The adoption of surrogate models can be an appropriate alternative approach to reduce computational costs that will arise with the high dimensionality accompanied by the early-stage design problems. By embracing PBD principles in early-stage designs, the construction industry can actively contribute to mitigating global warming effects and moving towards a more sustainable and resilient built environment. For example, (Zaker Esteghamati & Flint, 2021) proposed a framework for building a generalizable surrogate model for mid-rise reinforced concrete buildings to assess the seismic vulnerability and life cycle assessment. The surrogate model proved its efficiency not only for PBSD but also for PBWD. For instance, (Micheli, Alipour, et al., 2020b) developed multiple Kriging surrogate models for probabilistic cost assessment of tall buildings subjected to wind loads generated by a spectral approach. Each story had a surrogate model that accepted mass, stiffness, wind speed, and wind turbulence as inputs, while the maximum story drift and peak acceleration were the outputs that would be used in the cost assessment fragility curves. In addition, Surrogate models are used in aerodynamic mitigation and optimization of tall buildings, which is considered part of the PBWD philosophies (Bernardini, Spence, Wei, et al., 2015; Ding et al., 2019; Elshaer, Bitsuamlak, El-Damatty, et al., 2017; Elshaer

& Bitsuamlak, 2018; Qiu et al., 2021). When it comes to layout optimization, the core of the early-stage design, limited studies could be found considering the shear wall layout optimization (Alanani & Elshaer, 2023; H. Lou et al., 2021b; H. P. Lou et al., 2021; Y. Zhang & Mueller, 2017; X. Zhou et al., 2022). The previous studies focused on adopting static wind loads, while few studies considered the dynamic nature of wind (Alanani et al., 2024; Bobby et al., 2016; Gomez et al., 2021; Noormohamadian & Salajegheh, 2021). It can be noticed that optimization techniques aim to minimize the environmental impact of construction while ensuring the building's structural integrity and safety. Employing advanced optimization methods allows engineers to explore various design alternatives, evaluate the environmental implications, and arrive at an optimal solution that strikes a balance between structural efficiency and minimized embodied carbon emissions. While the Performance-based design approach provides resilient designs that are considered more optimal than deterministic designs, achieving such results requires linear or nonlinear analysis that adopts time history analysis to capture structural capacity degradation using dynamic loads. Yet the integration of optimization into the preliminary design stage is essential for maintaining the optimal designs in advanced design stages, achieving sustainable construction practices and mitigating the building sector's contribution to climate change.

In this study, a Performance-based wind design framework is introduced to early-stage design where the MWFRS layout should be identified. A Deep Neural Network (DNN)-based surrogate model is adopted to provide a computationally efficient evaluation for objective functions and constraints. The adopted surrogate model is built based on an automated FEM-generated database using ETABS (CSI, 2018) and (MATLAB, 2023) code. This surrogate model proved its ability to capture the critical engineering demand parameters required for PBWD. The inclusion of time history analysis during the optimization process has been challenging, as it often requires

simplifying the structural system. However, using the surrogate model significantly reduces the computational time for the optimization process. A non-gradient optimization algorithm, specifically a genetic algorithm, is employed to identify the optimal shear wall layout and columns' locations against dynamic wind and gravity loads, as specified by (ASCE, 2022).

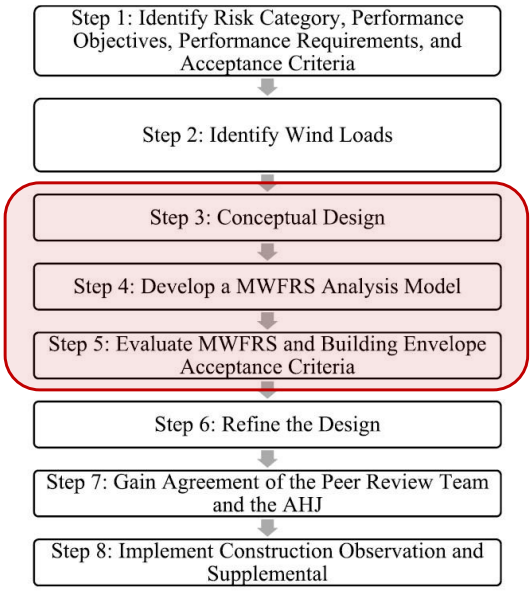

Fig. 4-1 ASCE PBWD pre-standards procedure (Abdelwahab et al., 2023)

4.2. Adopting performance-based wind design for tall building optimization

In the last few decades, multiple studies have been conducted to provide a framework for applying PBD concepts to wind loads. The PBWD pre-standards published by the ASCE are a result of the multiple studies conducted to standardize the process of applying PBWD for tall buildings (ASCE, 2019). It offers clear performance objectives, ensuring that buildings meet specified standards under varying hazard levels. Moreover, it incorporates acceptance criteria for overall system performance, encompassing both structural and building envelope aspects. This comprehensive guideline covers critical aspects of PBWD, such as risk categorization, dynamic analysis (both linear and nonlinear), procedures for different wind loads, and requirements for MWFRS. Fig. 4-1 shows the procedure prescribed by the ASCE and presented by (Abdelwahab et al., 2023). It goes

through several steps, from identifying the risk and the performance objectives with the accompanying acceptance criteria to gaining agreement from the peer review team and implementing the construction observations and supplementals.

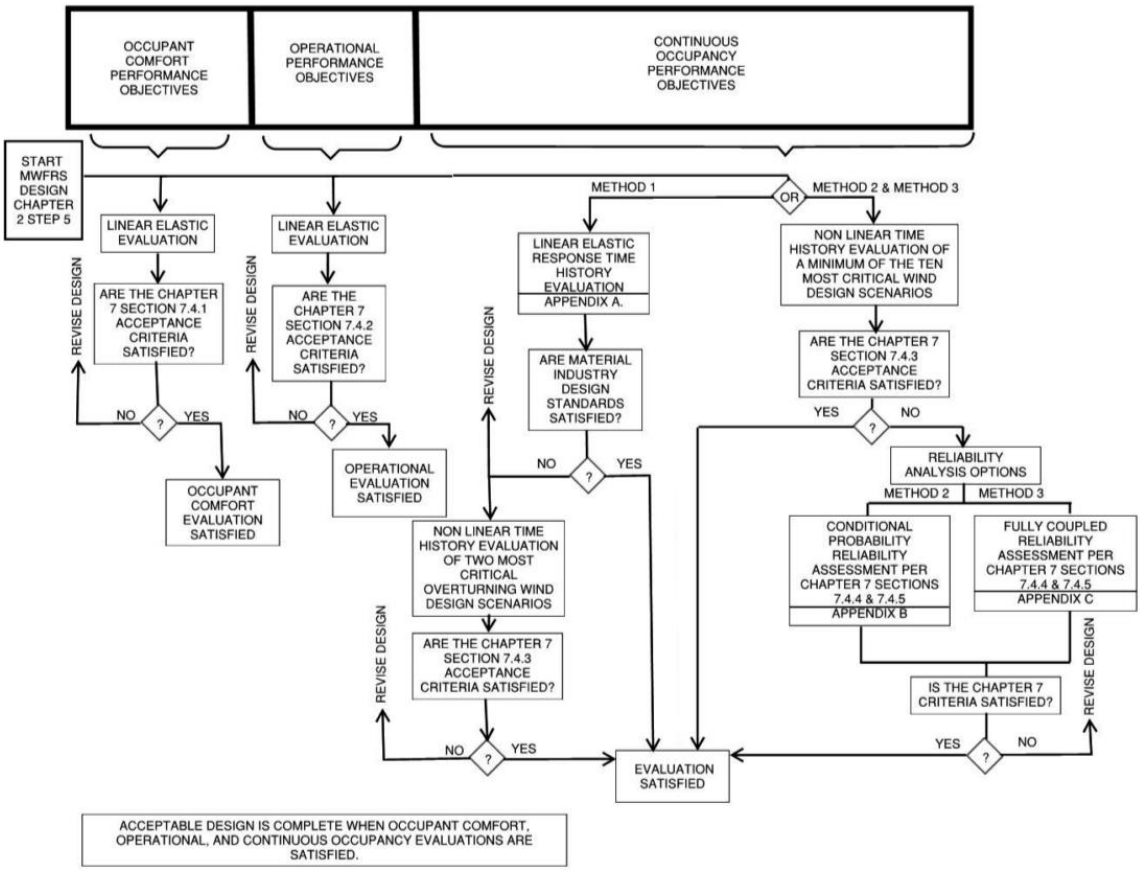

Fig. 4-2 Outline of PBWD MWFRS analysis and acceptance methods for each performance objective (ASCE, 2019)

There are three main objectives that were identified by the pre-standards (ASCE, 2019): (i) Occupant Comfort (OC), (ii) Operational and (iii) Continuous Occupancy (CO). These objectives define the desired performance for MWFRS, the building's envelope and the non-structural components and systems (e.g., cladding).

The Occupant Comfort objective is to maintain an elastic behaviour for the structural system with an independence of risk categories. Using frequency-dependent peak acceleration limits minimizes

the building motion and vibration at a design wind of mean recurrence interval (MRI) of 1-month, 1-year, and 10-year mean. For Operational objectives, elastic behaviour is also maintained, and the building should remain operational during windstorms of the selected risk category of II, III, IV at 10, 25 and 50-years MRI, respectively. The peak drift ratio is recommended to be H/400 to H/500, where H is the total height of the building, while no residual drift is allowed. For the non-structural elements, the deformation damage index (DDI) method can be used based on the displacement of four nodes at the damage zone. Regarding the Continuous Occupancy objectives, minor yielding is allowed at the deformation-controlled elements of the MWFRS while maintaining a low probability of minor or total collapse for all risk categories at an MRI of 700, 1700 and 3000 years. In addition, the building envelope should be designed to resist a wind-driven rain of a 25-year MRI for risk category II and a 50-year MRI for risk categories III and IV while having all non-structural components attached. Regarding the design of the MWFRS, a peak drift ratio of H/200 to H/300 is permitted. In contrast, the residual drift ratio, which occurs after experiencing minor inelastic behaviour, shall not exceed H/1000 or h/1000, where h is the story height. Regarding the strength limits, three main methods can be adopted, as shown in Fig. 4-2. It can be noticed that the design methodology should go through either linear or nonlinear time history analysis and multiple iterations are required to get a satisfactory design that can meet the acceptance criteria.

The ASCE prestandards have provided various recommendations to reduce the dynamic wind-induced responses, either by altering the buildings' outer shape to reduce the captured wind load, altering the structural properties of the buildings, or adding supplementary damping. Consequently, developing an optimization framework within the design process becomes necessary for the sake of the applicability and affordability of the PBWD procedures.

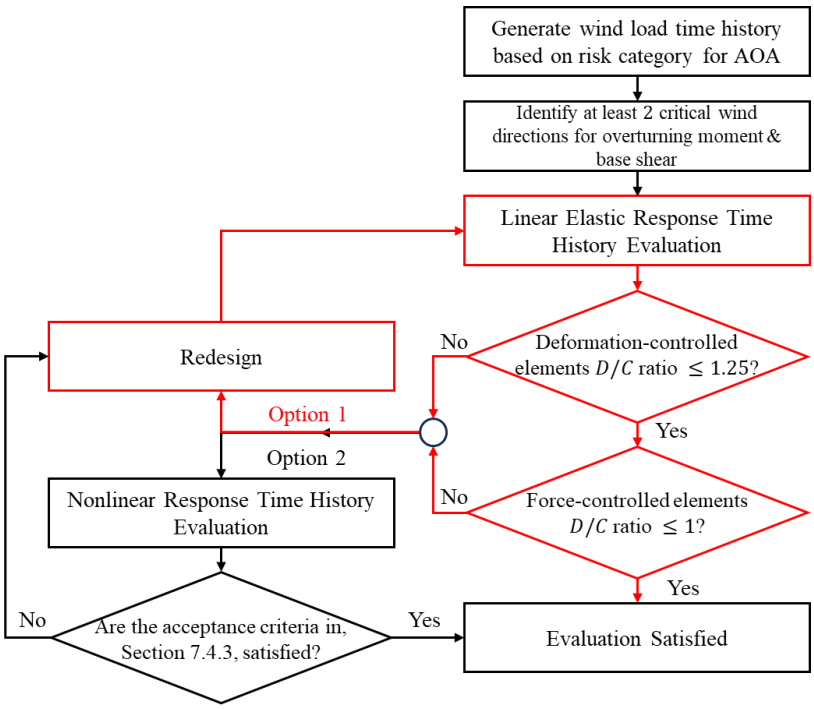

Fig. 4-3 Method 1 procedure for Continuous Occupancy performance objective of MWFRS

Previous research has focused on Occupant Comfort (OC) performance (Bernardini, Spence, Kwon, et al., 2015; Fu et al., 2018) with limited studies on Continuous Occupation (CO) performance (S. M. J. Spence & Kareem, 2014). Accordingly, this study will focus on the applicability of an optimization algorithm within the CO design procedure for the MWFRS, precisely the plan layout of MWFRS. Including the nonlinear behaviour within a high-dimensional problem is believed to be computationally challenging. In the developed framework, linear time history analysis (LTHA) is preferred to reduce the computational cost accompanied by the nonlinear time history analysis (NLTHA); thus, method-1 is selected where using an optimization algorithm can be adopted to systematically select a structural layout that will satisfy the acceptance criteria and avoid NLTHA within the conceptual design process of the MWFRS, as shown in Fig. 4-3.

4.3. Structural-Wind Optimization Framework (SWOF)

SWOF was initially developed to provide a deterministic-based design utilizing the National Building Code of Canada (NBCC) (Alanani et al., 2024; Alanani & Elshaer, 2023). The current study makes multiple improvements to the framework to embrace Performance-Based Wind Design (PBWD) principles, incorporating time history analysis based on the latest published prestandards (ASCE, 2019). This developed framework leverages the advancements in wind engineering to offer a comprehensive approach to structural optimization. As shown in Fig. 4-4, The framework is based on a Non-dominated Sorting Genetic Algorithm-II (NSGA-II) with a validated Deep Neural Network (DNN) used for objective functions and constraints evaluations through the optimization process to ensure that the acceptance criteria for the continuous occupancy (CO) performance objectives are maintained.

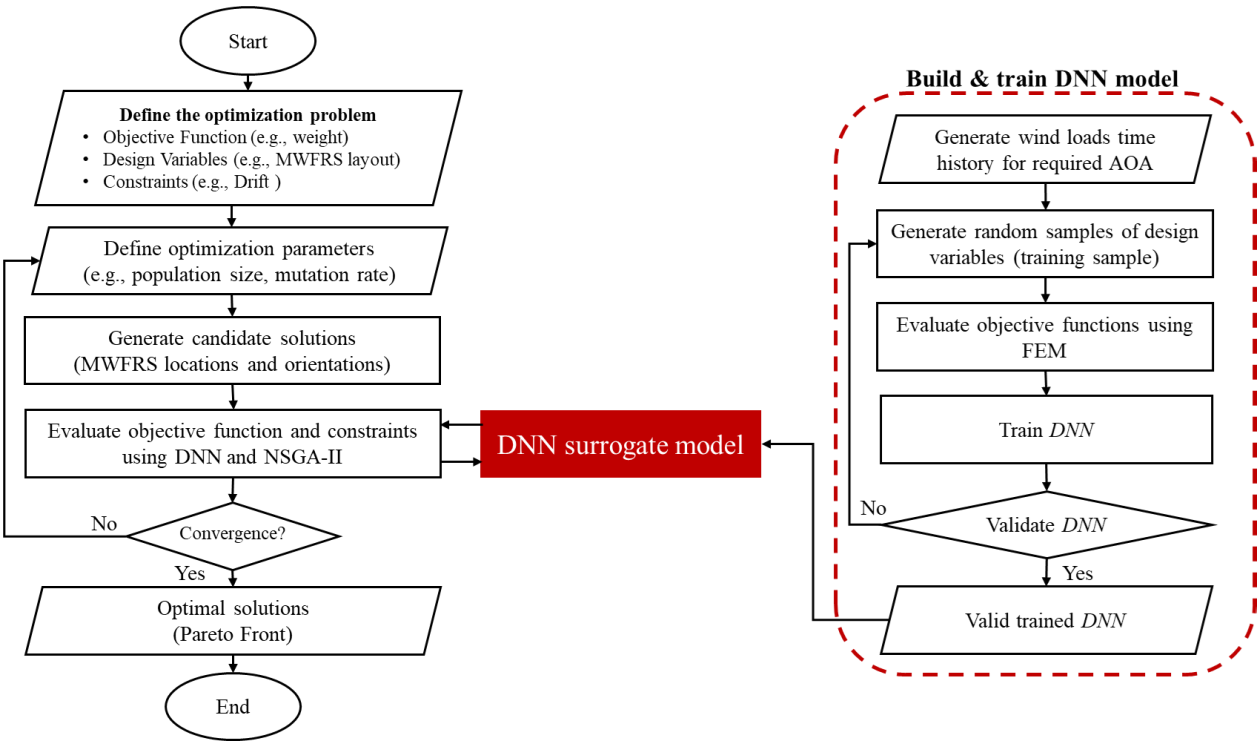

Fig. 4-4 Structure wind optimization framework (SWOF) flowchart (Alanani et al., 2024)

4.3.1. Case study

A three-dimensional rectangular 20-story reinforced concrete residential building is adopted for this case study, according to (Alanani & Elshaer, 2023). The MWFRS is chosen as a shear wall system, while columns are utilized as a Gravitational Force Resisting System (GFRS). The building stands at a 70 m height, with each story having a height of 3.5m. A dead load of 5 kN/m^2, and a live load of 1.9 kN/m^2 are added to all the floors' slabs. For material properties of all reinforced concrete elements, a concrete compressive strength of $f_c' = 35\ MPa$ and reinforced steel of yielding strength $f_y = 413\ MPa$ are used. The dimensions and thickness of reinforced concrete columns and shear walls are fixed throughout the whole process. A domain of all possible positions of shear walls and columns is identified based on a proposed architectural layout and thorough consideration of non-structural elements. To determine the length and shape of shear walls, a discretization of this domain is executed, employing a predefined segment size of 1.0 m. This process results in the division of the domain into 170 segments of shear walls, each measuring 1.0 m, as shown in Fig. 4-5. In every model, distinct column locations are determined to prevent overlap between shear wall segments and columns. The distribution of columns is governed by a predefined span of 6 m, to minimize alterations in the slab's straining actions as vertical supports are strategically placed, whether columns or shear walls in those areas.

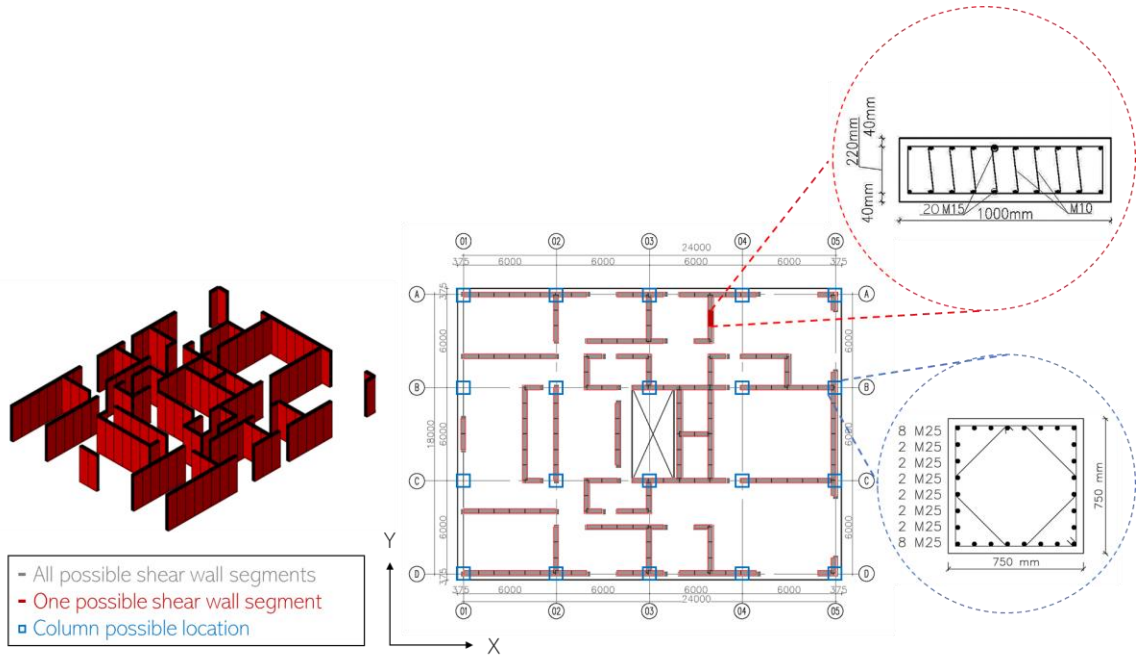

Fig. 4-5 The case study building plan layout with structural details and domain.

4.3.2. Wind load generation

The determination of wind speeds should be carried out using probabilistic wind climate analysis responses at varying return periods based on specified risk categories. For the sake of demonstration, risk Category II is chosen with an MRI of 700. In order to generate a turbulent inflow, the consistent discrete random flow generation (CDRFG) (Aboshosha et al., 2015) technique is utilized with a mean hourly wind speed at 33 ft height, $\bar{v}_{3600} = 39.68\, m/s$. Later on, the framework output results are compared to ASCE 7-22 (ASCE, 2022), an equivalent 3-second gust wind speed, to quantify the effect of time history analysis over the directional procedure method within the optimization framework. Turbulent intensity, turbulence length scale and velocity profile regression coefficients are used as per (Elshaer et al., 2016).

A validation model for an experimental wind tunnel test is conducted on a selected tall building, which is explained in detail in section 3.3.1.1. This step provides a validated computational domain that can be used later in the adopted case study.

The previously validated computational domain and boundary conditions are used to investigate the aerodynamic performance of the selected building. The chosen case study building replaces the Commonwealth Advisory Aeronautical Research Council (CAARC) building bluff body with the dimensions described in section 4.3.1. In order to extract wind load time histories, the building is discretized into 20 derived surfaces representing the tributary area of each storey in the building. These surfaces are responsible for integrating forces over time in the x and y directions. As shown in Fig. 4-6, a sample of wind load time history at the 10th floor is generated for longitudinal direction (Y-axis), across direction (X-axis) and torsional direction (Z-axis). For simplification, eight angles of attack are tested (i.e., 0^o, $45^o, 90^o, 135^o, 180^o, 225^o, 270^o, 360^o$). Then, the generated time histories for wind loads are defined in the FEM model as time history functions and applied at each storey's center of gravity.

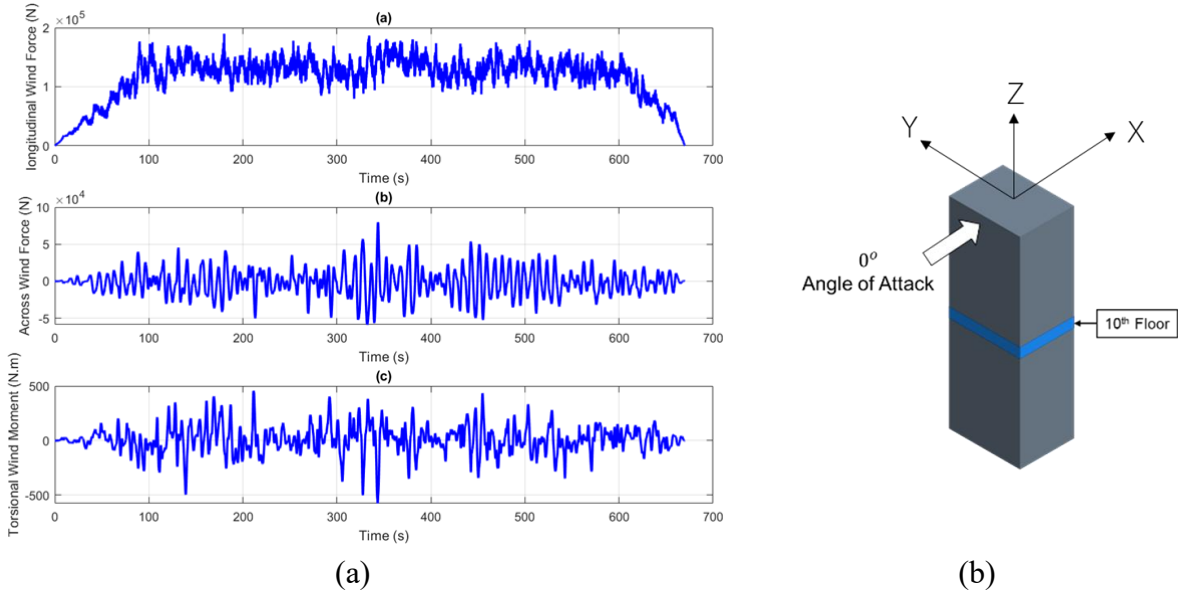

(a) (b)

Fig. 4-6. (a) Longitudinal and across wind forces and torsional wind moment time history at the 10th floor, AOA=0^o (b) Highlighted derived surface for the 10th floor

4.4. Surrogate model development

Throughout the literature review, it has been demonstrated that the usage of surrogate models improves the affordability of objective function evaluation, especially those computationally expensive (Abu-Zidan & Nguyen, 2023; Lalonde et al., 2021; W. T. Lu et al., 2023). This section outlines the process of building an efficient surrogate model capable of approximating the structural response based on various combinations of shear wall segments. The initial step involves employing a systematic sampling technique to ensure a representative set of data points for training the DNN. Latin Hypercube Sampling (LHS) is selected for its ability to efficiently cover the multidimensional design space (McKay et al., 1979), providing a diverse set of 1000 samples, ensuring that each design variable contributes to all generated samples with the same probability of occurrence. Each sample represents a unique configuration of 170 binary variables corresponding to the layout's presence or absence of shear walls. Three main structural parameters are chosen as constraints for the optimization problem: (i) the peak drift, (ii) the demand-to-capacity ratio for columns and (iii) the demand-to-capacity ratio for walls. All training samples are numerically modelled through ETABS OAPI (CSI, 2018) via (MATLAB, 2023). The process of identifying parameters and hyperparameters is established using performance metrics: The mean squared error (MSE) and the coefficient of determination (R-squared), as presented in equations (4-1) and (4-2).

$$MSE = \frac{1}{n}\sum_{i=1}^{n}\left(y_{predicted\,i} - y_{actual\,i}\right)^2 \tag{4-1}$$

$$R = \sqrt{1 - \frac{SSR}{SST}}, \tag{4-2}$$

$$SSR = \sum_{i=1}^{n}\left(y_{predicted\,i} - y_{actual\,i}\right)^2,$$

$$SST = \sum_{i=1}^{n} \left(y_{actual\,i} - \bar{y}_{actual} \right)^2$$

The architecture for the proposed DNN is shown in Fig. 4-7, where eight hidden layers of 400 nodes are used with eight attached bias nodes for each layer. Two transfer functions are used; all hidden layers included Saturating linear transfer functions except those in blue that used the Hyperbolic tangent sigmoid transfer function.

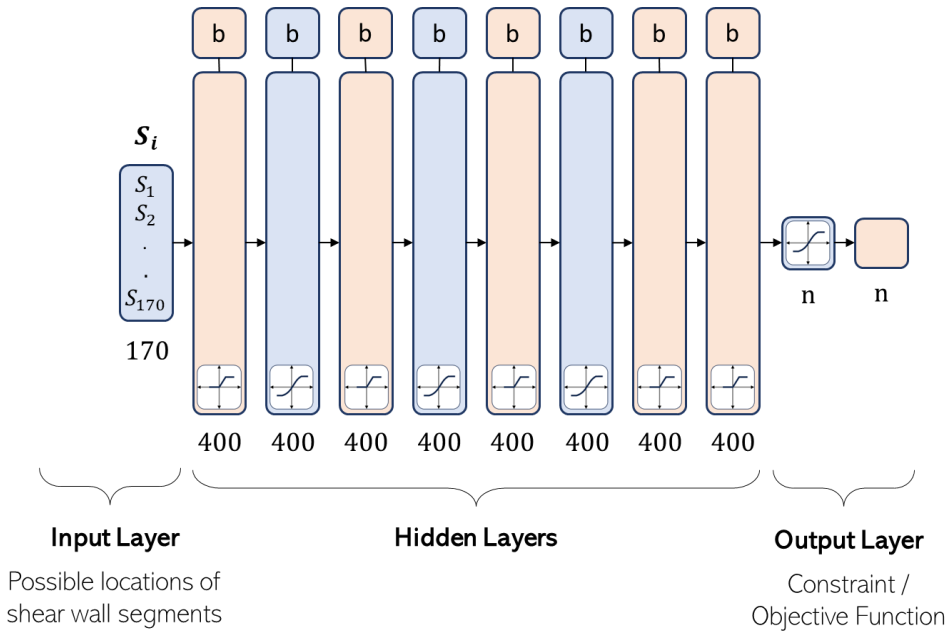

Fig. 4-7 Proposed Deep Neural Network (DNN) architecture.

The DNN is trained using a subset of the data (70%) while reserving the remaining portion for validation. The training process minimizes a defined loss function through backpropagation and optimization techniques. Mean Squared Error (MSE) is chosen as the loss function to measure the disparity between the predicted and actual structural responses. As shown in Fig. 4-8, the training process is stopped once no progress is noticed in the validation results to avoid overfitting the trained model. It can be noticed that 85% of samples do not exceed 10% error, which indicates the efficiency of the developed model, as shown in Fig. 4-9

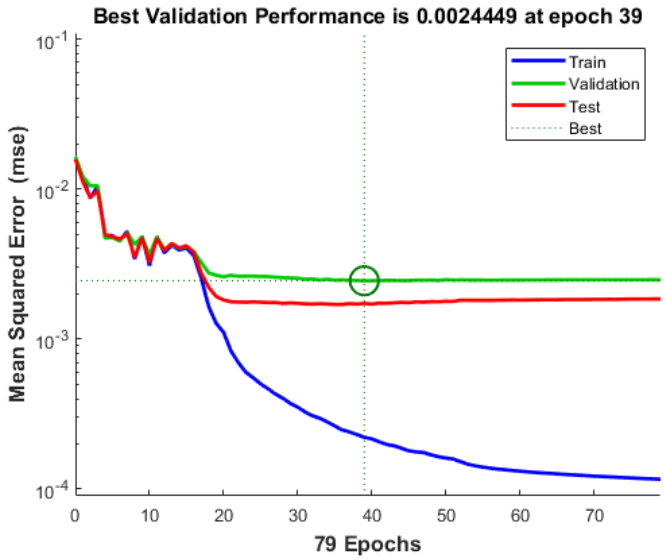

Fig. 4-8 Mean Square Error for D/C_{wall} DNN

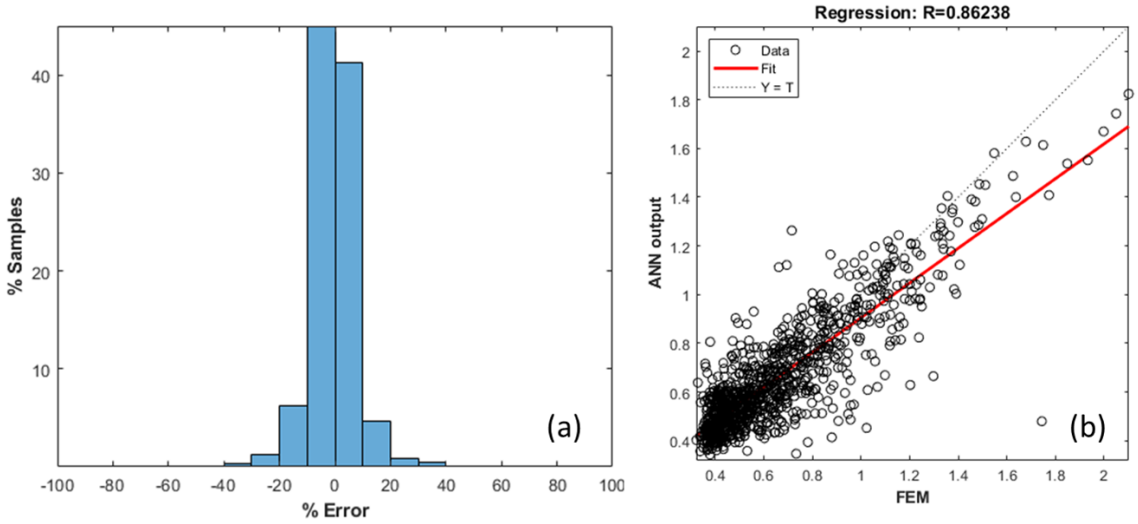

Fig. 4-9 (a) Error Histogram, and (b) Regression plot for D/C_{wall} results

4.5. Optimization Problem definition

By formulating the problem as a multi-objective optimization task, we aim to concurrently lower the structural material by minimizing (a) the total number of shear wall segments, (b) the number of piers (connected shear wall segments), and (c) the torsional effect via lowering eccentricity distance between the center of mass and center of rigidity ($e_{C_M C_R}$). These three objectives are aimed to be lowered while ensuring the satisfaction of the performance criteria constraints of (i)

peak drift Δ_{peak}, (ii) demand-to-capacity ratio (D/C) of the building's beams, and (iii) D/C of the columns in accordance with the PBWD standards (ASCE, 2019). The optimization variables encompass the MWFRS layout, directly impacting the building's overall structural integrity and response to dynamic wind loads. The layout shown in Fig. 4-5 will go through a preprocessing stage in which it will be discretized into 1 m segments, and each segment will be represented as a binary design variable. In this representation, a value of 1.0 indicates that the segment is active and utilized in the design, while a value of 0 signifies that the segment is inactive. Equation (4-3) shows the mathematical formulation of the optimization problem. S_i is a set of design variables representing each shear wall segment and C_T is the set of constraints. Based on the (ASCE, 2019), the peak drift, Δ_{peak}, should not exceed $\frac{H}{200:300}$, noting that H is the total height of the building and this limit should be applied on at least two orthogonal direction of building's plan. In addition, deformation-controlled elements of MWFRS, shear walls in our case $(D/C)_{walls}$, demand-to-capacity ratio should not exceed the 1.25 while force-based elements should not exceed 1. It' s worth noting that to leverage the capabilities of the algorithm in identify the length and shape of shear walls without getting standalone single segments that can behave as a column due to the small aspect ratio that equals to 3.33, the N_s constraint is introduced to identify the number of standalone segments that is not attached to any other group of shear walls using the graphs model algorithm. Moreover, a sub-process is introduced to the algorithm to only allow symmetric layouts around the longer side center line of the building. The population generation of shear wall segments is limited to 80 segments from the upper half of the layout then symmetrical elements are selected from the other half to ensure yielding a symmetric layout for shear walls.

$$
\begin{aligned}
&find\ S_i = (S_1, S_2, S_3, \dots, S_N) \\
&minimize \left(\sum_{i=1}^{N} S_i\ , N_p, e_{C_M C_R} \right) \\
&Subjected\ to: \\
&\quad C_{Total} = \Big(\Delta_{peak_x} \leq 300\ mm, \Delta_{peak_y} \leq 300\ mm, \\
&\qquad\qquad (D/C)_{walls} \leq 1.25, (D/C\ )_{Columns} \leq 1, N_s = 0 \Big) \\
&\quad Where\ S_i \in \{0,1\}\ (i = 1,2, \dots, N\ ), N = 170
\end{aligned}
\tag{4-3}
$$

Regarding the NSGA-II parameters, they are identified based on a trial-and-error procedure yielding to the presented values in Table 4-1.

Table 4-1 NSGA-II parameters

						Constraints (C_{Total})			
Population size	Number of generations	Mutation function	Mutation scale	Mutation shrink	Crossover ratio	Δ_{peak}	$(D/C)_{Columns}$	$(D/C)_{walls}$	N_s
5000	2000	"Mutation gaussian"	1	0.5	0.8	0.25	1	1.25	0

4.6. Results and discussion

4.6.1. Non-dominated sorting genetic algorithm-II

This section presents the output of the optimization process, and it shows how the Non-dominated Sorting Genetic Algorithm II (NSGA-II) is utilized to achieve a Pareto front representing optimal designs. The algorithm was executed for six independent runs, each with a different population size, ensuring the robustness and convergence of the optimization procedure. For the sake of demonstration, the eccentricity objective function convergence is presented in Fig. 4-10, while a similar observation has been noticed at the other two objective functions where thousands of possible layouts are tested.

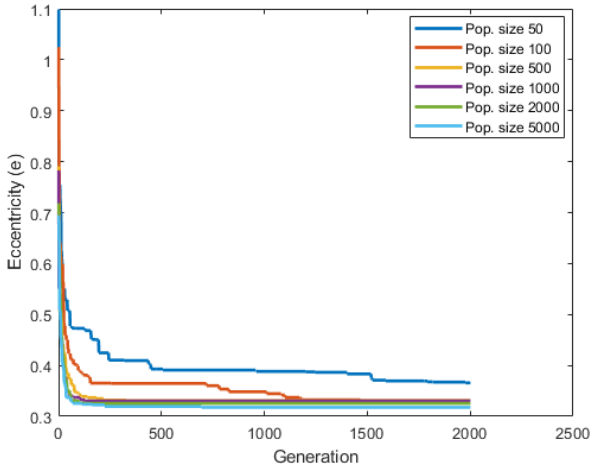

Fig. 4-10 Fitness function of the eccentricity objective function through different population sizes

The NSGA-II algorithm operates through multiple generations of evolving populations (Deb et al., 2002b). Parents are selected based on their dominance and crowding distance at each generation, subsequently undergoing crossover and mutation to generate offspring. The offspring, combined with the parent population, undergoes non-dominated sorting to identify Pareto fronts. The selection process then chooses individuals for the next generation, considering dominance and crowding distance, as shown in Fig. 4-11. The concept of dominance plays a crucial role in NSGA-II, where a solution dominates another solution if it is equal or better in all objectives and strictly better in at least one. During the non-dominated sorting, individuals are categorized into fronts based on their dominance relationships. Crowding distance is then calculated within each front to guide the selection. It measures the density of solutions around an individual. Solutions at the extremities of a front have higher crowding distances, indicating greater diversity. This diversity promotes a well-distributed Pareto front, avoiding solutions clustering in specific regions.

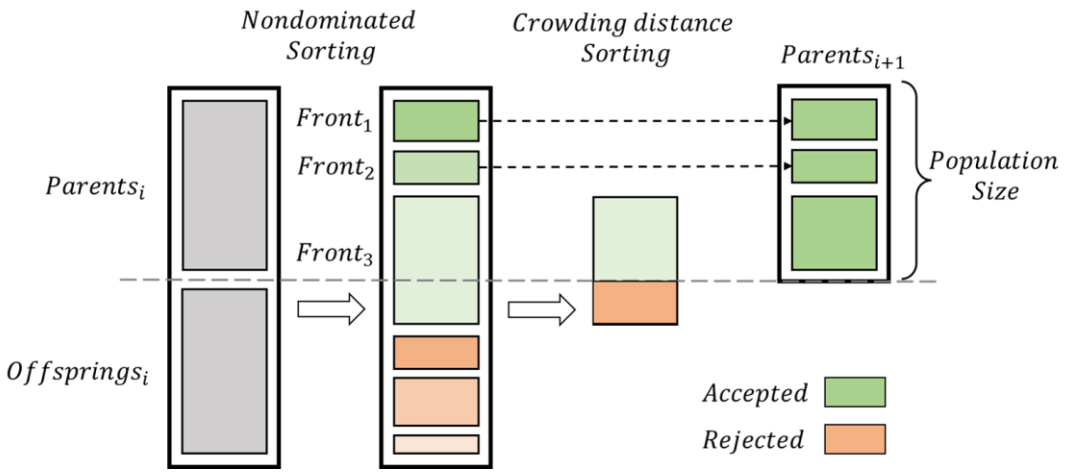

Fig. 4-11 NSGA-II procedure (based on (Deb et al., 2002b))

The obtained 3D Pareto front provides a comprehensive view of trade-offs between structural weight, number of piers, and eccentricity, as shown in Fig. 4-12. The convex shape of the front implies that as optimization tends towards reducing the number of piers and segments, the associated increase in eccentricity is moderated. These results empower structural engineers and designers with a set of options, allowing them to tailor solutions based on project-specific constraints and preferences. In this case study, one solution will be selected based on the least number of shear wall segments and the least number of piers possible with a convenient eccentricity that does not trigger a severe torsional behaviour, as shown in Fig. 4-13. The selected layout can be considered one of the optimal solutions on the bounds of the Pareto front to investigate the efficiency of the proposed framework. Later in this paper, the structural nonlinear behaviour will be studied to quantify how much nonlinearity can be induced with the proposed PBWD D/C for deformation-controlled elements (i.e., shear walls).

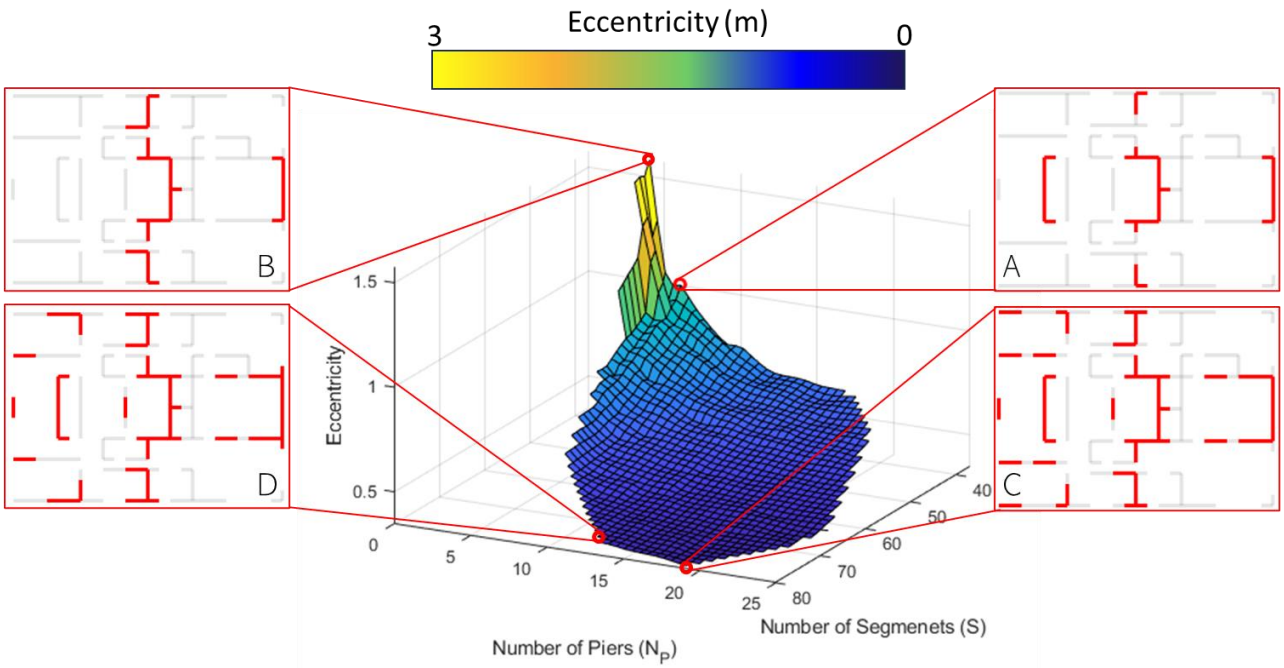

Fig. 4-12 3D Pareto Front with five samples of possible MWFRS layouts

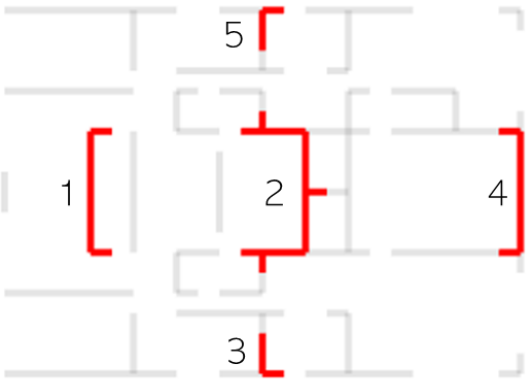

Fig. 4-13 Selected optimal layout-A

4.6.2. Linear Time History Analysis (LTHA)

In this study, Linear Time History Analysis (LTHA) was utilized as the numerical assessment for the generated training samples to assess the dynamic response of the structure under wind loading conditions. The LTHA was implemented using modal superposition to solve the dynamic equations. Three main wind load components are applied: along-wind, across-wind, and torsional wind loads are applied by use of validated Computational Fluid Dynamics (CFD) simulations,

capturing the intricate flow patterns and variations in wind speed. The P-Delta effect, accounting for geometric nonlinearity, was considered in the analysis using dead loads and 50% of live loads in an iterative procedure till convergence is achieved, as recommended by the prestandards (ASCE, 2019). By incorporating the modal superposition time domain analysis, mode shapes are determined accurately, with an output time step of 0.1s, including the P-delta effect yielding the natural frequency of the first three modes of the optimal solution to be $f_1 = 0.143\,Hz$, $f_2 = 0.33\,Hz$, and $f_3 = 0.42\,Hz$. A modal damping ratio of 5% is defined based on the (ASCE, 2022). As shown in Fig. 4-14, it can be noticed that the ASCE code regulations can provide acceptable accuracy that is slightly higher than the time-history analysis for along wind direction of a 0^o AOA. Regarding the across-wind behaviour, as presented in Fig. 4-15, the LTHA shows a lower response in the peak drift than the code values that reach 15 %. This can be related to the conservative considerations of the ASCE code specifications that were found to have more variance in across wind pressure coefficients compared to wind tunnel results where the dominancy of wake-induced effects is present (Badri et al., 2015; Kijewski, T; Kareem, 1998; Kwon & Kareem, 2013).

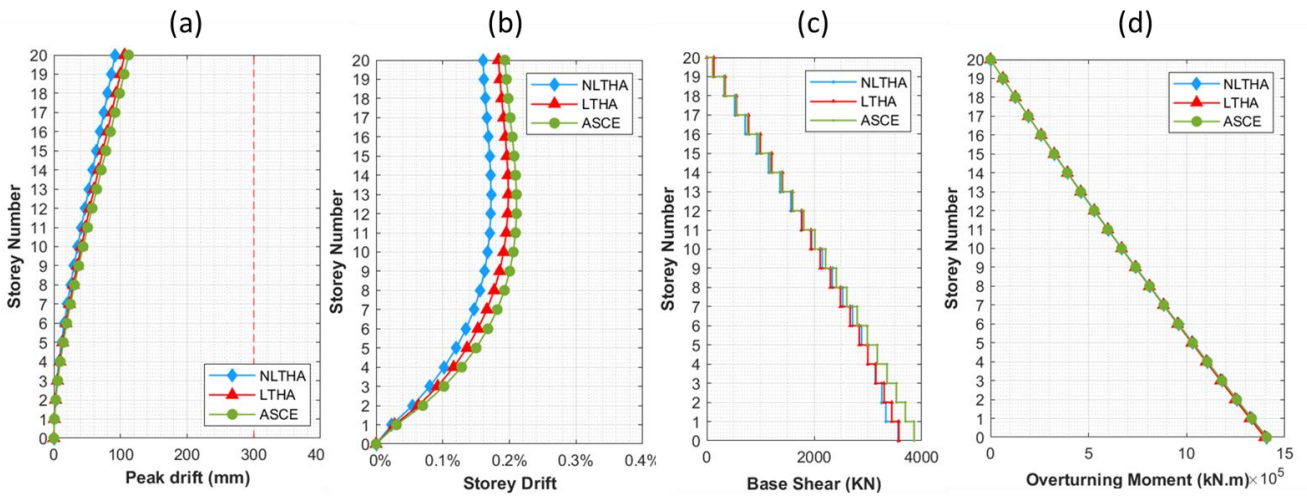

Fig. 4-14 Structural response via along wind load: (a) peak drift, (b) storey drift, (c) base shear, and (d) overturning moment of layout-A

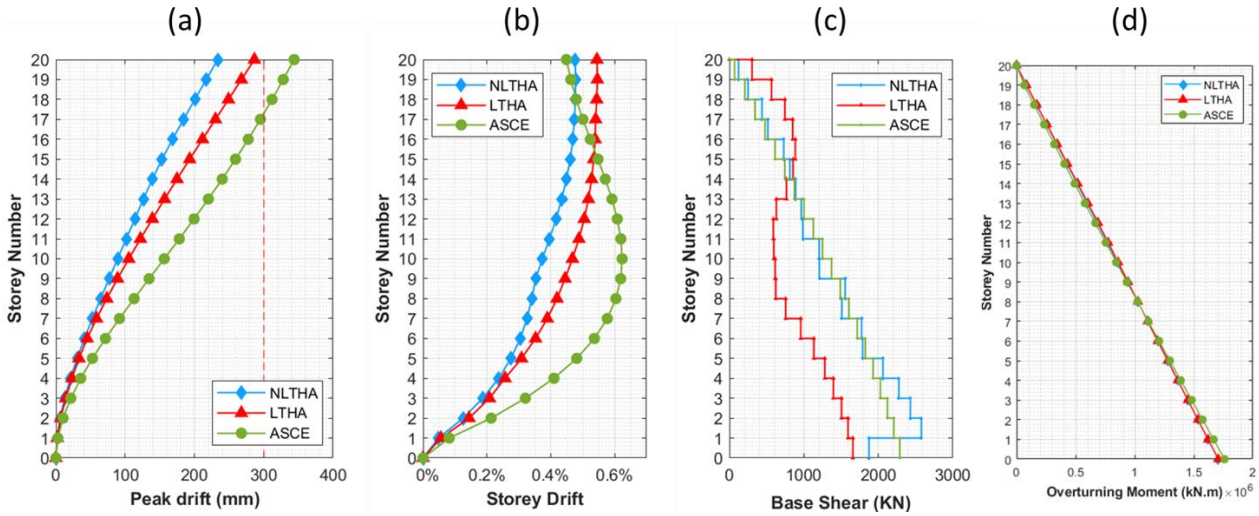

Fig. 4-15 Structural response via across wind load: (a) peak drift, (b) storey drift, (c) base shear, and (d) overturning moment of layout-A

4.6.3. Nonlinear Time History Analysis (NLTHA)

Since the proposed framework yielded a $(D/C)_{wall} > 1$, it is required to apply NLTHA to quantify the true response of the shear wall and to check that the peak residual story drifts are within the required limit of $H/1000$ and $h/1000$ per story. A computationally efficient nonlinear modal time history analysis, namely the Fast Nonlinear Analysis (FNA) method (Wilson, 2002) is adopted as

it is applicable for small to moderate inelastic deformations (Jeong et al., 2021). Adopting accurate modelling of deterioration incorporating geometric and material properties is essential to capture the strength and stiffness degradation. Material properties should be presented using well-established constitutive models to represent the fibre behaviour for concrete (Mander et al., 1988) and for steel (Menegotto & Pinto, 1973). The deterioration in deformation-controlled elements (i.e., Shear wall elements) is modelled using fiber hinges of coupled axial loads, P_1 , and bending moment around the strongest axes, M_3. The hysteresis behaviour of each fiber follows a force-deformation curve based on the ((FEMA) & (ASCE), 2000). Consequently, neither effective stiffness nor the code strength reduction factors are included through the NLTHA. Three main load combinations are proposed by the PBWD prestandards (ASCE, 2019), as presented in equations (4-4), (4-5), and (4-6), where D_L is dead load, L is expected live load, L_r live load at roof, and W_{MRI} is wind load at specific MRI. As shown in Fig. 4-16, almost zero inelastic deformation has been noticed in the main orthogonal directions, and it can be explicitly noted in Fig. 4-17, where all shear walls did not exceed 51% of the deformation required to reach the yielding capacity. When we delve deeper into the edge fiber behaviour of the dominant pier shown in Fig. 4-18, it can be noticed that yielding stress was not reached. Yet, showing the interaction behaviour of axial loads P_1, and moments around both axes M_2 and M_3. The loads are incubated by the yielding surface as shown Fig. 4-19 where the two extreme AOA loads are plotted.

$$LC1 = 1.0D_L + 1.0L + 1.0W_{MRI} \quad (4\text{-}4)$$

$$LC2 = 1.2D_L + 1.0L + 0.5L_r + 1.0W_{MRI} \quad (4\text{-}5)$$

$$LC3 = 0.9D_L + 1.0W_{MRI} \quad (4\text{-}6)$$

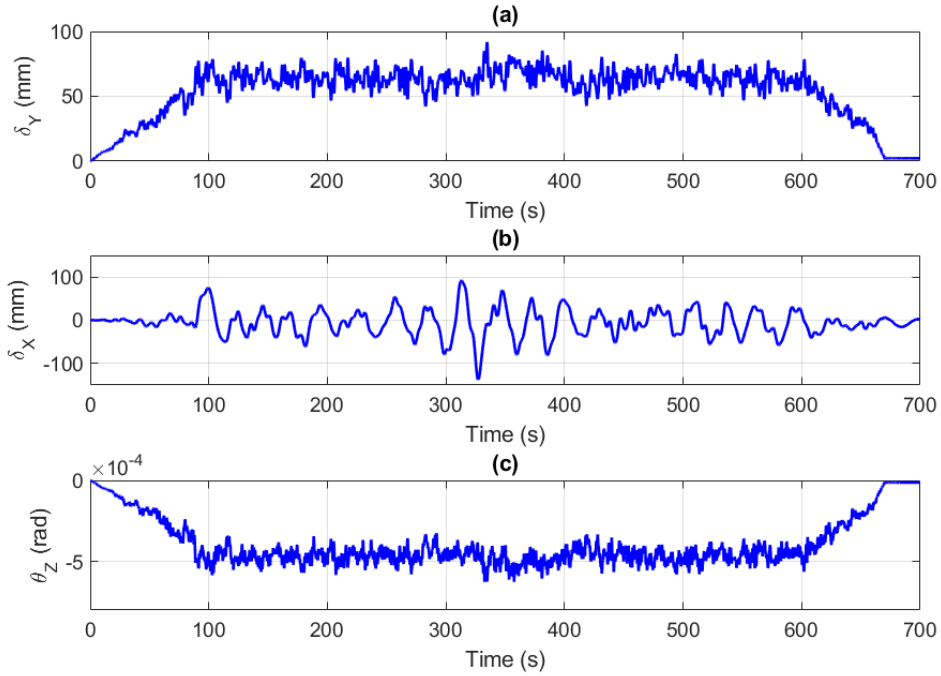

Fig. 4-16 Peak drift in the (a) x-direction, (b) y-direction and (c) the rotation time history at the top story by LC2

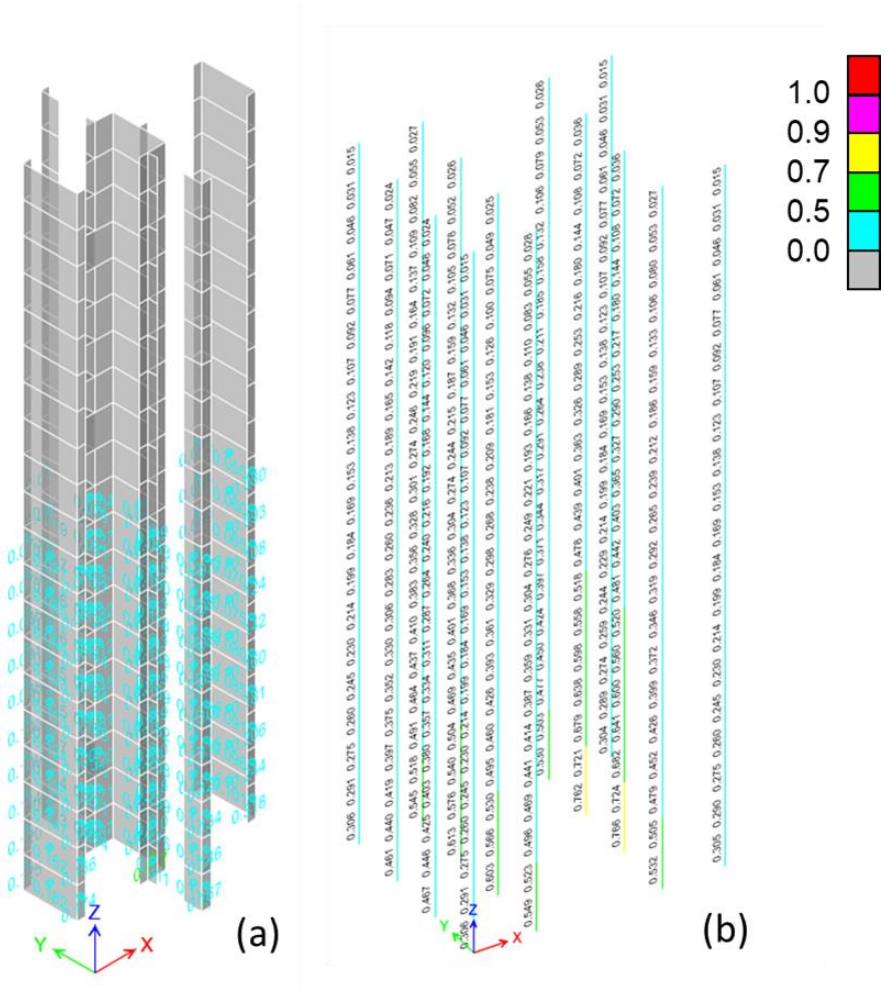

Fig. 4-17 (a) Performance D/C results for shear walls, and (b) strength capacity results for columns

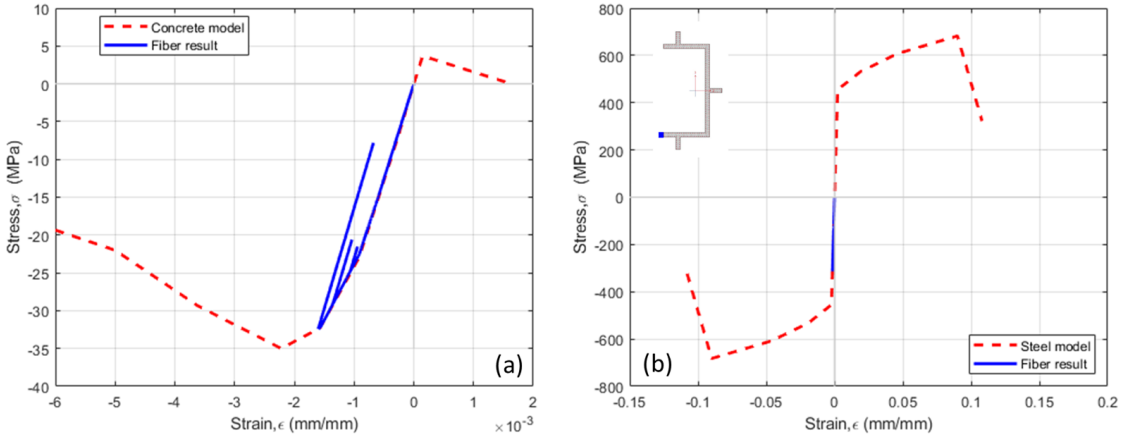

Fig. 4-18 Edge fiber stress-strain results for (a) concrete and (b) steel reinforcement at Pier-2

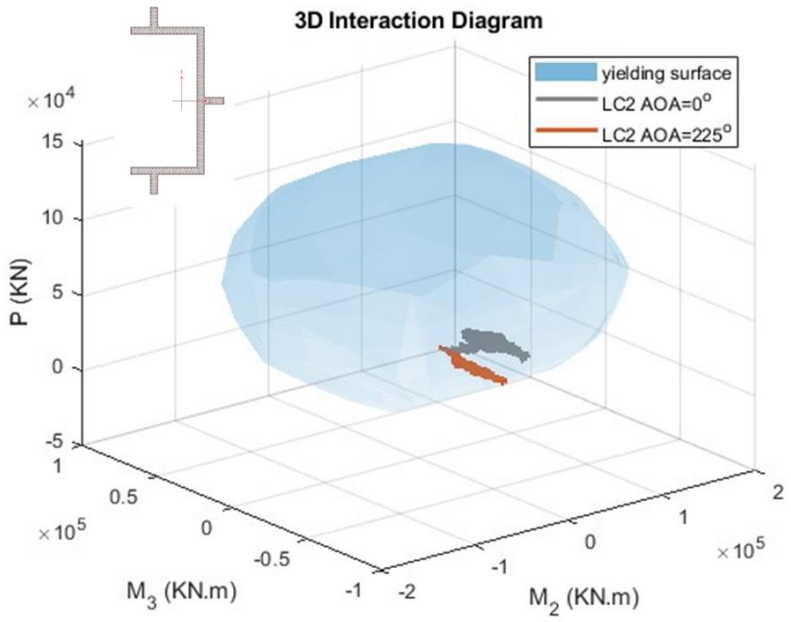

Fig. 4-19 $P_1 - M_2 - M_3$ Interaction diagram for Pier-2 with internal loads due to 0^o and 225^o Angles of Attack (AOA)

4.7. Conclusion

In this paper, a layout optimization framework is presented for tall buildings subjected to stochastic wind loads. The developed framework is compatible with the recommendation of the PBWD prestandards (ASCE, 2019) by considering three objective functions: the total number of shear wall segments ($\sum S_i$) as a representation of total material volume, the total number of formulated piers (N_P), and the eccentricity ($e_{C_M C_R}$) of the center of rigidity (C_R) from the center of mass (C_M) as a representation of torsional behaviour, while constraints are defined based on the prestandards allowable demand-to-capacity ratio for force-controlled and deformation-controlled elements in addition to the peak drift ratios. This framework focuses on the Continuous Occupancy (CO) performance with Linear Time History Analysis (LTHA) using wind loads time-histories of 8 wind angles of attack. To overcome the challenges of the domain complexity, a Non-Dominant Sorting Genetic Algorithm (NSGA-II) is used that managed to adopt 170 design variables to yield a 3D Pareto front of possible solutions that are not dominated by any other solution based on the

provided criteria. The developed DNN-based surrogate model that tested a very large number of possible layouts in a few minutes makes it computationally efficient. It also shows a high capability in capturing the structural response of a FEM output subjected to CFD-generated wind loads with an error of less than 10% for 85% of generated samples. A case study of a 70 m tall building is presented to show the applicability of the developed framework. Furthermore, a comparison is made between the framework's optimal layout behaviour, the ASCE 7-22 directional procedure generated wind loads, and nonlinear time history analysis (i.e., FNA method) to quantify the effectiveness of the developed framework. It was found that the ratio identified by the PBWD prestandards (ASCE, 2019) for allowable demand-to-capacity ratio for deformation-controlled MWFRS required more research to ensure that limited nonlinearity can occur under dynamic wind loading using LTHA.

4.8. References

Abdelwahab, M., Ghazal, T., Nadeem, K., Aboshosha, H., & Elshaer, A. (2023). Performance-based wind design for tall buildings: Review and comparative study. *Journal of Building Engineering*, *68*(November 2022), 106103. https://doi.org/10.1016/j.jobe.2023.106103

Abu-Zidan, Y., & Nguyen, K. (2023). A machine learning approach for calibrating ABL profiles in large-eddy simulations. *Journal of Wind Engineering and Industrial Aerodynamics*, *232*, 105277. https://doi.org/10.1016/J.JWEIA.2022.105277

Adams, M., Burrows, V., & Richardson, S. (2019). Bringing embodied carbon upfront: Coordinated action for the building and construction sector to tackle embodied carbon. In *World Green Building Council*. https://www.worldgbc.org/sites/default/files/WorldGBC_Bringing_Embodied_Carbon_Upfront.pdf

Alanani, M., Brown, T., & Elshaer, A. (2024). Mulit-objective structural layout optimization of tall buildings subjected to dynamic wind loads. *Journal of Structural Engineering*. https://doi.org/10.1061/JSENDH/STENG-12366

Alanani, M., & Elshaer, A. (2023). ANN-based optimization framework for the design of wind load resisting system of tall buildings. *Engineering Structures*, *285*, 116032. https://doi.org/10.1016/j.engstruct.2023.116032

Applied Technology Council. (1996a). ATC 32, Improved Seismic Design Criteria for California Bridges: Resource Document. *Design*, *1996*.

Applied Technology Council. (1996b). *ATC 40, Seismic Evaluation and Retrofit of Concrete Buildings*.

ASCE. (2017). Minimum Design Loads for Buildings and Other Structures. In *ANSI/ASCE Standard* (Issue 7 98). American Society of Civil Engineers. https://doi.org/10.1061/9780872629042

ASCE. (2019). Prestandard for Performance-Based Wind Design V1.1. In *Prestandard for Performance-Based Wind Design V1.1*. American Society of Civil Engineers. https://doi.org/10.1061/9780784484739

ASCE. (2022). Minimum Design Loads for Buildings and Other Structures. In *ANSI/ASCE Standard* (Issue 7 98). American Society of Civil Engineers. https://doi.org/10.1061/9780872629042

Badri, A. A., Hussein, M. M., & Attia, W. A. (2015). Study of wind tunnel test results of high-rise buildings compared to different design codes. *Wind and Structures*, *20*(5), 623–642. https://doi.org/10.12989/was.2015.20.5.623

Bernardini, E., Spence, S. M. J., Kwon, D.-K., & Kareem, A. (2015). Performance-Based Design of High-Rise Buildings for Occupant Comfort. *Journal of Structural Engineering*, *141*(10), 1–14. https://doi.org/10.1061/(asce)st.1943-541x.0001223

Bernardini, E., Spence, S. M. J., Wei, D., & Kareem, A. (2015). Aerodynamic shape

optimization of civil structures: A CFD-enabled Kriging-based approach. *Journal of Wind Engineering and Industrial Aerodynamics*, *144*, 154–164.

Bezabeh, M., Bitsuamlak, G., & Tesfamariam, S. (2020). Performance-based wind design of tall buildings: Concepts, frameworks, and opportunities. *Wind and Structures*, *31*(2), 103–142. https://doi.org/10.12989/was.2020.31.2.103

Bobby, S., Spence, S. M. J., & Kareem, A. (2016). Data-driven performance-based topology optimization of uncertain wind-excited tall buildings. *Structural and Multidisciplinary Optimization*, *54*(6), 1379–1402. https://doi.org/10.1007/s00158-016-1474-6

Cerè, G., Rezgui, Y., Zhao, W., & Petri, I. (2022). Shear walls optimization in a reinforced concrete framed building for seismic risk reduction. *Journal of Building Engineering*, *54*(May), 104620. https://doi.org/10.1016/j.jobe.2022.104620

CSI. (2018). *ETABS building analysis and design* (2018.1.1). Computers and Structures, Inc. www.csiamerica.com

Deb, K., Pratap, A., Agarwal, S., & Meyarivan, T. (2002). A fast and elitist multiobjective genetic algorithm: NSGA-II. *IEEE Transactions on Evolutionary Computation*, *6*(2), 182–197. https://doi.org/10.1109/4235.996017

Ding, F., Kareem, A., & Wan, J. (2019). Aerodynamic Tailoring of Structures Using Computational Fluid Dynamics. *Structural Engineering International*, *29*(1), 26–39. https://doi.org/10.1080/10168664.2018.1522936

Elshaer, A., & Bitsuamlak, G. (2018). Multiobjective Aerodynamic Optimization of Tall Building Openings for Wind-Induced Load Reduction. *Journal of Structural Engineering*, *144*(10), 4018198. https://doi.org/10.1061/(ASCE)ST.1943-541X.0002199

Elshaer, A., Bitsuamlak, G., El-Damatty, A., & El Damatty, A. (2017). Enhancing wind performance of tall buildings using corner aerodynamic optimization. *Engineering Structures*, *136*, 133–148. https://doi.org/10.1016/j.engstruct.2017.01.019

Federal Emergency Management Agency (FEMA). (1997). NEHRP Guidelines for the Seismic Rehabilitation of Buildings. *Federal Emergency Management Agency Developed by the Applied Technology Council*, *October*.

FEMA P58-6. (2018). Guidelines for Performance-Based Seismic Design of Buildings. *Fema P-58-6*, *6*(December), 92. https://www.fema.gov/media-library/assets/documents/90380

Fu, J., Zheng, Q., Huang, Y., Wu, J., Pi, Y., & Liu, Q. (2018). Design optimization on high-rise buildings considering occupant comfort reliability and joint distribution of wind speed and direction. *Engineering Structures*, *156*(November 2017), 460–471. https://doi.org/10.1016/j.engstruct.2017.11.041

Gomez, F., Spencer, B. F., & Carrion, J. (2021). Topology optimization of buildings subjected to stochastic wind loads. *Probabilistic Engineering Mechanics*, *64*(July 2020), 103127. https://doi.org/10.1016/j.probengmech.2021.103127

Huang, M. F., Chan, C. M., & Lou, W. J. (2012). Optimal performance-based design of wind

sensitive tall buildings considering uncertainties. *Computers and Structures*, *98–99*, 7–16. https://doi.org/10.1016/j.compstruc.2012.01.012

IBC. (2021). *International Building Code* (Vol. 0, Issue October 2020). https://www.accessengineeringlibrary.com/content/book/9781264270118

IPCC. (2023). Summary for policymakers. In: Climate Change 2023: Synthesis Report. A report of the Intergovernmental Plane on Climate Change. *Journal of Crystal Growth*, *2*, 36.

Jeong, S. Y., Alinejad, H., & Kang, T. H.-K. (2021). Performance-Based Wind Design of High-Rise Buildings Using Generated Time-History Wind Loads. *Journal of Structural Engineering*, *147*(9), 04021134. https://doi.org/10.1061/(asce)st.1943-541x.0003077

Kijewski, T; Kareem, A. (1998). Dynamic wind effects : a comparative study of provisions in codes and standards with wind tunnel data. *Wind & Structures*, *1*(1), 77–109.

Kwon, D. K., & Kareem, A. (2013). Comparative study of major international wind codes and standards for wind effects on tall buildings. *Engineering Structures*, *51*, 23–35. https://doi.org/10.1016/j.engstruct.2013.01.008

Lagaros, N. D., Bakas, N., & Papadrakakis, M. (2009). Optimum design approaches for improving the seismic performance of 3D RC buildings. *Journal of Earthquake Engineering*, *13*(3), 345–363. https://doi.org/10.1080/13632460802598594

Lalonde, E. R., Vischschraper, B., Bitsuamlak, G., & Dai, K. (2021). Comparison of neural network types and architectures for generating a surrogate aerodynamic wind turbine blade model. *Journal of Wind Engineering and Industrial Aerodynamics*, *216*, 104696. https://doi.org/10.1016/J.JWEIA.2021.104696

Lou, H., Gao, B., Jin, F., Wan, Y., & Wang, Y. (2021). Shear wall layout optimization strategy for high-rise buildings based on conceptual design and data-driven tabu search. *Computers & Structures*, *250*, 106546. https://doi.org/10.1016/j.compstruc.2021.106546

Lu, W. T., Phillips, B. M., & Jiang, Z. (2023). Surrogate-based cyber-physical aerodynamic shape optimization of high-rise buildings using wind tunnel testing. *Journal of Wind Engineering and Industrial Aerodynamics*, *242*, 105586. https://doi.org/10.1016/J.JWEIA.2023.105586

Mander, J. B., Priestley, M. J. N., & Park, R. (1988). Theoretical Stress-Strain Model for Confined Concrete. *Journal of Structural Engineering*, *114*(8), 1804–1826. https://doi.org/10.1061/(ASCE)0733-9445(1988)114:8(1804)

MATLAB. (2023). *MATLAB and Statistics Toolbox Release 2023b* (9.10). The MathWorks Inc.

McKay, M. D., Beckman, R. J., & Conover, W. J. (1979). A Comparison of Three Methods for Selecting Values of Input Variables in the Analysis of Output from a Computer Code. *Technometrics*, *21*(2), 239. https://doi.org/10.2307/1268522

Menegotto, M., & Pinto, P. E. (1973). Method of Analysis for Cyclically Loaded R. C. Plane Frames Including Changes in Geometry and Non-Elastic Behavior of Elements under Combined Normal Force and Bending. *Proceedings of IABSE Symposium on Resistance*

and Ultimate Deformability of Structures Acted on by Well Defined Loads, 15–22. https://cir.nii.ac.jp/crid/1571980075471506816

Methods, C., Mech, A., Schuëller, G. I., & Jensen, H. A. (2008). Computational methods in optimization considering uncertainties – An overview. *Computer Methods in Applied Mechanics and Engineering*, *198*(1), 2–13. https://doi.org/10.1016/j.cma.2008.05.004

Micheli, L., Alipour, A., & Laflamme, S. (2020). Multiple-Surrogate Models for Probabilistic Performance Assessment of Wind-Excited Tall Buildings under Uncertainties. *ASCE-ASME Journal of Risk and Uncertainty in Engineering Systems, Part A: Civil Engineering*, *6*(4). https://doi.org/10.1061/ajrua6.0001091

Mokarram, V., & Banan, M. R. (2018). An improved multi-objective optimization approach for performance-based design of structures using nonlinear time-history analyses. *Applied Soft Computing Journal*, *73*, 647–665. https://doi.org/10.1016/j.asoc.2018.08.048

Noormohamadian, M., & Salajegheh, E. (2021). Evaluation and minimization of moment coefficient of tall buildings with trilateral cross-section via a surrogate model. *SN Applied Sciences*, *3*(2). https://doi.org/10.1007/s42452-020-04128-5

Petrini, F., & Ciampoli, M. (2012). Performance-based wind design of tall buildings. *Structure and Infrastructure Engineering*, *8*(10), 954–966. https://doi.org/10.1080/15732479.2011.574815

Preetha Hareendran, S., Alipour, A., Shafei, B., & Sarkar, P. (2022). Performance-Based Wind Design of Tall Buildings Considering the Nonlinearity in Building Response. *Journal of Structural Engineering*, *148*(9), 1–19. https://doi.org/10.1061/(asce)st.1943-541x.0003312

Qiu, Y., San, B., He, H., & Zhao, Y. (2021). Surrogate-based aerodynamic optimization for enhancing the shelter effect of porous fences on a triangular prism. *Atmospheric Environment*, *244*(September 2020). https://doi.org/10.1016/j.atmosenv.2020.117922

Spence, S. M. J. J., & Arunachalam, S. (2022). Performance-Based Wind Engineering: Background and State of the Art. *Frontiers in Built Environment*, *8*(March), 1–11. https://doi.org/10.3389/fbuil.2022.830207

Spence, S. M. J., & Kareem, A. (2014). Performance-based design and optimization of uncertain wind-excited dynamic building systems. *Engineering Structures*, *78*, 133–144. https://doi.org/10.1016/j.engstruct.2014.07.026

Suksuwan, A., & Spence, S. M. J. J. (2019). Performance-based design optimization of uncertain wind excited systems under system-level loss constraints. *Structural Safety*, *80*(June 2018), 13–31. https://doi.org/10.1016/j.strusafe.2019.03.004

Valdebenito, M. A., & Schuëller, G. I. (2010). *A survey on approaches for reliability-based optimization*. 645–663. https://doi.org/10.1007/s00158-010-0518-6

Wen, Y. . (2001). Reliability and performance-based design. *Structural Safety*, *23*(4), 407–428. https://doi.org/10.1016/S0167-4730(02)00011-5

Wilson, E. L. (2002). Three-Dimensional Static and Dynamic Analysis of Structures. In *Journal*

of neurophysiology (Vol. 90, Issue 3). http://www.ncbi.nlm.nih.gov/pubmed/17267222

Zaker Esteghamati, M., & Flint, M. M. (2021). Developing data-driven surrogate models for holistic performance-based assessment of mid-rise RC frame buildings at early design. *Engineering Structures*, *245*. https://doi.org/10.1016/j.engstruct.2021.112971

Zhang, Y., & Mueller, C. (2017). Shear wall layout optimization for conceptual design of tall buildings. *Engineering Structures*, *140*, 225–240. https://doi.org/10.1016/j.engstruct.2017.02.059

Zhou, X., Wang, L., Liu, J., Cheng, G., Chen, D., & Yu, P. (2022). Automated structural design of shear wall structures based on modified genetic algorithm and prior knowledge. *Automation in Construction*, *139*(January), 104318. https://doi.org/10.1016/j.autcon.2022.104318

CHAPTER 5

5. DATA-DRI EN SURROGATE MODELS FOR ESTIMATING TALL BUILDING WIND RESPONSE

5.1. Introduction

The last few decades have witnessed an increasing demand to adopt performance-based design (PBD) frameworks that aim to ensure tall buildings' safety, functionality, and resilience under various loading conditions, with the wind being a predominant factor (Abdelwahab et al., 2023). In contrast to the traditional structural design practices that rely on the equivalent static wind load method, the performance-based wind design (PBWD) considers the unique characteristics and dynamic nature of wind forces acting on tall structures, especially those of high natural period that require a wind tunnel test (Iancovici et al., 2022). It allows for a more holistic evaluation, considering factors like wind-induced vibrations, occupant comfort, and structural reliability (S. M. J. J. Spence & Arunachalam, 2022). However, deploying the PBWD is challenging in the conceptual design phase due to the multiple uncertainties and the high computational cost required to consider such dynamic behaviour, especially when multiple design iterations are needed. The exhaustive search design approach will be cumbersome to yield an economical design efficiently. Thus, it is recommended to adopt an appropriate optimization algorithm that can handle the high dimensionality of the tall buildings' structures. The recently published PBWD prestandards advocated the utilization of optimization frameworks in the PBD process to enhance the applicability of PBWD frameworks (ASCE, 2019). This direction has highlighted the need to develop surrogate models that promptly provide accurate and rapid estimation for structural and performance assessments using statistical models (Westermann & Evins, 2019). These models act much faster than analytical or physics-based models to provide parameters of interest. Since the 1980s, Machine Learning (ML) algorithms have shown promising performance in capturing the

nonlinearity of structural response through different ways of application, either through developing data-driven materials models, structural health monitoring or predicting the structural response (Darko et al., 2020; Sayed et al., 2023; Sun et al., 2021; C. Wang et al., 2022).

Regarding Main Wind Force Resisting Systems (MWFRS), shear walls are considered one of the most typical structural elements used to resist wind loads. The recently developed ML models have shown competitive performance compared to those of mechanically driven models for structural element behaviour (e.g., shear walls) (Siam et al., 2019; Solorzano & Plevris, 2023b, 2023a; C. Wang et al., 2022). For instance, Mangalathu et al. explore the use of machine learning and artificial intelligence in failure mode identification of concrete shear walls (Mangalathu et al., 2020). The authors created a database of 393 reinforced concrete shear walls with rectangular or non-rectangular sections. They generated input parameters to capture geometry, material properties, and reinforcement details of shear walls. Eight machine learning models were evaluated, including Decision Trees, Random Forest and Ensemble learning, with Random Forest having the highest accuracy for the training set. The model had an 84% precision in identifying the flexure-shear failure mode for the test set. Moreover, the prediction of the backbone curves, which is essential in the nonlinear analysis of PBD, is also possible by ML models. Another study aims to develop predictive models for backbone curves using a comprehensive shear wall experimental database of 500 samples and the Gaussian Process Regression (GPR) machine learning method (Deger & Taskin, 2022). Based on twelve wall design properties, the models predict seven backbone curve variables and four limit states, such as cracking, yielding, peak shear strength, and ultimate deformation capacity. The models are recommended for walls controlled by shear or shear-flexure interaction with an accuracy of 80%. Regardless of the black box concept that most ML models are known for, the interpretability of some models, like Genetic

Programming, makes use of the ML capability to enhance the analytical governing equations used in describing the element's mechanical behaviour. The study by (G. Ma et al., 2023) proposes a backbone curve model for RC walls using Genetic programming-based symbolic regression (GP-SR). GP-SR is a white-box model with the advantage of obtaining functional correlations between inputs and outputs without assuming a functional form, in contrast to traditional machine learning techniques. The study addressed four failure modes: shear sliding, shear, flexure-shear, and flexure, where a SHAP-based feature selection method (Lundberg et al., 2017) was adopted to avoid poor generalization performance. Five machine learning models were applied to 388 existing RC walls with various failure modes, with XGB showing the best prediction performance. The GP-SR model predicted the characteristic points for the backbone curve better than ASCE 41-17 (ASCE, 2017). The model also outperformed existing empirical models in predicting shear strength. The failure mode of RC walls needs to be determined before estimating the backbone curve. The development of data-driven models contributed not only to the component level but also showed excellence on the system level. For example, the study by (Vaseghiamiri et al., 2020) introduces an innovative approach for constructing a probabilistic surrogate Single Degree of Freedom (SDOF) model characterized by a multilinear backbone curve, serving as a representative model for Multi-Degree of Freedom (MDOF) systems. The methodology focused on seismic risk and resilience analyses and parametric studies, maintaining a reasonable level of accuracy. The process involves designing 60 distinct Special Moment-Resisting Frame (SMF) buildings and conducting probabilistic pushover analyses to generate 25,200 pushover curves for training. Bayesian linear regression equations are then derived from the resulting 25,200 backbone realizations, predicting key parameters based on the fundamental period of the MDOF structure. Not only seismic excitation is considered but also wind loading which might be more challenging

due to the multiple time history load functions that should be applied on the structural model (Hareendran & Alipour, 2022; Micheli, Hong, et al., 2020). For example, (Micheli, Alipour, et al., 2020b) developed a multiple-surrogate models framework for probabilistic assessment of wind-excited tall buildings under uncertainties. The framework divides the structural system into subsystems, each represented by a surrogate model with small inputs and outputs vectors. The Kriging metamodel was used as the surrogate model trained by samples ranging from 600 to 1000. The results showed that the multiple-surrogate models accurately predicted the building's floor response with an average error of 12.5% and a cost loss probability curve with low computational demand.

On the other hand, the inclusion of such computationally efficient models either in optimization or in sensitivity analysis at the early stage of design added value for enhancing the design process where discrete, complex and non-convex optimization problems are now possible thanks to the computational speed provided by the data-driven surrogate models to deploy the fitness function through non-gradient based optimization algorithms (Mistakidis & Stavroulakis, 1998). This can be seen in the study by (Tseranidis et al., 2016), who examined multiple ML-based surrogate models to optimize the structure of trussed elements. (Elshaer, Bitsuamlak, & El-Damatty, 2017) used an ANN-based surrogate model to modify the corner radius of tall buildings in order to reduce the captured wind load through the optimized applied aerodynamic modifications. In addition, the surrogate model makes it possible to select an optimal shape for openings in tall buildings to enhance their aerodynamic behaviour (Elshaer & Bitsuamlak, 2018). Beyond surrogate models, deep learning can regenerate designs for layout through generative adversarial networks (GANs), as shown in (Liao et al., 2021; Oh et al., 2019), without an explicit definition of optimization algorithms. To enable broader application of optimization frameworks, especially those coupled

with PBWD, a surrogate model capable of capturing tall building wind response is required. The existing literature falls short in providing a thorough examination of developing a surrogate model that is capable of capturing the total performance of a tall building with a shear wall system as an MWFRS. The data-driven surrogate models have proven their efficiency, yet choosing the appropriate model requires a comparative study of different models to choose the best-performing model with the least amount of data and the highest correlation.

This study explores the accuracy of developing a data-driven surrogate model that can capture the structural response of tall buildings subjected to dynamic wind load, either global performance (e.g., peak drift) or structural elements' demand-to-capacity ratio (e.g., MWFRS and Columns). A comparative study is held between various data-driven models that have been previously used in literature for capturing element behaviour and assessing them in a system-level behaviour, including: (1) Ridge Regression (RDG) (Sun et al., 2021), (2) Decision Trees (DT) (Barros et al., 2023; Junda & Málaga-Chuquitaype, 2024), (3) Random Forests (RF) (Voulpiotis et al., 2022; C. Zhou et al., 2023), (4) Extreme Gradient Boosting (XGB) (L. Ma et al., 2022; T. Zhang et al., 2024), (5) Support Vector Machines (SVM) (Funk et al., 2023; Liu & Guo, 2021; Yetilmezsoy et al., 2021), and (6) Deep Neural Networks (DNN) (Akinosho et al., 2020; Kallioras & Lagaros, 2021; Lieu et al., 2022; Pizarro & Massone, 2021b). The main contribution of the developed surrogate model is to serve as a fitness function evaluator that is capable of deriving an optimization algorithm to identify the optimal layout of the structural system of tall buildings in the conceptual phase design.

5.2. Usage of the surrogate model in PBWD optimization framework

The utilization of surrogate models varies across a spectrum of applications. These models can be adapted in digital twin development (L. Wang et al., 2023), where they serve as efficient

alternatives for high-fidelity simulations, enabling real-time performance monitoring and decision-making. Additionally, surrogate models are vital in sensitivity analysis, showing the impact of input variations on system responses. Their role extends to reliability analysis, aiding in assessing structural robustness and performance under uncertainties and risk quantification. Moreover, these models play a pivotal role in optimization processes, guiding the exploration of design spaces for optimal solutions. In the case of tall building design, the optimization problem becomes discrete non-convex with multiple local minima, which makes using a non-gradient algorithm preferable to identify the optimal layout (Mistakidis & Stavroulakis, 1998). The proposed surrogate model can be coupled with an adequate optimization algorithm to reduce the time required for exploring thousands of samples required by the non-gradient algorithm (e.g., Genetic Algorithm) to find the optimal layout for the MWFRS (e.g., shear walls) in the initial design stage, which is a budget-sensitive item, as shown in Fig. 5-1. In this study, the focus is on developing a surrogate model capable of capturing the relationship between the crude topology of a structural system and the structural response required for evaluation. A case study building is adopted based on a previously developed optimization framework (Alanani & Elshaer, 2023, 2024). Starting with an architectural layout and thorough consideration of non-structural elements, a domain of all possible positions of shear walls and columns is identified. To determine the length and shape of shear walls, a discretization of this domain is executed, resulting in the division of the domain into 170 segments of shear walls, each measuring 1.0 m. In every model, distinct column locations are determined to prevent overlap between shear wall segments and columns. The distribution of columns is governed by a predefined span of 6.0 m, to minimize alterations in the slab's straining actions as vertical supports are strategically placed, whether columns or shear walls in those areas. Afterwards, a training database is prepared to build the required ML-based surrogate model. As

presented in Fig. 5-2, wind load time history is generated via an experimentally validated CFD model (Alanani et al., 2024a; Alanani & Elshaer, 2022) that later is applied to the building using a Finite Element Model (FEM). Based on the PBWD prestandards, all wind angles of attack (AOA) should be considered. For simplification, eight main AOA are considered in CFD analysis, with an increment of 45^o, to produce wind response for each load combination. The envelope of all AOA demand forces will be used for demand-to-capacity calculations for both shear walls and columns. For the sake of comparison, the training process for the generated database is done in two stages: the first is considering the envelope behaviour of the 8 AOA responses to generate one surrogate model for all AOA, and the second is by considering a single AOA for each model. Latin Hypercube Sampling (LHS), by (McKay et al., 1979), is selected to generate the training data for its ability to efficiently cover the multidimensional design space, providing a diverse set of 1000 layout samples. Each sample represents a unique configuration of 170 binary variables corresponding to the layout's presence or absence of shear walls. Four primary structural responses are chosen to train the ML models, which has been previously adopted as the constraints for the optimization problem: (1) peak interstory drift, (2) peak deflection, (3) demand-to-capacity ratio for columns and (4) demand-to-capacity ratio for walls. These structural parameters are recorded in a database that will be used by the current proposed ML pipeline within a comparative study to choose an efficient surrogate model capable of driving the optimization fitness function.

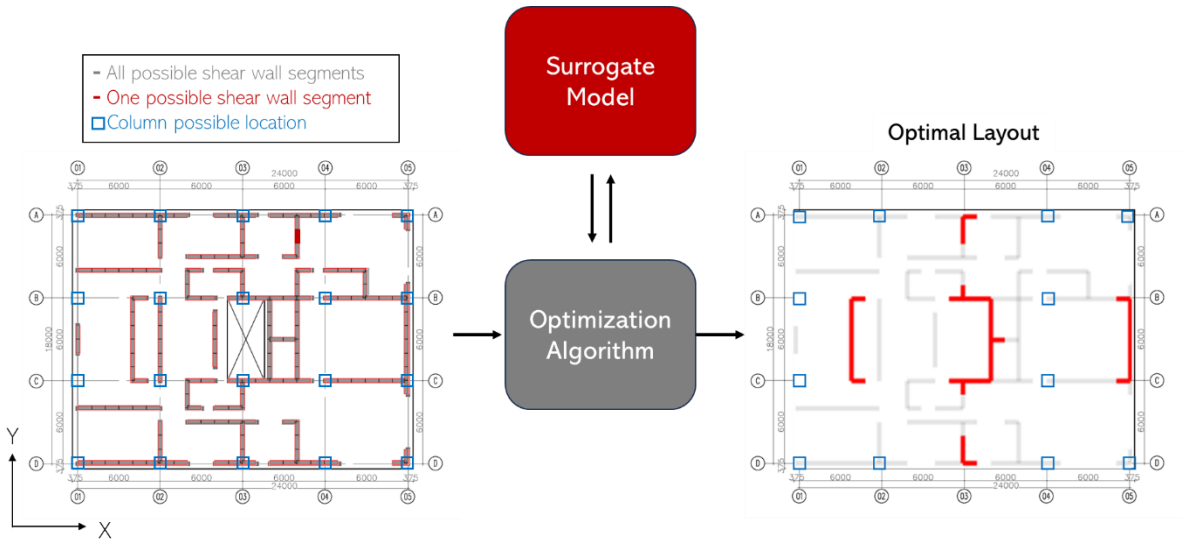

Fig. 5-1 Surrogate model attached to an optimization algorithm.

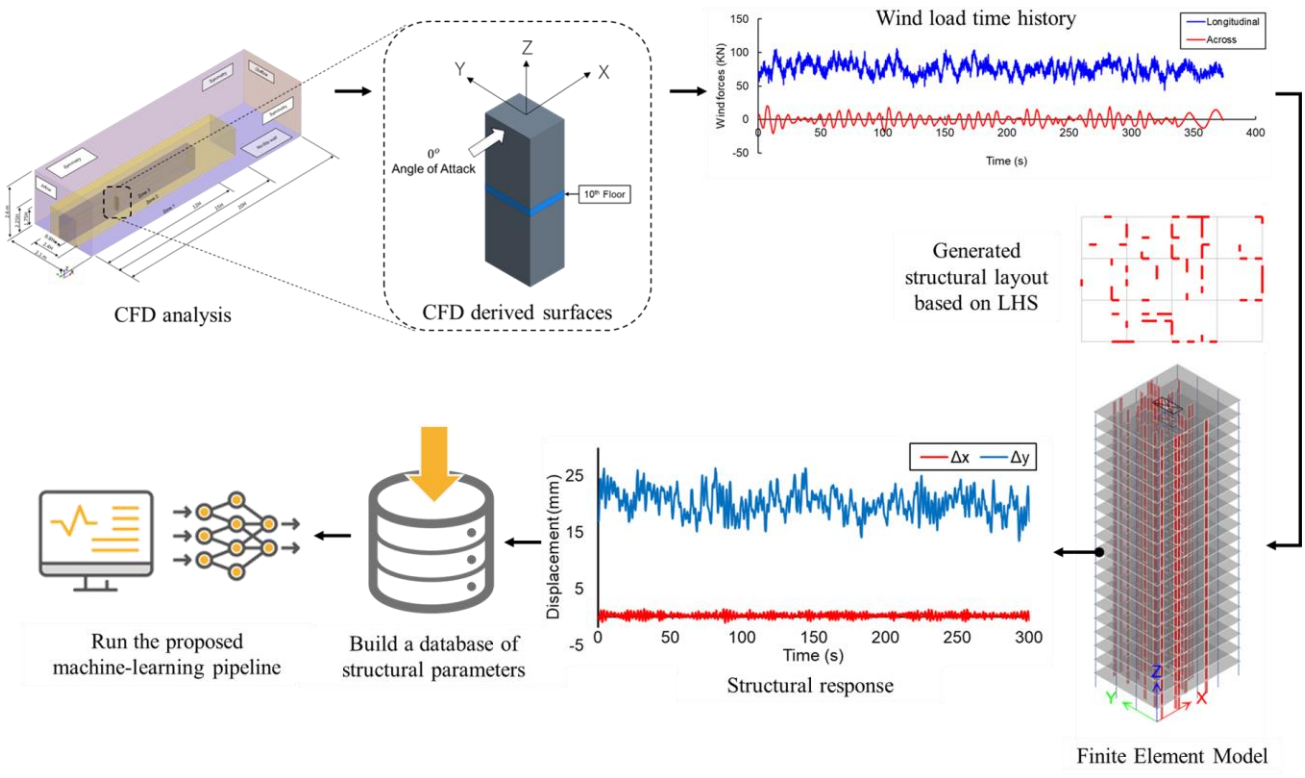

Fig. 5-2 The process of preparing a training database for the proposed ML-based surrogate model.

5.3. Regression Models

5.3.1. Ridge Regression (RR)

Ridge Regression is a shrinkage technique, also known as Tikhonov regularization (Hoerl & Kennard, 1970) or L2 regularization, used for dealing with multicollinearity and preventing overfitting in predictive modelling that incorporates a regularization term by penalizing large coefficients. It is an extension of the least square method, which minimizes the sum of squared differences between observed and predicted values, known as the residual sum of squares (RSS) and can be calculated using equation (5-1), where n is the number of observations, y_i is the observed value of the i^{th} observation and y_i' is the predicted value of the same i^{th}observation. Since it is a form of linear regression, so β_o is the intercept and the β_j is the slope coefficient for the predictor x_{ij} and p is the number of predictors.

$$RSS = \sum_{i=1}^{n}(y_i - y_i')^2 = \sum_{i=1}^{n}\left(y_i - \beta_o - \sum_{j=1}^{p}\beta_j x_{ij}\right)^2 \quad (5\text{-}1)$$

It is advantageous when dealing with multicollinearity, where predictor variables are highly correlated. The regularization term, also known as the L2 penalty, is added to the ordinary least squares objective function. In this model, the ridge regression coefficient, $\hat{\beta}^{Ridge}$, is meant to be minimized. While t is the constraint that ensures the weight vector does not grow too large, which helps control model complexity.

$$\hat{\beta}^{Ridge} = argmin_{\beta_j}\left\{RSS + \lambda\sum_{j=1}^{p}\beta_j^2\right\} \quad (5\text{-}2)$$

Subject to $\sum_{j=1}^{p}\beta_j^2 \leq t$

5.3.2. Decision Trees (DT)

The Decision Trees regression model can be considered one of the interpretable machine learning algorithms employed for classification and regression tasks. In this chapter, the DT model was proposed to be studied for its workability with binary and discrete data (Hastie et al., 2009). In this model, the dataset is recursively partitioned into subsets based on the most significant features, creating a tree-like structure where each internal node represents a decision, and each leaf node provides the final prediction. The splitting process is guided by criteria such as minimizing mean squared error, enabling the algorithm to capture complex nonlinear relationships between input features and the target variable. Decision tree regression is particularly advantageous for its ability to handle numerical and categorical data, and its intuitive representation facilitates a clear understanding of the decision-making process. The algorithm starts with growing a huge tree T_o then prune it back to create a subtree. The decision to prune the subtree depends on the lowest rate of test errors. The validation set technique or cross-validation can be used to estimate the test error of a subtree. However, since there is a multitude of potential subtrees, computing the cross-validation error for each one would be cumbersome. Instead, choosing a limited number of trees is possible using cost-complexity pruning, as shown in equation (5-3). The α is a tuning parameter that corresponds to the subtree $|T|$ where it represents the number of terminal nodes of the tree, and the predictor space is divided by R_m rectangular regions of m terminal nodes. Similar to the ridge regression, the ${y_i}'_{R_m}$ is the predicted value, and it was noticed that by increasing the α parameter, more subtrees get pruned. Thus, instead of taking into account each potential subtree,

caution must be exercised to prevent overfitting, especially with deep trees and various regularization techniques. DT models have been used for structural applications, for example, damage prediction of reinforced concrete buildings subjected to earthquakes, as presented by (Karbassi et al., 2014). Its effectiveness as a surrogate model is studied in this study.

$$C_\alpha(T) = \sum_{m=1}^{|T|} \sum_{i:x_i \in R_m} \left(y_i - {y_i}'_{R_m}\right)^2 - \alpha|T| \tag{5-3}$$

5.3.3. Random Forests (RF)

The previously explained DT models can achieve satisfactory results, yet high variance with low bias can occur. Thus, the bootstrap aggregation (i.e., bagging) reduces the high variance by building multiple B trees using B bootstraps to reduce the variability of each predictor. The Random Forest algorithm leverages the concept of bagging. However, it uses a modified approach to decorrelate predictors through splitting the predictors and avoiding the selection of all predictors at each bootstrap. RF is considered an ensemble learning method that leverages the strength of multiple decision trees to enhance predictive accuracy and robustness. In the context of Random Forest, decision trees act as the building blocks, collectively forming a forest that harnesses the strengths of multiple models. The ensemble approach excels in handling noisy data and capturing complex relationships. For instance, a sample size of N can be divided into multiple bootstraps B, and then a random forest tree T_b can be built till the minimum node size n_{min}. Then, the selection of random predictors m is done where $m \leq p$, noting than p is the total number of predictors. The optimal number of split points among variables m is identified, and then the total ensemble is $\{T_b\}_1^B$. For any prediction afterwards, the equation (5-4) can be used.

$$\hat{f}_{RF}^{B}(T) = \frac{1}{B}\sum_{b=1}^{B} T_b(x) \tag{5-4}$$

5.3.4. Extreme Gradient Boosting (XGB)

The extreme gradient boosting developed for decision tree algorithms stands out as a solid and effective ensemble learning algorithm (Chen & Guestrin, 2016). XGB shares a lineage with decision trees, at which it integrates shallow decision trees sequentially, each correcting the errors of its predecessor. Yet, it diverges from Random Forest's ensemble construction. XGB focuses on a sequential construction of decision trees, where each successive tree corrects the flaws of the previous ones, as opposed to building parallel decision trees individually. Furthermore, XGB improves its capacity to manage complex relationships and outliers by including a regularization component in the objective function. Unlike bagging, XGB relies on a weighted procedure of building trees of predictors based on previously built trees. In bagging, multiple trees are built based on the bootstrap and then combined with averaging. In XGB, trees are fitted based on the error of previously developed models using a shrinkage factor λ to slow the learning process and form simpler trees that provide more bias and less variance. Based on gradient boosting concepts, XGB builds a sequence of decision trees and iteratively improves forecasts by regularized learning and sparsity-aware split findings by minimizing the loss function in equation (5-5), measuring the difference between actual and predicted values, $\sum_i l({y_i}'_i, y_i)$, in addition to regularization term, $\sum_k \Omega(f_k)$, of the k^{th} tree. The first part of the regularization term controls the strength of the penalty. A higher γT value leads to more aggressive pruning, where T is the total number of trees as a penalization for tree complexity. The second part of the regularization is a leaf score magnitude that penalizes the magnitude of the scores, $\|w\|^2$, assigned to the leaf nodes. The regularization parameters γ and λ) are hyperparameters that need to be tuned during the model

training process. A higher value for these parameters increases the regularization strength, leading to more aggressive pruning and smaller leaf scores. XGB has proven its capability to predict the capacity of structural elements trained on a FEM-generated database (Haggag et al., 2024).

$$\mathcal{L} = \sum_i l({y_i}'_i, y_i) + \sum_k \Omega(f_k) \tag{5-5}$$

Where $\Omega(f) = \gamma T + \frac{1}{2}\lambda\|w\|^2$

5.3.5. Support Vector Machines (SVM)

Support Vector Machines (SVM) represent powerful machine learning algorithms renowned for their effectiveness in classification and then developed for regression tasks. SVM operates by finding an optimal hyperplane that best separates data points belonging to different classes, maximizing the margin between the classes. Unlike decision trees, SVM does not rely on an ensemble approach but focuses on finding the most efficient decision boundary (Cortes et al., 1995). SVM excels in scenarios with high-dimensional data and is particularly effective when clear linear separability exists. While decision trees and random forests construct a hierarchy of decision rules, XGB sequentially builds an ensemble of weak learners. SVM's strength lies in its ability to handle complex decision boundaries in both linear and nonlinear cases through the use of kernels, providing flexibility compared to XGB. However, SVM may be less interpretable than decision trees and lack the ensemble approach of random forests and XGB. The choice between SVM, decision trees, random forests, and XGB depends on the nature of the data, interpretability requirements, and the trade-off between computational complexity and predictive performance. SVR consists of a regularization parameter, C, that controls the trade-off between fitting the training data and having a smooth decision boundary. Additionally, it relies on kernels like the linear, polynomial, Gaussian (RBF), and sigmoid kernels to handle nonlinear relationships by

transforming the data into higher-dimensional spaces as shown in equation (5-6), where k is the kernel function, and M is the total number of samples of N number of predictors x. It is a reformulation of the basic regression function, where $h(x)$ is the basis function while to find β, β_o a minimization for equation (5-7) should be conducted. w indictes the normal vector of the hyperplane, while b is the intercept. ζ_i are the distances of points on the wrong side of their margin, and ε indicates the soft margin. Hyperparameter tuning can be achieved by finding optimal C and Kernel parameters.

$$f(x) = \sum_{m=1}^{M} \beta_m h_m(x) + \beta_o = \sum_{i=1}^{N} a_i k(x, x_i)^d \tag{5-6}$$

$$\min_{w,b,\zeta_i,} \frac{1}{2}\|w\|^2 + C\sum_{i=1}^{N}(\zeta_i + \zeta_i^*) \tag{5-7}$$

Subjected to $y_i(w, x_i - b) \leq \varepsilon + \zeta_i$

5.3.6. Deep Neural Networks (DNN)

Deep neural networks are forms of artificial neural networks with more than one hidden layer of neurons that show remarkable capabilities in handling complex data through nonlinear learning algorithms. In contrast to traditional ML models like Decision Trees (DT), Random Forests (RF), Support Vector Machines (SVM), and Gradient Boosted Trees (XGB), DNNs operate on a different paradigm that is considered the foundation of deep learning models (Li et al., 2021). Their interconnected layers of nodes, which can be mathematically presented as A_k equation (5-8), where k is the number of nodes, enables them to extract hierarchical features from raw data automatically. While tree-based models excel in interpretability, DNNs trade interpretability for unparalleled predictive power in large-scale, high-dimensional datasets. The equations governing DNNs involve forward and backward passes through the network, with parameters updated using

gradient-based optimization algorithms like Stochastic Gradient Descent (SGD). The activation functions, such as ReLU, introduce nonlinearities, as shown in equation (5-9), where $h_k(x)$ is a nonlinear activation function, enhancing the model's capacity to capture intricate patterns. The flexibility and scalability of DNNs come at the cost of increased complexity and the need for substantial amounts of labelled data for training.

$$A_k = h_k(x) = g(w_{k_o} + \sum_{j=1}^{p} w_{k_j} x_j) \tag{5-8}$$

$$f(x) = \beta_o + \sum_{k=1}^{K} \beta_k h_k(x) = \beta_o + \sum_{k=1}^{K} \beta_k g\left(w_{k_o} + \sum_{j=1}^{p} w_{k_j} x_j\right) \tag{5-9}$$

The fitting of neural networks consists of two main functions: feed-forward and backpropagation, which are done by minimizing the loss function in equation (5-10), where θ is assumed to be the vector of all parameters. The gradient descent, shown in equation (5-11), derives the loss function toward an optimal value and then updates the parameters θ as shown in equation (5-12). The backpropagation process is evident through the chain rule that distributes a fraction of residuals to each parameter. Through literature, DNN has excelled as a regression surrogate model. For instance, The DNN-surrogate model developed by (Solorzano & Plevris, 2023a) is capable of predicting the nonlinear curve of a lateral pushover analysis applied over RC shear walls using the wall's geometry, properties, and loading conditions to get the corresponding nonlinear pushover curve discretized into six segments.

$$R(\theta) = argmin_{\{w_k\}_1^k,\beta} \frac{1}{2}\sum_{i=1}^{n}\left(y_i - f(x_i)\right)^2 \quad (5\text{-}10)$$

$$\nabla R(\theta^m) = \frac{\partial R(\theta)}{\partial \theta}|_{\theta=\theta^m} \quad (5\text{-}11)$$

$$\theta^{m+1} \leftarrow \theta^m - \rho\, \nabla R(\theta^m) \quad (5\text{-}12)$$

5.4. Development of surrogate models

In this study, a pipeline has been built using Python's built-in libraries (e.g., NumPy and Tensorflow) for developing an ML-based surrogate model using an offline synthetically developed database using (MATLAB, 2023) and ETABS OAPI (CSI, 2018), as shown in Fig. 5-4. As mentioned in section 5.2, the surrogate model's main objective is to act as an alternative model that can predict the structural response (e.g., drift, displacement and D/C) based on the shear walls' and columns' layout variations. The model inputs are defined as N binary design variables that represent the location of each shear wall segment, where 0 and 1 mean inactive and active shear wall segments, respectively. The required structural outputs are as follows: (1) peak displacement (Δ_{peak}), (2) peak drift (δ_{peak}), (3) peak demand-to-capacity ratio of columns ($D/C_{columns}$) and (4) peak demand-to-capacity ratio of walls (D/C_{walls}). The required database is generated using the Latin Hypercube Sampling (LHS) technique, where the generated sample data distribution is shown in Fig. 5-3. LHS is a strategic sampling technique employed in the field of experimental design and uncertainty quantification (McKay et al., 1979). Unlike random sampling methods, LHS ensures a more even and representative exploration of the input space $[s_1, s_2, \dots, s_N]$. The fundamental principle involves dividing each input variable into intervals of equal probability and selecting one sample from each interval, ensuring that all intervals are sampled once. This approach ensures uniform input space coverage and minimizes the risk of oversampling or undersampling. While the primary objective is to efficiently sample across the entire input domain,

LHS also enhances the exploration of potential correlations between variables. The process starts with dividing the design domain into n intervals as mentioned in equation (5-13) at which for each design variable a random binary value is selected. For each selection a check is done to ensure that the probability of each variable is not exceeded.

$$s_{i,j} = [(i-1) \times \frac{upper\ bound_i\ -\ lower\ bound_i}{n} + \ lower\ bound_i + rand(0,1))] \tag{5-13}$$

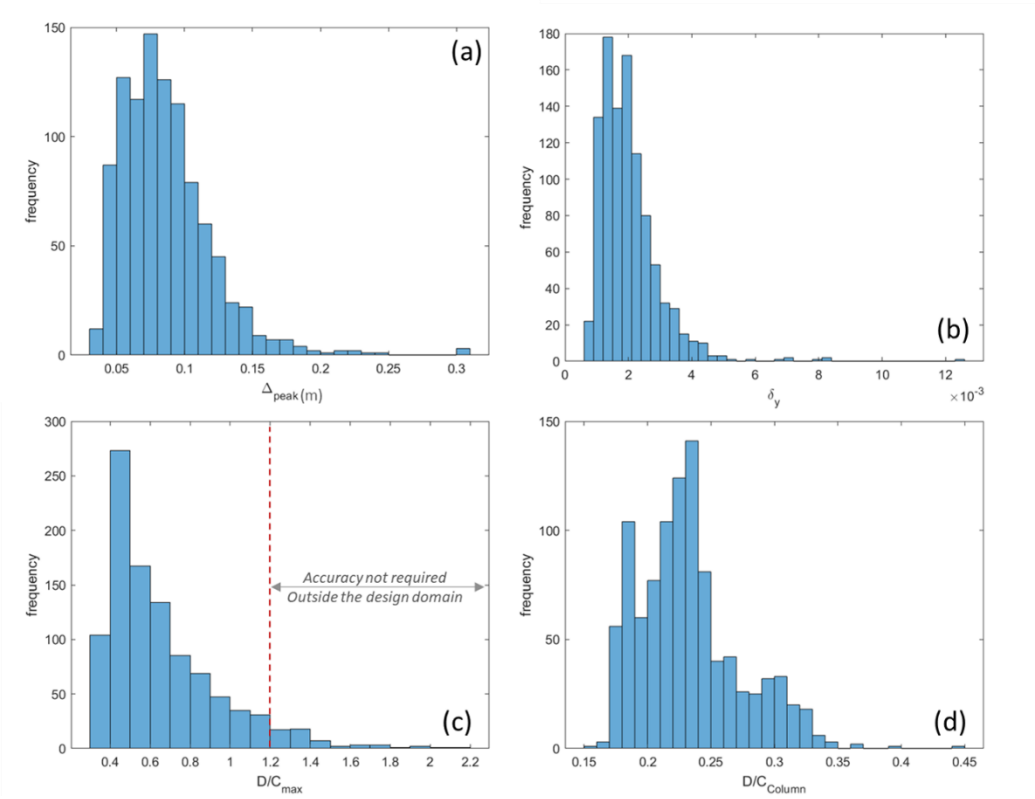

Fig. 5-3 Structural response data distribution for 1000 generated samples using LHS

The preprocessing of data through normalization is done to reduce the skewness found in the data distribution and to enhance the model's consistency by reducing the sensitivity to the scale of the data. Then, the generated dataset, of size $n = 1000$, gets split into 80% for training and 20% for testing. While the testing set is held for performance evaluation, the training set will go through a cross-validation process in which parameters and hyperparameters will be tuned via a grid search

algorithm. The grid search algorithm systematically evaluates a predefined hyperparameter grid, exhaustively testing different combinations to identify the set that maximizes model effectiveness. This method provides an exhaustive search over specified hyperparameter values, offering a comprehensive understanding of the parameter space.

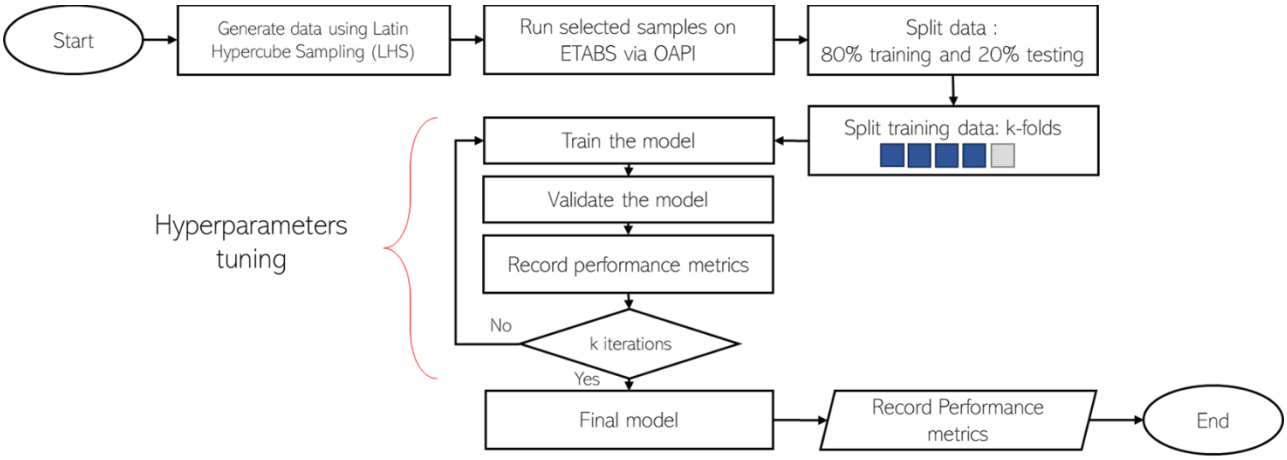

Fig. 5-4 ML-based surrogate model's developing pipeline

5.4.1. Model cross-validation, testing, and hyperparameter tuning

Cross-validation is a crucial machine-learning technique used to assess a model's performance and generalization ability. Its primary purpose is to provide a more reliable estimate of a model's performance on unseen data compared to a single train-test split. The key idea is to simulate how the model would perform on different subsets of the data. In this study, a K-fold cross-validation technique is adopted (Stone, 1974). This approach divides the dataset into K equally sized folds, where K is chosen as five folds in this study. The model is trained and validated K times, each using a different fold as the validation set and the remaining $K-1$ folds as the training set. This process ensures that every data point is used for validation exactly once to avoid overfitting or underfitting. Then, the performance of each fold is recorded, and the average of all folds is considered to indicate how the model is generalized and how reliable it is in prediction. Within the K-fold loop, the hyperparameter optimization process is applied to do an exhaustive search for the

optimal combination of hyperparameters. Hyperparameters are considered the external configuration required for the training process, and they differ based on each ML model. For example, the neural networks' hyperparameters are the number of neurons and layers, while the decision trees rely on the tree's depth as a hyperparameter. All hyperparameters used in this study for all ML models are mentioned in Table 5-1.

Table 5-1 Hyperparameters configuration for each ML model

ML model	Hyperparameters
Ridge regression (RDG)	$\lambda \in [10^{-6}, 10^{6}]$
Decision Trees (DT)	Maximum depth: [1,21] Minimum sample split: $m \in \{1,2,3,5,10,20\}$ Minimum sample leaf: $T \in \{1,5,10,20,50,100\}$
Random Forest (RF)	Number of predictors: $p \in [10,200]$ Maximum number of samples: $B \in [\,5, 10]$ Minimum node size: $n_{min} \in \{2, 5, 10\}$
Extreme Gradient Boosting (XGB)	Column sample by tree: [0,1] Max depth: [50,1050] Number of estimators: [50,200]
Support Vector Regression (SVR)	Kernel Type: {Linear, Polynomial, Radial basis function (RBF), Sigmoid} C (Regularization Parameter): $C \in [10^{-6}, 10^{6}]$ SVR Margin: $\varepsilon \in [0.1,10]$
Deep Neural Networks (DNN)	Number of hidden layers: [1,12] Number of neurons: [10,800] Learning rate: $\alpha \in [10^{-4}, 0.1]$ Activation Function: $\{Sigmoid, Tanh, RelU\}$

Within each iteration of the K-fold cross-validation loop, model parameters, representing the internal aspects of the algorithm, are adjusted to enhance learning capabilities. Parameters are the internal variables that the model learns from the training data. These are the coefficients in a linear regression, weights in a neural network, or split points in a decision tree. The identification parameters are based on performance metrics, which is this study's mean square error (MSE). This dual optimization strategy, encompassing both hyperparameter and parameter tuning, ensures a

comprehensive exploration of the model's potential. After updating the models with the optimal parameters and hyperparameters, all models will be tested against the previously held test data, and a comparison will be made based on the performance metrics mentioned in Table 5-2, where y_i is the actual value and $y_i{}'$ is the corresponding prediction, while $\bar{y}$ and $\bar{y'}$ are the mean values of them respectively.

Table 5-2 Statistical performance metrics

Statistical performance metrics	formula	
Coefficient of determination (R^2)	$R^2 = 1 - \frac{\sum_{i=1}^{n}(y_i - y_i{}')^2}{\sum_{i=1}^{n}(y_i - \bar{y})^2}$	(5-14)
Pearson Correlation Coefficient (Pearson R)	$\text{Pearson R} = \frac{\sum_{i=1}^{n}(y_i{}' - \bar{y'})(y_i - \bar{y})}{\sqrt{\sum_{i=1}^{n}(y_i{}' - \bar{y'})^2 \sum_{i=1}^{n}(y_i - \bar{y})^2}}$	(5-15)
Mean Absolute Error (MAE)	$MAE = \frac{1}{n}\sum_{i=1}^{n}\lvert(y_i - y_i{}')\rvert$	(5-16)
Root Mean Squared Error (RMSE)	$RMSE = \sqrt{\frac{\sum_{i=1}^{n}(y_i - y_i{}')^2}{n}}$	(5-17)
Symmetric Mean Absolute Percentage Error (SMAPE)	$SMAPE = \frac{1}{n}\sum_{i=1}^{n}\frac{\lvert(y_i - y_i{}')\rvert}{\frac{1}{2}(\lvert y_i\rvert + \lvert y_i{}'\rvert)} \times 100$	(5-18)
Error percentage	$Error\% = \frac{y_i - y_i{}'}{y_i} \times 100$	(5-19)

5.5. Results and Discussion

5.5.1. Assessment of the training samples performance for different surrogate models

In this section, a comparison is made between the previously proposed machine learning models in order to identify which model is more reliable to build on and which can be coupled with an appropriate optimization algorithm for early-stage design to identify the structural system layout. The pipeline previously described split the dataset into 80% for training and 20% for testing. Throughout the training process, which uses the cross-validation concept, R^2 was recorded to show how different folds perform and to evaluate the model's goodness of fit. It measures how well the model's predicted values match the dataset's observed values. R^2 is a single value between 0 and

1, where 1 indicates a perfect fit, and 0 indicates that the model does not explain any variability in the response variable, essentially equivalent to a constant model that predicts the mean of the response for all observations. In Fig. 5-5, The distribution of the R^2 is presented for all structural parameters required for optimization: (1) peak deflection, (2) peak interstory drift, (3) maximum D/C in shear walls and (4) maximum D/C in columns. It can be noticed that DNN models show a high capability of training compared to other ML models that can reach R^2 of 0.99 in capturing the maximum demand-to-capacity ratio of shear walls with a very low standard deviation that indicates, the model is generalized on data. However, this metric is not enough and might be deceiving since, in testing shown in Fig. 5-6, the DNN model showed an overfitting behaviour since it dropped in performance similar to other models. It is worth mentioning that the D/C_{walls} is quite challenging nonlinear problem that required fine considerations through the whole pipeline, starting from sampling through feature selection and ending with ML-model selection. In cases of predicting the peak displacement and interstory drift, the relationship to the crude topology of the MWFRS is more robust since it is directly proportional to the inertia, compared to the demand-to-capacity ratio, which might require more data, different features or more variational samples, and this will be discussed in section 5.5.3. When it comes to the generalization of models through training, the decision-tree model falls short with a high standard deviation of R^2 in almost all models and that can happen based on the random initial start of each fold where the pruning of the tree differs significantly based on the chosen depth. DT is one of the most sensitive models to hyperparameter tuning, affecting its performance tremendously. Surprisingly, the SVR model did not perform as expected, especially in the case of peak interstory drift; it can be related to the presence of outliers that might affect the accuracy of the hyperplane created for the prediction. In contrast, XGB models showed a decent performance in training quality that comes after DNN.

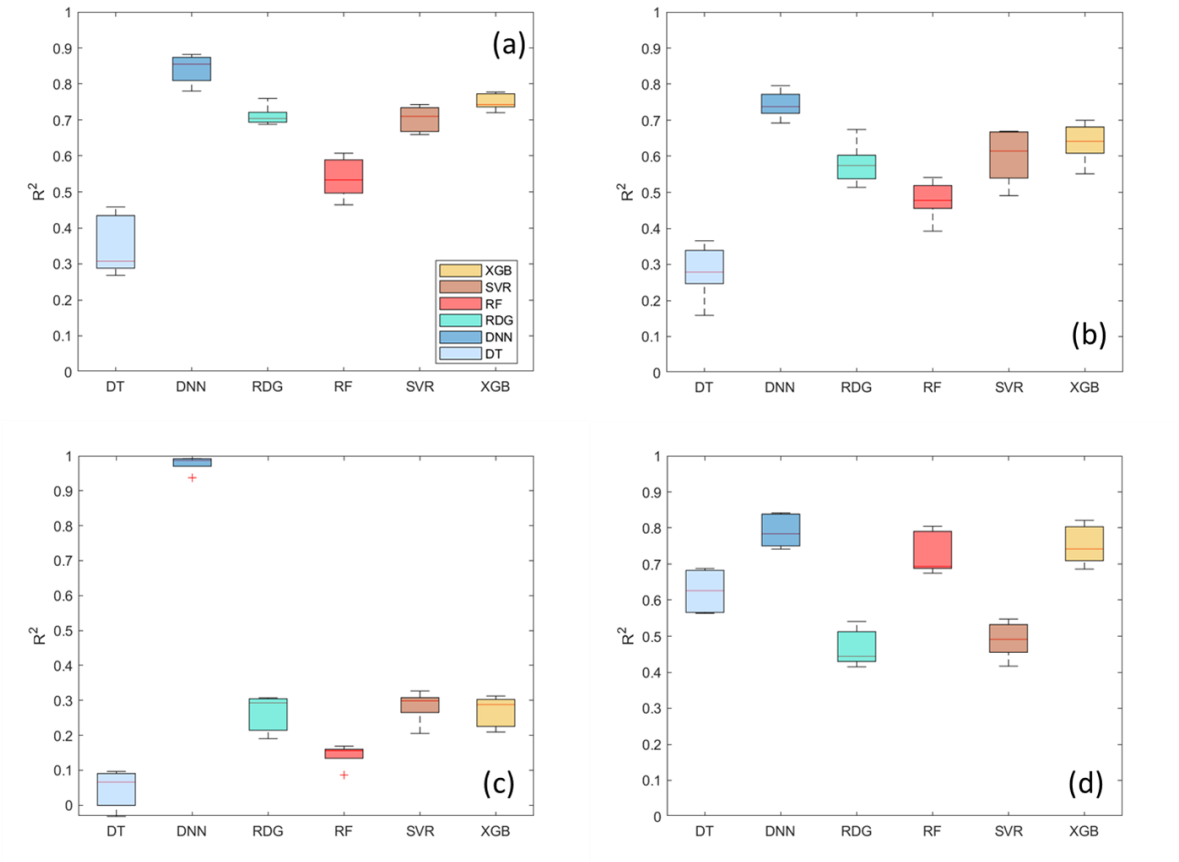

Fig. 5-5 Coefficient of determination box plot for 5-fold through the cross-validation training of different ML models: (a) peak deflection, (b) peak interstory drift, (c) maximum D/C in shear walls and (d) maximum D/C in columns.

5.5.2. Assessment of testing samples performance for different surrogate models

For a better interpretation of the developed model, the comparison will be held on the test dataset through R^2 and error distribution all over the samples presented in Fig. 5-7. Among all proposed surrogate models, DNN and XGB outperform other models. For peak deflection, DNN and XGB reached an $R^2 = 0.77$, with a neglibile exceedance of XGB over DNN, while for the error distribution, XGB mean error is ~17% with 50% of error below 20%. While SVR model R^2 is 0.68 for peak drift, the mean error is ~18%, which shows a slightly better error distribution than DNN, which got a mean error of 20%. When it comes to the behaviour of the peak interstory drift, which is dependent on the building's deflection. The DNN showed a significant overperformance compared to the rest of the models, with R^2 of 0.63 and half of the test set error is below the 30%,

relying on its capabilities to capture nonlinearity. The deviation between different structural parameters, shown using the R^2, indicates that the complexity of all parameters is not the same, and the grid search yields different optimal hyperparameters for each structural parameter even when using the same ML model. In contrast to the D/C_{walls}, the maximum $D/C_{columns}$ was a bit easier to capture the behaviour due to the fact that columns are mainly responsible for transferring most of the vertical loads in the form of axial straining actions and no bending moment is allowed. The deviation of R^2 between the proposed ML models is minimal compared to other structural parameters. Even decision trees that poorly behaved in previous structural parameters showed a significant improvement in predicting the $D/C_{columns}$. While XGB is showing a better R^2 of 0.71, which is better than the DNN and RF of 0.68. The analysis of error reveals a contrasting perspective compared to the R^2values, indicating nuances in the performance assessment of the models. The error, representing the differences between predicted and actual values, shows that the DNN has a lower standard deviation, and 75% of samples are getting an error of less than ~20% compared to the XGB of ~25% and RF of ~27%.

Furthermore, selecting an appropriate ML-based surrogate model for each structural parameter depends on the performance metric used for comparison. Thus, a unified reference performance index is developed that combines multiple performance metrics in a weighted manner to provide a single index to facilitate the process of selection. The reference index, based on literature, is a weighted sum of 10% Pearson-r, 30% R^2, 30% SMAPE, and 30% RMSE. All error values are normalized for a better presentation of indices, noting that the inverse value is considered for error metrics since a higher error indicates a lower performance. In Fig. 5-8, a spider web plot is employed to compare all the normalized performance metrics of all ML models. DNN and XGB can be selected for the peak deflection, while for peak interstory drift and $D/C_{Columns}$, DNN

outperformed all proposed ML models. For the D/C_{walls}, the SVR scored the highest R^2 among other model yet the reference index showed a similar value for both XGB and SVR.

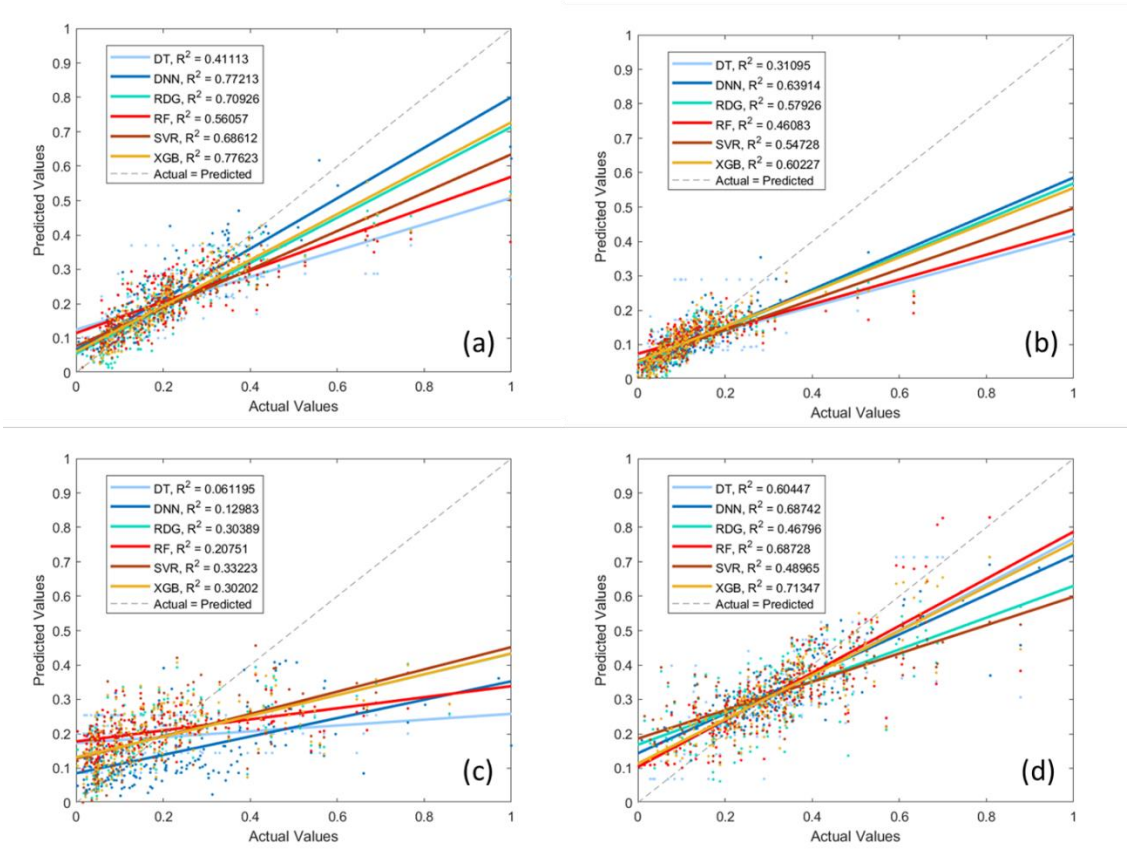

Fig. 5-6 Actual and predicted values representation for: (a) peak deflection, (b) peak interstory drift, (c) maximum D/C in walls and (d) maximum D/C in columns

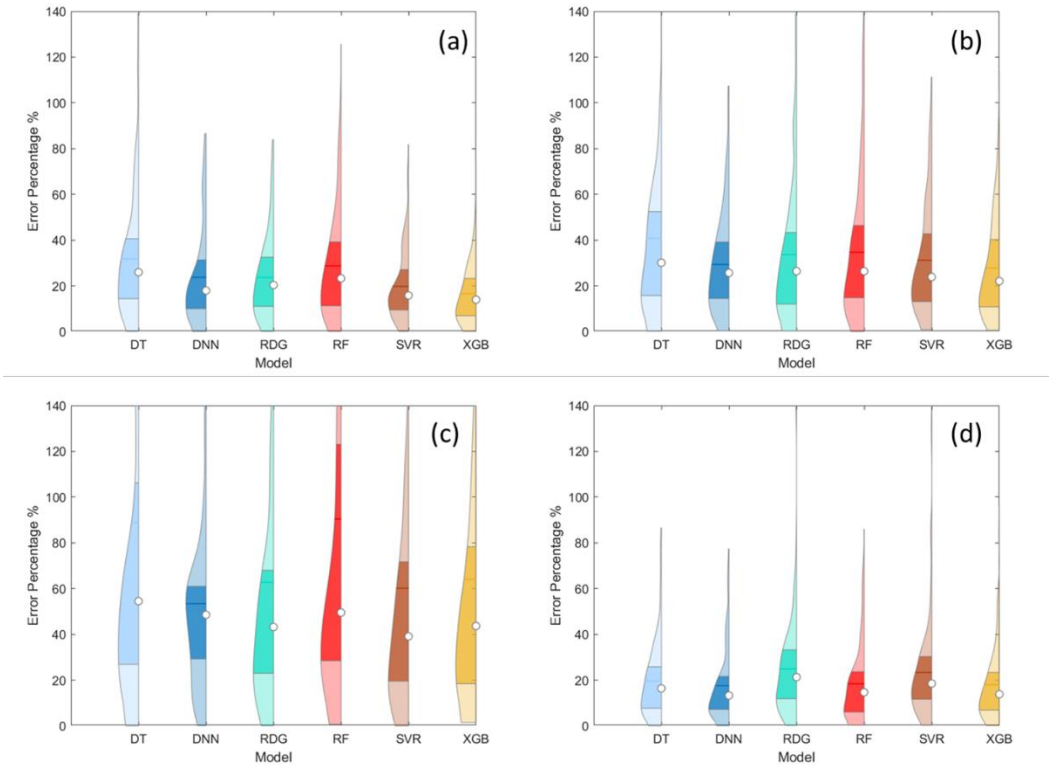

Fig. 5-7 Error distribution percentage of different ML models for: (a) peak deflection, (b) peak interstory drift, (c) maximum D/C in shear walls and (d) maximum D/C in columns

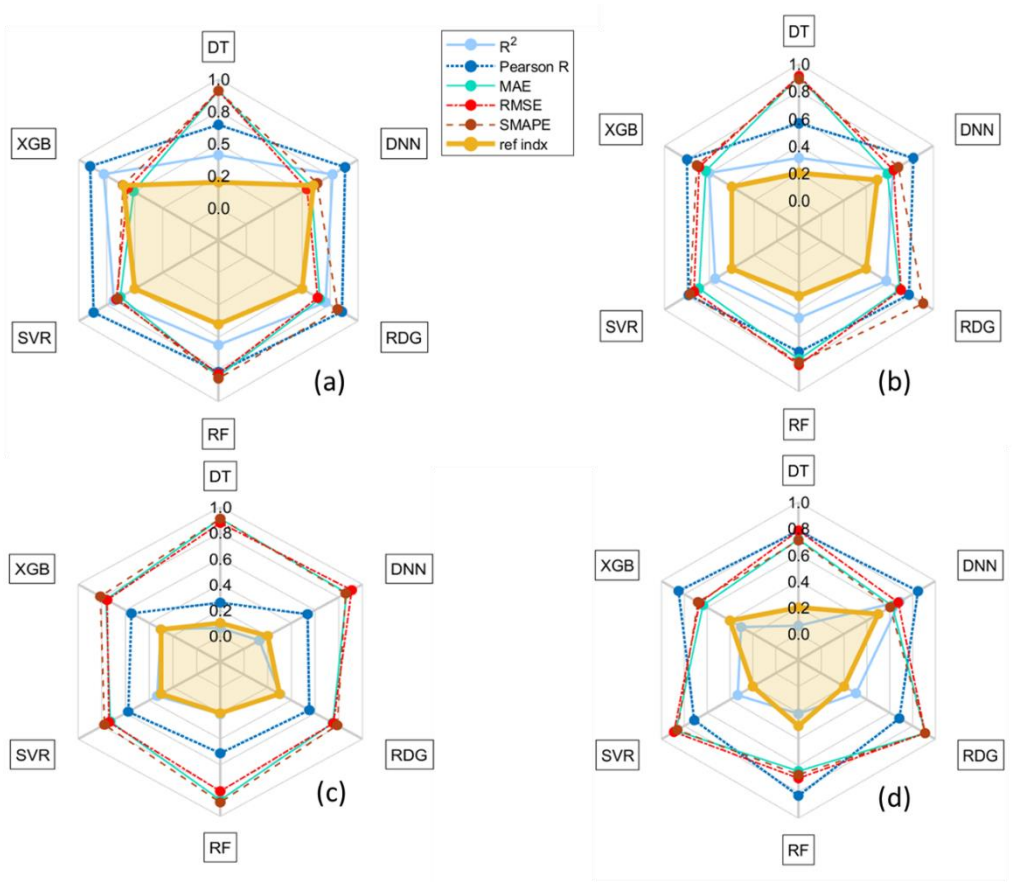

Fig. 5-8 Performance metrics of different ML-based surrogate models (a) peak deflection, (b) peak interstory drift, (c) maximum D/C in shear walls and (d) maximum D/C in columns

5.5.3. The effect of considering a single wind angle of attack on surrogate models

The demand-to-capacity ratio of MWFRS, D/C_{walls}, is a crucial parameter that, if considered in the optimization problem, will be an added value that can reduce the required effort in the final design stages, and an adequately performing surrogate model will enhance the results of selecting an optimal structural layout for tall buildings. As a result, to enhance the capability of ML models in capturing this structural behaviour, a strategic approach involves reducing the complexity of structural parameters by considering the resulted maximum D/C_{walls} of one angle of attack (AOA) wind loading per surrogate model instead of considering the maximum D/C_{walls} out of 8 AOA wind loads per model. By applying this enhancement to the same training and testing data set. It shows a significant improvement in the performance metrics, as shown in Fig. 5-9. The DNN

model returned to be the best-performing model with an increase in the test sample. R^2 that reached 0.55. DNN did not only overperform in the coefficient of determination but also the reference index confirmed that even the error distribution was better. Comparing the proposed enhancement to the previously developed model, the mean error dropped from ~50% to ~21%, as shown in Fig. 5-10. Thus, as a form of model enhancement, increasing the training data sample showed a noticeable increase in the coefficient of determination of testing data, reaching 0.84 with an almost 50% increase in the R^2value. Doubling the database size through increasing the total training and testing samples from 1000 to 2000 increased the ability of the DNN model to capture the maximum D/C_{walls} in the dynamic model. While a marginal increase occurred in the mean error for the DNN model of double sample size, labelled as 1 $AOA\ DNN \times 2$, from ~21% to ~25%, the total error of 50% of the data dropped from ~36% to ~28%. Since the database size is doubled, 50% of the new data equals 1000 samples. This increase can be noticed in the spike of the reference index shown in Fig. 5-10 (c), which indicates that not only the goodness of fit but also the distribution of error through RMSE and SMAPE has been improved.

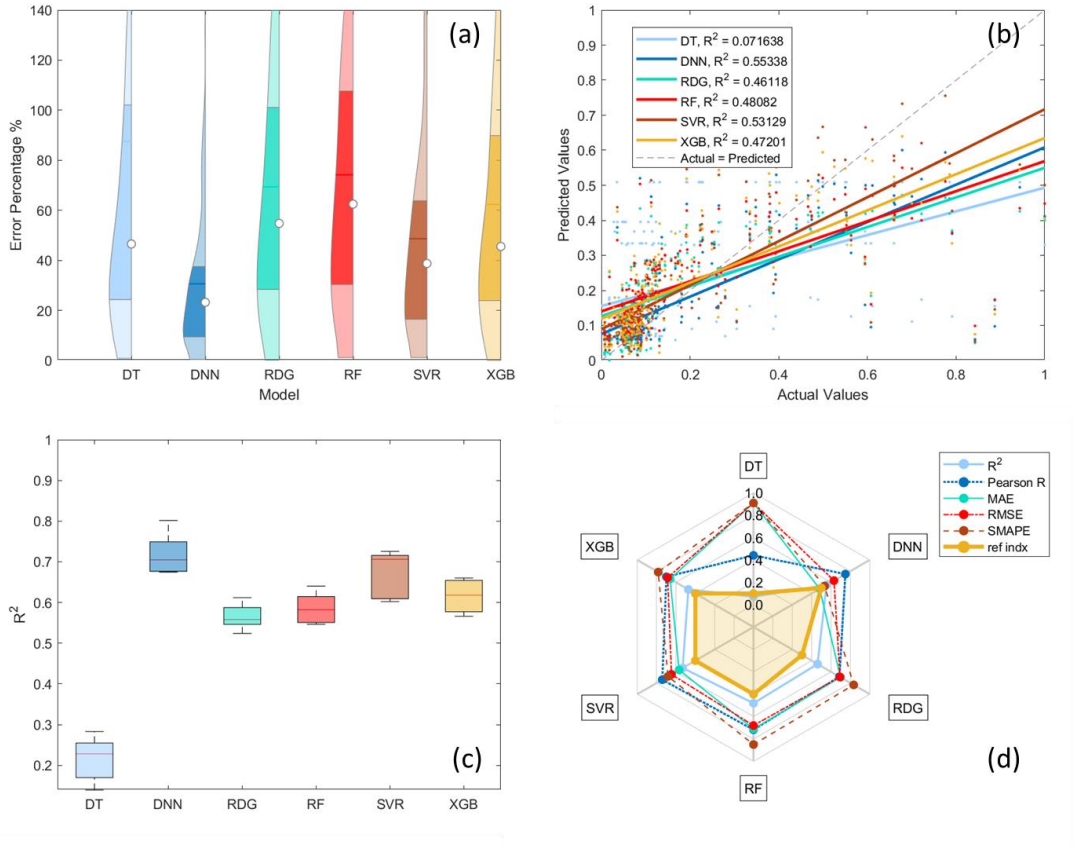

Fig. 5-9 A comparison of different ML models for a 1 AOA scenario using: (a) error %, (b) actual and predicted values representation, (c) 5-fold coefficient of determination distribution, and (d) performance metrics.

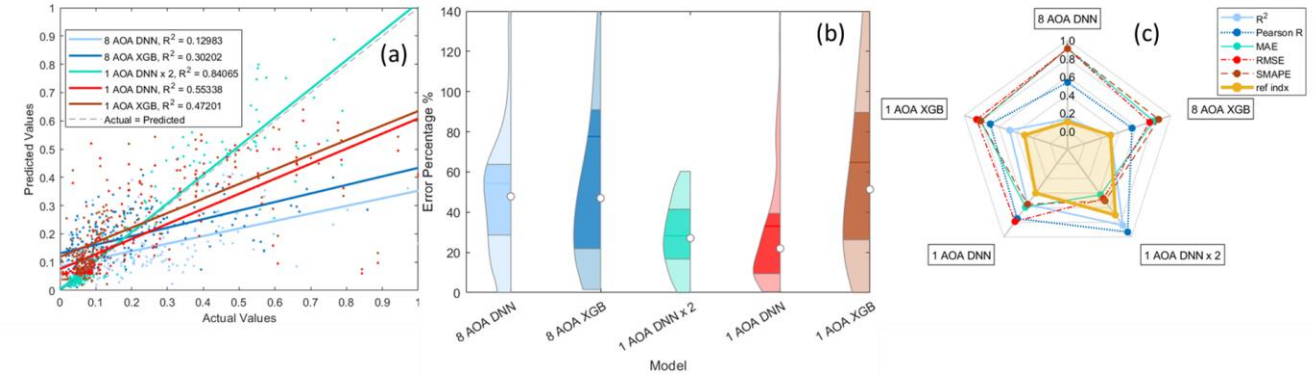

Fig. 5-10 A comparison between best performing ML models for 1 and 8 AOA scenarios: (a) error %, (b) coefficient of determination, (c) 5-fold coefficient of determination distribution, and (d) performance metrics.

5.6. Conclusion

This research endeavours to address the challenges faced in predicting the dynamic behaviour of wind-excited tall buildings by providing a framework for developing and applying data-driven surrogate models. The findings of this study highlight the significant potential of surrogate models in tall building design processes, especially when deployed within an optimization framework where discrete, complex and non-convex optimization problems are now possible thanks to the computational speed provided by the data-driven surrogate models to derive the fitness function. A case study tall building is adopted where a structural system layout should be identified in the initial stage. Thus, an efficient surrogate model is identified through a comparative study of multiple recommended machine-learning algorithms, including: (1) Ridge Regression (RDG), (2) Decision Trees (DT), (3) Random Forests (RF), (4) Extreme Gradient Boosting (XGB), (5) Support Vector Machines (SVM), and (6) Deep Neural Networks (DNN). The developed surrogate model objective is to capture the relationship between the topology of tall buildings (i.e., shear wall segments) and structural performance typically required for PBWD: (a) peak interstory drift, (b) peak deflection, (c) demand-to-capacity ratio for columns and (d) demand-to-capacity ratio for walls. For models' comparison, four performance metrics have been combined in a weighted sum formula to form a single reference index that eases the decision-making process. When considering eight wind AOA, XGB and DNN models have shown an adequate capability in capturing the performance of peak deflection, peak interstory drift and demand-to-capacity ratio of columns with an R^2 of 0.77, 0.68 and 0.71, respectively. While XGB and DNN overperformed other proposed ML models, all models showed a low performance for the maximum demand-to-capacity ratio for shear walls due to the complexity of such parameters that rely on the load, the topology, and the design code regulations. Considering the maximum D/C_{walls} of one angle of attack (AOA) wind loading per surrogate model instead of considering the maximum D/C_{walls} out of 8 AOA wind

loads per model reduced the complexity of the relationship required to be captured. Consequently, DNN outperformed all other proposed models with a testing R^2 of 0.55 and Pearson r of 0.81, with 50% of the error below 30%. While the range of training R^2 showed a value between 0.69 and 0.82, exceeding all other models. Among all proposed data-driven surrogate models, it can be deduced that DNN is the best surrogate model, capturing the required structural response thanks to its deep learning capabilities. In addition, multiple surrogate models showed more efficiency than single models that require more data and more complex models to be captured.

5.7. References

Abdelwahab, M., Ghazal, T., Nadeem, K., Aboshosha, H., & Elshaer, A. (2023). Performance-based wind design for tall buildings: Review and comparative study. *Journal of Building Engineering*, *68*(November 2022), 106103. https://doi.org/10.1016/j.jobe.2023.106103

Akinosho, T. D., Oyedele, L. O., Bilal, M., Ajayi, A. O., Delgado, M. D., Akinade, O. O., & Ahmed, A. A. (2020). Deep learning in the construction industry: A review of present status and future innovations. *Journal of Building Engineering*, *32*. https://doi.org/10.1016/j.jobe.2020.101827

Alanani, M., Brown, T., & Elshaer, A. (2024). Mulit-objective structural layout optimization of tall buildings subjected to dynamic wind loads. *Journal of Structural Engineering, ASCE*, 1–30. https://doi.org/10.1061/JSENDH/STENG-12366

Alanani, M., & Elshaer, A. (2022). Structural Layout Optimization of Tall Buildings Against Wind Load. *Proceedings of the Canadian Society of Civil Engineering Annual Conference 2022*. https://www.researchgate.net/publication/361756060_Structural_Layout_Optimization_of_Tall_Buildings_Against_Wind_Load

Alanani, M., & Elshaer, A. (2023). ANN-based optimization framework for the design of wind load resisting system of tall buildings. *Engineering Structures*, *285*, 116032. https://doi.org/10.1016/j.engstruct.2023.116032

Alanani, M., & Elshaer, A. (2024). Performance-based layout optimization framework of tall buildings subjected to dynamic wind load (submitted). *Journal of Wind Engineering and Industrial Aerodynamics*.

ASCE. (2017). Minimum Design Loads for Buildings and Other Structures. In *ANSI/ASCE Standard* (Issue 7 98). American Society of Civil Engineers. https://doi.org/10.1061/9780872629042

ASCE. (2019). Prestandard for Performance-Based Wind Design V1.1. In *Prestandard for Performance-Based Wind Design V1.1*. American Society of Civil Engineers. https://doi.org/10.1061/9780784484739

Barros, B., Conde, B., Cabaleiro, M., & Riveiro, B. (2023). Design and testing of a decision tree algorithm for early failure detection in steel truss bridges. *Engineering Structures*, *289*, 116243. https://doi.org/10.1016/J.ENGSTRUCT.2023.116243

Cortes, C., Vapnik, V., & Saitta, L. (1995). Support-vector networks. *Machine Learning 1995 20:3*, *20*(3), 273–297. https://doi.org/10.1007/BF00994018

CSI. (2018). *ETABS building analysis and design* (2018.1.1). Computers and Structures, Inc. www.csiamerica.com

Darko, A., Chan, A. P. C., Adabre, M. A., Edwards, D. J., Hosseini, M. R., & Ameyaw, E. E. (2020). Artificial intelligence in the AEC industry: Scientometric analysis and visualization of research activities. *Automation in Construction*, *112*, 103081. https://doi.org/10.1016/J.AUTCON.2020.103081

Deger, Z. T., & Taskin, G. (2022). A novel GPR-based prediction model for cyclic backbone curves of reinforced concrete shear walls. *Engineering Structures*, *255*, 113874. https://doi.org/10.1016/j.engstruct.2022.113874

Elshaer, A., & Bitsuamlak, G. (2018). Multiobjective Aerodynamic Optimization of Tall Building Openings for Wind-Induced Load Reduction. *Journal of Structural Engineering*, *144*(10), 4018198. https://doi.org/10.1061/(ASCE)ST.1943-541X.0002199

Elshaer, A., Bitsuamlak, G., & El Damatty, A. (2017). Enhancing wind performance of tall buildings using corner aerodynamic optimization. *Engineering Structures*, *136*, 133–148. https://doi.org/10.1016/j.engstruct.2017.01.019

Funk, S., Airoud Basmaji, A., & Nackenhorst, U. (2023). Globally supported surrogate model based on support vector regression for nonlinear structural engineering applications. *Archive of Applied Mechanics*, *93*(2), 825–839. https://doi.org/10.1007/s00419-022-02301-3

Haggag, M., Elruby, A. Y., Ismail, M. K., AbdelAleem, B. H., & El-Dakhakhni, W. (2024). Failure mode and capacity prediction for bolted T-stub connections using ensemble learning. *Journal of Constructional Steel Research*, *212*, 108288. https://doi.org/10.1016/J.JCSR.2023.108288

Hareendran, S. P., & Alipour, A. (2022). Prediction of nonlinear structural response under wind loads using deep learning techniques. *Applied Soft Computing*, *129*, 109424. https://doi.org/10.1016/j.asoc.2022.109424

Hastie, T., Tibshirani, R., & Friedman, J. (2009). The Elements of Statistical Learning. In *Springer series in statistics* (Vol. 27, Issue 2). Springer New York. https://doi.org/10.1007/978-0-387-84858-7

Hoerl, A. E., & Kennard, R. W. (1970). Ridge Regression: Applications to Nonorthogonal Problems. *Technometrics*, *12*(1), 69–82. https://doi.org/10.1080/00401706.1970.10488635

Iancovici, M., Ionică, G., Pavel, F., Moța, F., & Nica, G. B. (2022). Nonlinear dynamic response analysis of buildings for wind loads. A new frontier in the structural wind engineering. *Journal of Building Engineering*, *47*(August 2021). https://doi.org/10.1016/j.jobe.2021.103708

Junda, E., & Málaga-Chuquitaype, C. (2024). Seismic acceleration demands in tall CLT buildings, predictive models and intensity measures. *Engineering Structures*, *298*, 117024. https://doi.org/10.1016/J.ENGSTRUCT.2023.117024

Kallioras, N. A., & Lagaros, N. D. (2021). DL-SCALE: a novel deep learning-based model order upscaling scheme for solving topology optimization problems. *Neural Computing and Applications*, *33*(12), 7125–7144. https://doi.org/10.1007/s00521-020-05480-8

Karbassi, A., Mohebi, B., Rezaee, S., & Lestuzzi, P. (2014). Damage prediction for regular reinforced concrete buildings using the decision tree algorithm. *Computers and Structures*, *130*, 46–56. https://doi.org/10.1016/j.compstruc.2013.10.006

Li, S., Snaiki, R., & Wu, T. (2021). A knowledge-enhanced deep reinforcement learning-based

shape optimizer for aerodynamic mitigation of wind-sensitive structures. *Computer-Aided Civil and Infrastructure Engineering*, *36*(6), 733–746. https://doi.org/10.1111/mice.12655

Liao, W., Lu, X., Huang, Y., Zheng, Z., & Lin, Y. (2021). Automated structural design of shear wall residential buildings using generative adversarial networks. *Automation in Construction*, *132*(February), 103931. https://doi.org/10.1016/j.autcon.2021.103931

Lieu, Q. X., Nguyen, K. T., Dang, K. D., Lee, S., Kang, J., & Lee, J. (2022). An adaptive surrogate model to structural reliability analysis using deep neural network. *Expert Systems with Applications*, *189*. https://doi.org/10.1016/j.eswa.2021.116104

Liu, Z., & Guo, A. (2021). Empirical-based support vector machine method for seismic assessment and simulation of reinforced concrete columns using historical cyclic tests. *Engineering Structures*, *237*, 112141. https://doi.org/10.1016/J.ENGSTRUCT.2021.112141

Lundberg, S. M., Allen, P. G., & Lee, S.-I. (2017). A Unified Approach to Interpreting Model Predictions. *Advances in Neural Information Processing Systems*, *30*. https://github.com/slundberg/shap

Ma, G., Wang, Y., & Hwang, H. J. (2023). Genetic programming-based backbone curve model of reinforced concrete walls. *Engineering Structures*, *283*, 115824. https://doi.org/10.1016/J.ENGSTRUCT.2023.115824

Ma, L., Zhou, C., Lee, D., & Zhang, J. (2022). Prediction of axial compressive capacity of CFRP-confined concrete-filled steel tubular short columns based on XGBoost algorithm. *Engineering Structures*, *260*, 114239. https://doi.org/10.1016/J.ENGSTRUCT.2022.114239

Mangalathu, S., Jang, H., Hwang, S. H., & Jeon, J. S. (2020). Data-driven machine-learning-based seismic failure mode identification of reinforced concrete shear walls. *Engineering Structures*, *208*, 110331. https://doi.org/10.1016/J.ENGSTRUCT.2020.110331

MATLAB. (2023). *MATLAB and Statistics Toolbox Release 2023b* (9.10). The MathWorks Inc.

McKay, M. D., Beckman, R. J., & Conover, W. J. (1979). A Comparison of Three Methods for Selecting Values of Input Variables in the Analysis of Output from a Computer Code. *Technometrics*, *21*(2), 239. https://doi.org/10.2307/1268522

Micheli, L., Alipour, A., & Laflamme, S. (2020). Multiple-Surrogate Models for Probabilistic Performance Assessment of Wind-Excited Tall Buildings under Uncertainties. *ASCE-ASME Journal of Risk and Uncertainty in Engineering Systems, Part A: Civil Engineering*, *6*(4). https://doi.org/10.1061/ajrua6.0001091

Micheli, L., Hong, J., Laflamme, S., & Alipour, A. (2020). Surrogate models for high performance control systems in wind-excited tall buildings. *Applied Soft Computing Journal*, *90*. https://doi.org/10.1016/j.asoc.2020.106133

Mistakidis, E. S. ., & Stavroulakis, G. E. . (1998). Nonconvex optimization in mechanics: Algorithms, heuristics and engineering applications by the F.E.M. In *Computers & Mathematics with Applications* (Vol. 36, Issue 8). https://doi.org/10.1016/S0898-1221(98)91119-1

Oh, S., Jung, Y., Kim, S., Lee, I., & Kang, N. (2019). Deep generative design: Integration of topology optimization and generative models. *Journal of Mechanical Design, Transactions of the ASME*, *141*(11). https://doi.org/10.1115/1.4044229

Pizarro, P. N., & Massone, L. M. (2021). Structural design of reinforced concrete buildings based on deep neural networks. *Engineering Structures*, *241*(March), 112377. https://doi.org/10.1016/j.engstruct.2021.112377

Sayed, Y. A. K., Ibrahim, A. A., Tamrazyan, A. G., & Fahmy, M. F. M. (2023). Machine-learning-based models versus design-oriented models for predicting the axial compressive load of FRP-confined rectangular RC columns. *Engineering Structures*, *285*, 116030. https://doi.org/10.1016/J.ENGSTRUCT.2023.116030

Siam, A., Ezzeldin, M., & El-Dakhakhni, W. (2019). Machine learning algorithms for structural performance classifications and predictions: Application to reinforced masonry shear walls. *Structures*, *22*, 252–265. https://doi.org/10.1016/J.ISTRUC.2019.06.017

Solorzano, G., & Plevris, V. (2023a). An Open-Source Framework for Modeling RC Shear Walls Using Deep Neural Networks. *Advances in Civil Engineering*, *2023*. https://doi.org/10.1155/2023/7953869

Solorzano, G., & Plevris, V. (2023b). DNN-MLVEM: A Data-Driven Macromodel for RC Shear Walls Based on Deep Neural Networks. *Mathematics*, *11*(10). https://doi.org/10.3390/math11102347

Spence, S. M. J. J., & Arunachalam, S. (2022). Performance-Based Wind Engineering: Background and State of the Art. *Frontiers in Built Environment*, *8*(March), 1–11. https://doi.org/10.3389/fbuil.2022.830207

Stone, M. (1974). Cross-Validatory Choice and Assessment of Statistical Predictions. *Journal of the Royal Statistical Society: Series B (Methodological)*, *36*(2), 111–133. https://doi.org/10.1111/J.2517-6161.1974.TB00994.X

Sun, H., Burton, H. V., & Huang, H. (2021). Machine learning applications for building structural design and performance assessment: State-of-the-art review. *Journal of Building Engineering*, *33*, 101816. https://doi.org/10.1016/j.jobe.2020.101816

Tseranidis, S., Brown, N. C., & Mueller, C. T. (2016). Data-driven approximation algorithms for rapid performance evaluation and optimization of civil structures. *Automation in Construction*, *72*, 279–293. https://doi.org/10.1016/j.autcon.2016.02.002

Vaseghiamiri, S., Mahsuli, M., Ghannad, M. A., & Zareian, F. (2020). Surrogate SDOF models for probabilistic performance assessment of multistory buildings: Methodology and application for steel special moment frames. *Engineering Structures*, *212*, 110276. https://doi.org/10.1016/J.ENGSTRUCT.2020.110276

Voulpiotis, K., Schär, S., & Frangi, A. (2022). Quantifying robustness in tall timber buildings: A case study. *Engineering Structures*, *265*, 114427. https://doi.org/10.1016/J.ENGSTRUCT.2022.114427

Wang, C., Song, L. han, & Fan, J. sheng. (2022). End-to-End Structural analysis in civil

engineering based on deep learning. *Automation in Construction*, *138*. https://doi.org/10.1016/j.autcon.2022.104255

Wang, L., Liu, H., Chen, Z., Zhang, F., & Guo, L. (2023). Combined digital twin and hierarchical deep learning approach for intelligent damage identification in cable dome structure. *Engineering Structures*, *274*, 115172. https://doi.org/10.1016/J.ENGSTRUCT.2022.115172

Westermann, P., & Evins, R. (2019). Surrogate modelling for sustainable building design – A review. *Energy and Buildings*, *198*, 170–186. https://doi.org/10.1016/j.enbuild.2019.05.057

Yetilmezsoy, K., Sihag, P., Kıyan, E., & Doran, B. (2021). A benchmark comparison and optimization of Gaussian process regression, support vector machines, and M5P tree model in approximation of the lateral confinement coefficient for CFRP-wrapped rectangular/square RC columns. *Engineering Structures*, *246*, 113106. https://doi.org/10.1016/J.ENGSTRUCT.2021.113106

Zhang, T., Xu, W., Wang, S., Du, D., & Tang, J. (2024). Seismic response prediction of a damped structure based on data-driven machine learning methods. *Engineering Structures*, *301*, 117264. https://doi.org/10.1016/J.ENGSTRUCT.2023.117264

Zheng, Y., Ge, Y., Muhsen, S., Wang, S., Elkamchouchi, D. H., Ali, E., & Ali, H. E. (2023). New ridge regression, artificial neural networks and support vector machine for wind speed prediction. *Advances in Engineering Software*, *179*, 103426. https://doi.org/10.1016/J.ADVENGSOFT.2023.103426

Zhou, C., Xie, Y., Wang, W., & Zheng, Y. (2023). Machine learning driven post-impact damage state prediction for performance-based crashworthiness design of bridge piers. *Engineering Structures*, *292*, 116539. https://doi.org/10.1016/J.ENGSTRUCT.2023.116539

CHAPTER 6

6. CONCLUSIONS AND RECOMMENDATIONS

6.1. Summary

This thesis provides a novel structural layout optimization framework for Main Wind Force Resisting Systems (MWFRS) of tall buildings using machine learning-based surrogate models. Various structural parameters have been studied to show their influence on the optimization process, including the interstorey drift, the building peak drift, the torsional effect, the demand-to-capacity ratio, shear walls base moment distribution, the number of formulated pier and the total number of shear wall segments. The use of SWOF has been extended to include dynamic wind loads generated via experimentally validated Computational Fluid Dynamics (CFD) Analysis to show the variability of generated optimal layout subjected to wind load time history through a linear time history analysis. SWOF enabled a reasonable compromise for various objective functions required in a practical application through multi-objective optimization where a Pareto Front is found as a group of possible optimal solutions. SWOF is also modified to fit the requirements of Performance-based Wind Design (PBWD) standards that use SWOF capabilities to capture linear time history analysis for wind-loaded structures. Finally, a comparative study is held on different machine learning models to assess the adequacy of computationally efficient surrogate models that are capable of deriving the optimization algorithm in exploring the layout search domain with sufficient accuracy.

6.2. Main Contributions

The main conclusions pertaining to the newly developed structural layout optimization framework are as follows:

- An optimization framework capable of handling plan layout problems is developed using genetic algorithms and ANN-based surrogate models to find optimal shear walls and columns layout of tall buildings subjected to wind loads. The ultimate limit state requirements were included implicitly in a computationally affordable manner.
- The adoption of a surrogate model within an evolutionary optimization algorithm makes it possible to find acceptable solutions for the non-convex problem of structural layout in a computationally affordable way.
- Newly defined objective functions (e.g., total number of piers) are included. Those functions enhanced the capability of SWOF to find a reasonable constructible layout that leverages the refinement and discretization options to reach a higher accuracy in finding the shear walls' length and shape.
- A practical database generation procedure is developed through coupling MATLAB and ETABS OAPI to create accessible FEM-generated databases for tall buildings' wind-structural performance. The developed code can automatically change the shear walls layout, change columns layout, assign pier labels for lumped shear wall segments and export required results.
- The developed framework, SWOF, showed the possibility of using linear time history analysis of wind-excited tall buildings by generating wind loads via experimentally validated CFD. The resulting layout showed that minimal considerations are required in

the final design stages since the framework pushes the design process to the limits of the considered design code, taking into account the serviceability limit states explicitly and the strength limit state implicitly.

- The developed framework, SWOF, adopted the multi-objective optimization algorithm that provides multiple possible solutions (i.e., Pareto Front) that provide stakeholders with multiple options that can facilitate the process of decision-making in identifying a final layout.
- The developed framework, SWOF, is modified to include the ultimate limit states explicitly through the demand-to-capacity ratio for MWFRS and structural elements, in addition to multiple angles of attachment for wind time history analysis, making it possible to fit the PBWD standards and requirements.
- The developed framework, SWOF, is fine-tuned to enhance constructability by allowing symmetrical layouts and penalizing layouts with standalone segments through accepting layouts with lumped shear wall segments. This penalization technique ensures a shear wall behaviour for shear wall elements instead of column behaviour.
- The machine learning-based surrogate model enables SWOF to discover thousands of possible layouts for the MWFRS, eliminating the need for direct integration of FEM within the optimization process.
- Deep neural networks showed their capabilities in capturing the nonlinear relationship between crude topology (i.e., structural layout) and tall buildings' performance. It was found that DNN overperformed previously used ML surrogate models. Moreover, it

significantly lowers the computational cost and eliminates the need for the direct integration of FEM and CFD within the optimization algorithm.

6.3. Future work and recommendations

- It will be valuable to investigate transforming the framework to use an adaptive surrogate by continuously updating the surrogate model parameters based on the evolving characteristics of the population samples initially generated through the optimization process to check the effectiveness of the computational time and surrogate model efficiency.

- Achieving a computationally efficient optimization process can be reached through comparing the evolutionary-based optimization algorithm with a gradient-based algorithm for a simplified representation of the structure with a modified convex version that can be achieved without being trapped in a local minimum.

- For more generalization of the developed framework, it will be beneficial to increase the design parameters (e.g., seismic loads) and change the structural systems (e.g., steel structures, bracing system and connections) that SWOF can tackle with an extension toward sizing optimization.

- It will be useful to develop a BIM tool that can read models from IFC models to identify possible structural system domains and generate a surrogate model for tall buildings based on prespecified parameters using FEM.

- More studies can be done on surrogate model behaviour to enhance its performance and reduce the margin of error. Since DNN showed an adequate performance, it can be compared to its counterparts of deep learning algorithms (e.g., Convolutional Neural Networks).